JOHANNES GUTENBERG UNIVERSITÄT MAINZ

Bioactive Polyphosphate-based Biomaterials: An Approach towards Improved Bone Replacement Implants

Dissertation
zur Erlangung des Grades
"Doktor der Naturwissenschaften"
am Fachbereich Biologie
der Johannes Gutenberg-Universität
in Mainz

vorgelegt von

Emad Tolba Adnan Tolba Eldeyaste

geboren am 04.07.1983 in Eldakahlia, Ägypten

Mainz, 2016

Dekan: Prof. Dr. Hans Zischler

Erster Berichterstatter: Prof. Dr. Werner E. G. Müller

Zweiter Berichterstatter: Prof. Dr. Bernhard Lieb

Tag der mündlichen Prüfung: 10.11.2016

Acknowledgement

The presented doctoral thesis has been performed in the ERC Advanced Investigator Grant Research Group at the Institute for Physiological Chemistry, University Medical Center of the Johannes Gutenberg University in Mainz. Foremost, I would like to express my gratitude to my supervisor Prof. Dr. Werner E. G. Müller for offering me the possibility to join his research group, for his scientific guidance and for his ongoing interest in the progress of this work. I further very much appreciate the possibility of active participation in numerous local and global scientific meetings, discussions, and conferences. I would also like to thank Prof. Dr. Heinz C. Schröder for his collaborative and constructive discussion and critical reading of the thesis and Prof. Dr. Xiaohong Wang for her advice, continuous motivation and providing excellent working conditions, as well as Prof. Dr. Bernhard Lieb for his support and help throughout my PhD work.

Furthermore, I am very grateful and would like to thank current and old members of our group for their collaboration and constructive discussions, as well as the personal cooperation, trips and their contribution to various leisure time activities. I am very thankful to Renate Steffen, Shunfeng Wang, Vladislav Grebenyuk, Dr. Klaus Kropf, Dr. Julia Markl, Dr. Sebastian Neumann and Dr. Alberto Manfrin. Thanks to Max Planck Institute for Polymer Research in Mainz, especially Dr. Rafael Muñoz-Espí and Dr. Frederik R. Wurm deserve thanks for X-ray diffraction experiments, as well as Gunnar Glaßer and [redacted] for allowing me to use both SEM and EDX analyses. My special thanks to Dr. Maria Kokkinopoulou for helping me with TEM measurements.

I would like to express my sincere thanks to my mother, brother, sister and my whole family. Really I have no words able to express my sincere gratitude and appreciation for their continuous encouragement and support and for all they did for me. Finally, I would like to present a special thank to my lovely wife Sara Ahmed for always being there for me. Thank you!

List of Publications

This PhD thesis is based on the following 6 articles in peer-reviewed journals:

1. Müller WEG, **Tolba E**, Schröder HC, Wang S, Glaßer G, Muñoz-Espí R, Link T &Wang XH (2015). A new polyphosphate calcium material with morphogenetic activity. Mater Lett. 148: 163-166.

2. Müller WEG, **Tolba E**, Schröder HC & Wang XH (2015). Polyphosphate: a morphogenetically active implant material serving as metabolic fuel for bone regeneration. Macromol Biosci. 15: 1182-1197.

3. Müller WEG, **Tolba E**, Feng Q, Schröder HC, Markl JS, Kokkinopoulou M & Wang XH (2015). Amorphous Ca^{2+}polyphosphate nanoparticles regulate ATP level in bone-like SaOS-2 cells. J Cell Sci. 128: 2202-2207.

4. Müller WEG, Schröder HC, **Tolba E**, Neufurth M, Diehl-Seifert B & Wang XH (2016).Mineralization of bone related SaOS-2 cells under physiological hypoxic conditions. FEBS J. 283: 74-87.

5. **Tolba E**, Müller WEG, Abd El-Hady BM, Neufurth M, WurmF, Wang S, Schröder HC & Wang XH (2016). High biocompatibility and improved osteogenic potential of amorphous calcium carbonate/vaterite. J Mater Chem B. 4: 376-386.

6. Müller WEG, **Tolba E**, Schröder HC, Muñoz-Espí R, Diehl-Seifert B &Wang XH (2016). Amorphous polyphosphate-hydroxyapatite: A morphogenetically active substrate for bone-related SaOS-2 cells in-vitro. Acta Biomater. 31: 358-367.

Abstract

New strategies for regeneration of damaged or diseased bone tissue are urgently needed because of difficulties and limitations in conventional therapies for repairing bone defects. Bone tissue engineering is a relatively new method for clinical treatment of massive bone injuries and deficiencies. The concept behind this approach is to deliver osteogenic cells and growth factors to injure site using an artificial matrix called scaffold. Therefore, there is an ever-growing need to design and develop bioactive scaffolding materials that provide the appropriate physical, chemical and biological microenvironments for guiding properly the cells during the regeneration process. Recently, inorganic polyphosphate (polyP), as a potent inducer for osteogenic cell activities, has become one of the most interesting research directions in bone tissue regeneration based on its capability to play numerous functions both in the extracellular and in the intracellular space. To date, there have been many studies dealing with this issue, but the results obtained are somewhat controversial. The mechanisms whereby inorganic polyP induces mineralization of hard tissues likely depend on a number of factors or conditions. In this PhD thesis, calcium polyphosphate (Ca-polyP) nanoparticles were prepared from sodium polyphosphate (Na-polyP) via a calcium/sodium ion exchange in aqueous solution at room temperature and used in cell culture experiments. The results indicate that exogenously administered Ca-polyP granules or nanoparticles indeed significantly promote the growth of cell and expression of the alkaline phosphatase (*ALP*) of osteoblast, like SaOS-2 cells. Upon these results, an approach has been introduced to incorporate polyP with the most common biominerals hydroxyapatite (HA) and calcium carbonate (CC) to enhance their biological actions. The microstructural characterization of the obtained calcium phosphate or carbonate phases show the ability to control nucleation and growth of these inorganic crystallites as a function of polyP content. After the physical-chemical and morphological characterization of the synthesized materials, they were assessed via studying their effects on cell activity and mineral deposition. The work presented here not only

highlights the role of polyP as a morphogenetically active material (i.e. promoting maturation and functional activity of bone forming cells) but also provides strong evidence that amorphous phases of calcium phosphate or carbonate have a potential during biomineralization of bone tissue to act as precursors or nucleation sites for deposition of the bone mineral hydroxyapatite both *in vitro* and *in vivo*. Finally, the thesis opens new perspectives and paves a way for the development and fabrication of novel multifunctional hybrid biomaterials for effective bone tissue engineering and other biomedical purposes in the future.

Zusammenfassung

Komplikationen Therapien von traumatischen und Knochenerkrankungen haben in den letzten Jahren zu einer verstärkten Entwicklung neuer Strategien zur Regeneration von erkranktem oder beschädigtem Knochengewebe geführt. Bei „Bone Tissue Engineering“ handelt es sich um eine relativ neue Technik zur klinischen Behandlung von Knochenverletzungen, sowie von Knochenerkrankungen. Das Ziel dieser Methode ist es, die gerichtete Rekrutierung von knochenbildenden Zellen und Wachstumsfaktoren in einen definierten dreidimensionalen Raum unter Zuhilfenahme einer künstlichen Matrix (Scaffold) anzustoßen. Für die Etablierung solcher Methoden ist die Entwicklung entsprechender Materialien, die als strukturelles Netzwerk für regenerative Prozesse dienen und die Proliferation sowie Differenzierung der knochenbildenden Zellen induzieren können, unabdingbar. In jüngster Zeit erwies sich die Anwendung anorganischer Polyphosphate (polyP), die in der Lage sind, sowohl das Wachstum als auch die Differenzierung der knochenbildenden Zellen zu induzieren, als eine der interessantesten Stategien im Bereich der Knochenregeneration. Polyphosphate als anorganische bioaktive Polymere zeichnen sich durch exzellente Biokompatibilität und Biodegradierbarkeit aus. Sie haben außerdem die Fähigkeit, vielfältige intra- und extrazelluläre Funktionen zu übernehmen. Polyphosphate und ihre Eigenschaften wurden in einer Reihe von Studien untersucht. Die veröffentlichten Ergebnisse sind jedoch teils widersprüchlich, was vermutlich damit zusammenhängt, dass die durch anorganische Polyphosphate induzierte Mineralisation von Hartgeweben aller Wahrscheinlichkeit nach von einer Vielzahl an Faktoren oder Bedingungen abhängt. Im Rahmen der vorliegenden Arbeit wurde Natrium-Polyphosphat (Na-polyP) als Vorstufe von Polyphosphat für die Herstellung von Calcium-Polyphosphat (Ca-polyP) Nanopartikeln verwendet. Die Herstellung der Partikel wurde über einen Calcium/Natrium-Ionenaustausch in wässriger Lösung bei Raumtemperatur durchgeführt. Anschließend wurden die Partikel für *in vitro* Zellkulturversuche genutzt. Die gewonnenen Ergebnisse zeigen, dass exogen verabreichtes Ca-polyPGranulat bzw. Nanopartikel im Vergleich zu Na-polyP tatsächlich zu einem deutlich gesteigerten Wachstum sowie zu einer stärkeren Expression der alkalischen Phosphatase in Knochen-bildenden SaOS-2 Zellen führt. Basierend auf diesen Daten wurde ein weiterer Ansatz entwickelt, bei dem Polyphosphat mit den wichtigsten Biomineralien des Knochens, Hydroxylapatit (HA) und Calciumcarbonat (CC), zusammengebracht wurde. Diese Kombination sollte zur Steigerung der biologischen Leistung der verwendeten Materialien führen. Anhand der durchgeführten mikrostrukturellen Charakterisierung der erhaltenen Calciumphosphat-oder Calciumcarbonat-Phasen konnte gezeigt werden,

dass sich sowohl die Nukleation als auch das Wachstum der anorganischen Kristallite über den Polyphosphat-Gehalt steuern lassen. Die vorliegende Arbeit stellt nicht nur die Wichtigkeit von Polyphosphat als morphogenetisch aktives Material mit der Fähigkeit zur Induktion von knochenbildenden Zellen heraus, sondern liefert auch deutliche Hinweise dafür, dass die amorphen Phasen von Calciumphosphat und Calciumcarbonat das Potential haben, als Vorstufen für die Ablagerung des Knochenminerals zu fungieren. Die im Rahmen dieser Arbeit erzielten Ergebnisse ebnen den Weg für neue Ansätze in der Entwicklung von multifunktionalen Hybrid-Biomaterialien, die zukünftig für ein erfolgreiches „Bone Tissue Engineering“ und weitere biomedizinische Anwendungen genutzt werden könnten.

Table of Contents

Chapter 1:

General introduction

1.1 Bone tissue

1.1.1 The basic structure and functions of bone

Bone or Osseous tissue is a dynamic connective tissue that undergoes continual changing or remodeling during human lifetime to attain and preserve body skeletal [1, 2]. Unlike other connective tissues, Bone tissue is defined as a tissue and as an organ. Bones have many functions, including the following [2-4]:

- **Support**: Bones provide a framework for the attachment of muscles and other tissues.
- **Protection***:* Bones such as the skull and rib cage protect internal organs from damage.
- **Mobility***:* Bones enable body movements by acting as levers and points of attachment for muscles.
- **Mineral storehouse***:* Bones serve as a reservoir for calcium, phosphorus and other ions for various cellular activities throughout the body.
- **Hematopoiesis:** The formation of different types of blood cells occurs in the bone marrow which found inside certain bones.
- **Energy storage***:* Lipids, such as fats, stored in adipose cells of the yellow marrow and serve as an energy reservoir.

More than 200 bones with different shapes form the skeleton of human body. They are assorted into four main groups: long, short, flat and irregular bones [4]. Bone as a tissue has different arrangement either in a compact form (also known as cortical bone) forming the outer layer of natural bones [3, 5] or in a cancellous bone (spongy bone) which is located under the compact bone and consists of a highly porous interconnected network of bone basic unites close to bone marrow [6].

1.1.2 Hierarchical organization of bone: a bottom up approach

Bone has architecture fashion with different levels of sophisticated hierarchical structures which are arranged in a way to minimize weight, disperse-bearing stresses at the joints, and sustain external loads in the body. Actually, bone as a framework tissue has an optimal combination of properties, namely high stiffness, strength and toughness with low weight or density [7–9]. These characters of bone tissue are attributed to its unique composition as a nanocomposite biological material with amazing hierarchical structures from nano to macrostructure as shown in **Fig. 1.1**. However, the composition and morphology of bone differ greatly according to the site in the skeleton, but the basic chemical or structural components of bone consisting of collagen matrix reinforced with calcium phosphate HA tiny crystals remains the same overall the human body[10].Bone tissue exhibits distinct levels of organization [7, 10]:

(i) **1st level** of bone tissue represented by the components of bone matrix which is mainly composed of two major molecules at the nanoscale namely, collagen and bone mineral HA. The collagen has a typical fibrous structure, whose diameter varies from 100 to 2000 nm. Similarly, bone mineral HA is in the form of nanocrystals, with a size of about 1.5 - 4 nm thick and 30-50nm length.

(ii) **2nd level** is formed of mineralized collagen fibrils [7, 11]. It had been proposed that these mineral needles are arranged in parallel like a stack of cards within the interstices of the fibril [12].

(iii) **3rd level** is the arrangement of mineralized collagen fibrils in parallel arrays, woven arrangements, or plywood-like structures [11, 12].

(iv) **4th level** is the parallel arrays, woven arrangements, plywood-like structures, and radial arrays like those found in dentin [13].

(v) **5th level** is the cylindrical structure called osteons. They are formed with significant cellular activity, osteoclasts resorb bone and form a small tunnel, and osteoblasts subsequently lay down lamellae in stacked layers until Haversian canal is left behind [9]. These channels transport nutrients to bone cells.

(vi) **6th level** of bone organization reflects the classification of osseous tissue as either spongy or compact. Spongy bone has a high porosity (75-95%), providing space for marrow and blood vessels, but has much lower compressive strength. Cortical bone is the dense outer layer (5-10% porosity) that supports various functions of bone [6, 14].

(vii) **7th level** is simply the whole bone on the macroscopic scale, incorporating all of the lower levels of arrangement [15].

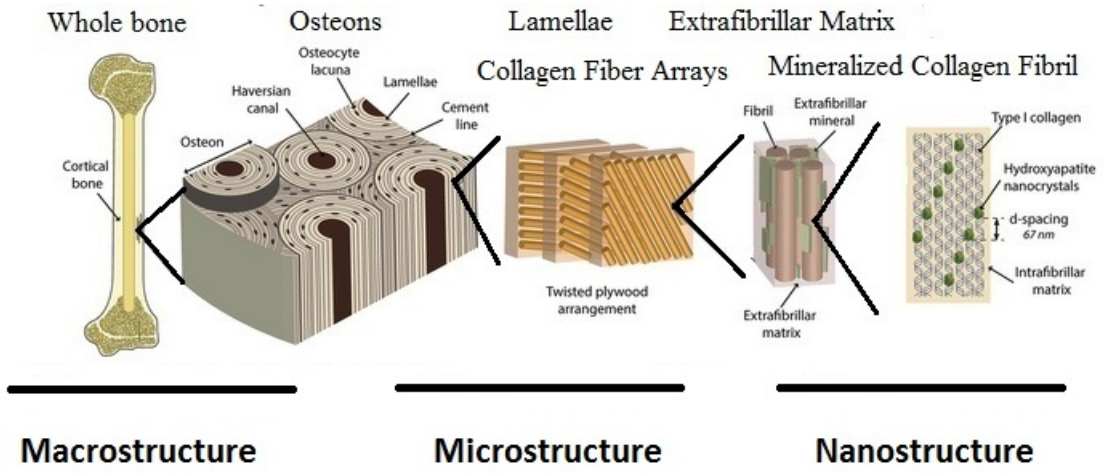

Figure 1.1.
Bone tissue exhibits a distinct hierarchical structural organization of its constituents on numerous levels including: macrostructure (cancellous and cortical bone), microstructure (Harversian systems, osteons and single trabeculae), and nanostructure (fibrillar collagen and embedded HA minerals) [15].

1.1.3 Molecular component of bone matrix

As mentioned before bone is composed of inorganic or mineral salts and organic matrix. The organic bone matrix contains collagenous proteins (90%), predominantly type I collagen, and noncollagenous proteins including osteocalcin, osteonectin, osteopontin, fibronectin and bone sialoprotein II, bone morphogenetic proteins, and growth factors [9]. Bone matrix plays important role in the release of several molecules that control bone cell functions activities in order to control bone tissue development and remodeling [16]. Bone defects are not only caused by loss of bone mass but also other

reasons, including changes or modifications of physical or chemical structure of bone matrix proteins and are of great importance to understanding and prediction of bone tissue complications.

Indeed, it is known that collagen plays a critical role in the structure and function of bone tissue [17]. Collagens are a family of structural proteins that are found in the extracellular matrix, which represents the main component of skin, blood vessel, tendon, cartilage and bone. Collagens account for approximately 25% of the total protein within the body. In the connective tissue, collagens constitute about 80% of all proteins. The chemistries underlying the formation of these tissues are quite similar and the fundamental differences are based on different hierarchical fibrillar architectures [9, 18]. The existence of more than 20 human collagens has been reported, many of them display a 67 nm periodicity, due to the axial packing of the individual collagen molecules [19]. Among them, collagen type I is the most abundant protein in the human body and provides much of the structural integrity for several connective tissue. The chemical structure of collagen is composed of the amino acids glycine, proline, and hydroxyproline, which together account for more than 50% of the amino acid composition, often as Gly-X-Y repeats (where X and Y are either proline or hydroxyproline) [20]. The collagen is synthesized intracellular, and then extruded to extracellular space where it undergoes fibrillogenesis, and subsequent self-assembly and mineralization [21]. Finally, it is important to note that the minerals are not directly bound to collagen, but bound through non-collagenous proteins (**Fig. 1.2**) [22].

The second important component in bone matrix is made up of the inorganic mineral HA (also called biological apatite). These tiny crystals are formed at the spaces left between the collagen fibers and exhibit the particular feature of being monodispersed and nanosized platelet or needle like crystal structure [18, 23]. The crystalline structure of HA, $Ca_{10}(PO_4)_6(OH)_2$, belongs to the hexagonal systems with lattice parameters a = b=9.423 Å and c = 6.875 Å [24]. The crystallographic axis c of these crystals is oriented in parallel to the collagen fibers [25]. Besides the main ions Ca^{2+}, PO_4^{3-} and OH^-, the

composition of bone mineral HA always includes ~4.5%CO_3^{2-}, and also a series of trace elements, mainly Mg^{2+}, Zn, Na^+, K^+, Cl^- and F^- which are known for their anabolic effects in bone metabolism [26]. These ions modify the lattice parameters of HA crystal structure as a consequence of different size of the substituting ions. This is an important difference between minerals grown in biological environment [27]. Hence, bone mineral is often described as a poorly crystalline carbonated apatite, which probably relates to the nanosize of the crystals as well as residual stresses in the crystal lattice due to substitution mechanisms with the addition of new ions into the crystal structure replacing both calcium and phosphate ions [28].

1.1.4 Bone matrix mineralization: how nature works

Composite materials are made by combining two or more distinct phases and called nanocomposite where one of the component has one dimensions in the nanometer size range [29]. Nature has a powerful ability to fabricate composite materials with remarkable and unique properties and functions [30, 31]. For instance, biological tissues such as bone, dentin and wood are nominated as natural composite materials. Bone is one of the biogenic ceramic–polymer nanocomposite materials that is still waiting for a man-made bone-like material. This could be due to the actual mechanism involved in the formation of bone nanocomposite material (Biomineralization process) remains poorly understood [32].

Generally, the building unit of natural bone tissues is mineralized collagen fibril, which is composed of organized collagen and HA [7, 33, 34]. Tropocollagen is the subunit of collagen fibrils formed of three polypeptide strands (each offset by one amino acid), approximately 300 nm long and 1.5 nm in diameter [21, 23, 35]. Each of the three chains forms a left-handed helical polyproline II type helix with three residues per turn. The tropocollagen units assemble in a parallel, quarter-staggered arrangement. There is a gap of 40 nm size, called the “hole zone”, in between the ends of each of these units, with 27 nm of overlap between adjacent units [35]. These hole zones are essential for mineralization process, as they appear to be the nucleation sites for HA mineral. The

crystals appear to grow and proliferate from this area. The size of the gap also appears to constrain the growth of HA crystals [36].

During mineralization process of collagen, nucleation sites are of great importance for the formation of the mineral crystals. In this regard, a number of reports suggested that the negatively charged carboxyl groups (–COOH), which are present in about 11% of the amino acid residues of collagen molecules, are the major nucleation sites for the mineralization of collagen fibrils, and the binding of calcium ions (Ca^{2+}) on these carboxyl groups is a key factor for the initial step of the biomineral nucleation [37, 38]. A subsequent study indicated that not only the carboxyl group, but also the carbonyl groups (C=O) on collagen serve as another site for nucleation of the HA crystals [21, 39]. The oxygen atoms of both types of groups react with Ca^{2+} as the core of non-homogenous nucleation reaction. The mineralized collagen fibrils further assemble to form bone matrix with a three-dimensional net structure as a template for further mineral deposition. Within the mineralized collagen, the conformation of the collagen protein changes and collagen fibrils cross-link through coordination bonding between saccharide hydroxyl and Ca^{2+}, thus making the collagen undissolvable in water [40, 41]. The assembly and organization of the collagen provide intramolecular space for the nucleation and growth of the HA crystals [24]. At the initial stage, the nucleation occurs within the gap and overlap regions created in the assembly of collagen molecules (**Fig.1.2**) [21]. After nucleation, the mineral crystals develop into small platelets, and grow in the direction of *c*-axis as a preferred orientation along and parallel to the long axis of a collagen fibril [25].

However, some reports have been conducted to develop bone-like material via physical mixing of nanosize HA with collagen or in situ nucleation and growth of HA in collagen solution; the obtained nanocomposites were very different from nanostructure and architecture of natural bone [42, 43]. Thus, It has been assumed that mineralization of collagen during bone formation can be achieved using a polymer-induced liquid-precursor (PILP) process [43]. In such a PILP process, a fluidic amorphous liquid-phase

mineral acts as a precursor for deposition and maturation of HA and the fluidic character enables the amorphous precursor to be naturally drawn into the nanoscale gaps and grooves of collagen fibrils by capillary action to facilitate intrafibrillar mineralization of type I collagen [44]. The amorphous precursor then solidifies and crystallizes upon loss of hydration waters into the more thermodynamically stable phase, leaving the collagen fibrils embedded with nano-sized HA crystals [25, 44, 45]. The existence of a transient precursor is an ongoing controversy in the field of bone biomineralization. It had been assumed that crystal growth during biomineralization occurs via an octacalcium phosphate (OCP) intermediate [38, 46, 47]. OCP has nearly the same crystal structure as HA but contains an extra hydrated layer that may be responsible for the observed plate-shaped crystals in natural bone. Further, Amorphous calcium phosphate (ACP) was also found to spontaneously precipitate to apatite at physiological values *in vitro* [48, 49]. As a result, the role of amorphous phases in mineralization of HA in biological tissues such as bone continues to be a subject of great research interest [50-52].

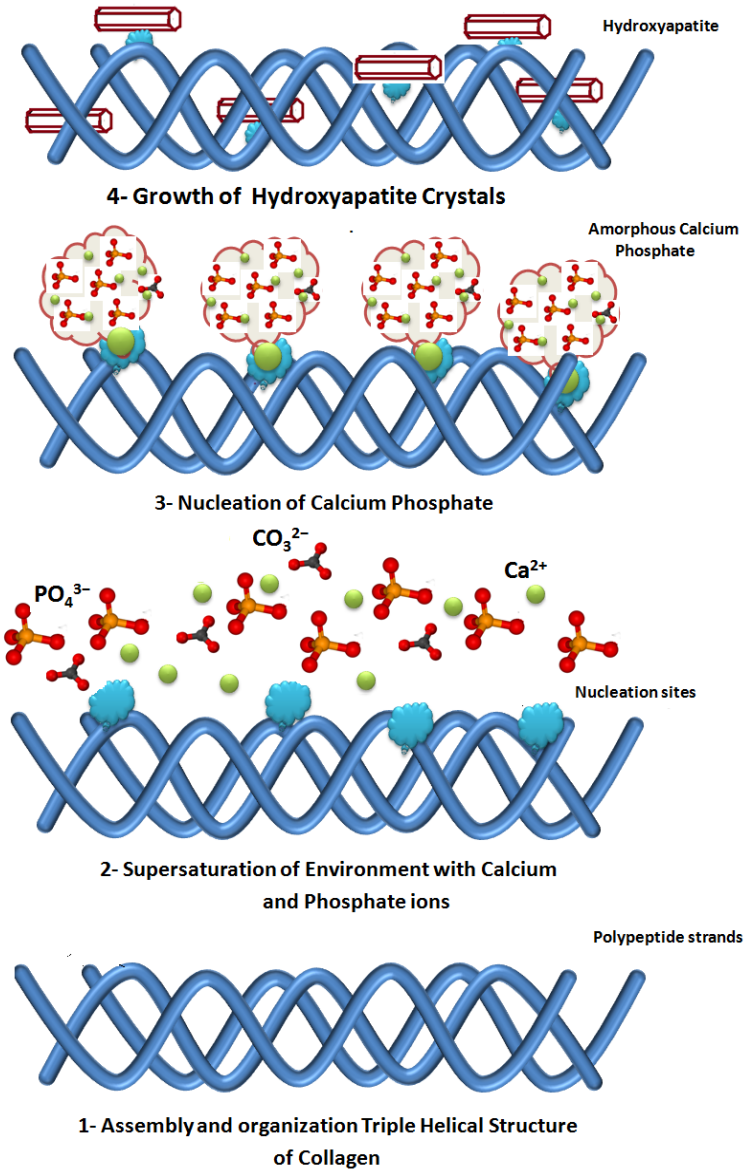

Figure 1.2.
Mechanism of nucleation and growth of HA crystals on collagen during bone matrix mineralization.

1.1.5 Cell types in bone tissue

The cellular components of bone tissue play an essential role in formation and control of bone metabolisms [53-56]. Five types of cells are found in bone tissue and involved in its biological activities [53, 57]: Osteoprogenitor cells, osteoblast cells, osteocytes

cells, lining cells and osteoclast cells. Each cell type has a different function and found in different locations in our bones. These cell names all start with "**Osteo**" because that is the Greek word meaning bone [57].

Osteoprogenitor cells (or ***osteogenic cells***) [55, 57] are undifferentiated cells with high mitotic activity. They are the only bone cells that divide. Immature osteogenic cells are found in the deep layers of the periosteum and the bone marrow. They differentiate and develop into bone forming cells osteoblasts.

Osteoblast cells [58] are responsible for formation of new bone tissue. They originate from the osteogenic cells and are related to structural cells. They have only one nucleus and work in teams to build bone. They produce new bone called "osteoid" which is made of mineralized collagen fibrils. They are found on the surface of the newly formed bone tissue.

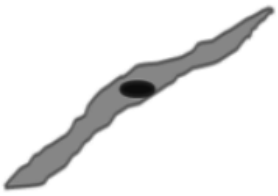

When a team of osteoblasts has finished closing up the gap, few of them become flat and look like pancakes. They line on the surface of the mature bone tissue. These old osteoblasts are called ***bone lining cells*** [57, 59]. They regulate passage of calcium and other ions into or out of the bone tissue and also respond to hormones by making special signal molecules to activate the osteoclasts.

Osteocyte Cells [60, 61] are inside the bone and long-lived cells, with a lifespan of up to 25 years. They also come from osteoblasts. Some of the osteoblasts turn into osteocytes while the new bone is being formed. They are not isolated from bone tissue and connected to each other to communicate during bone formation and resorption. These cells can sense pressures or cracks in the bone and help to direct where osteoclasts will dissolve the bone.

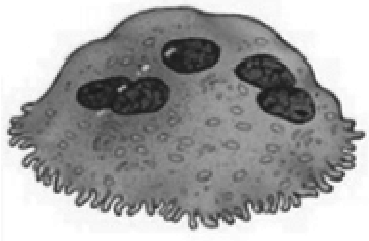

Osteoclast cells [62] are giant cells that dissolve the bone. They come from the bone marrow and are related to white blood cells. They are formed from two or more cells that fuse together, so the osteoclasts usually have more than one nucleus. They are found on the surface of the bone mineral next to the dissolving bone.

1.2 Bone tissue regeneration

1.2.1 Current scenarios of bone regeneration

Bone tissue has a powerful self-regenerative capacity as part of the healing process after injury, as well as during skeletal growth and continuous remodeling throughout human body development [63-66]. Natural bone regeneration following damage can be defined as interdependent series of biochemical pathways targeting the activation of different cellular and molecular responses. It is mainly consisted of two steps: clean-up or resorption of broken bone parts by osteoclasts followed by the rearrangement of bone matrix through the osteoblasts. The entire process is controlled by intracellular and extracellular signalling molecules in order to optimise regeneration process [65, 67]. These signals include the action of several hormones, such as parathyroid hormone, vitamin D, growth hormone, steroids and calcitonin, as well as a number of

bone marrow-derived membrane and soluble cytokines and growth factors [64, 67]. Unlike in other tissues, most of bone tissue fractures heal without the formation of a scar and regenerates with its pre-existing form [66].

Unfortunately, in some cases bone auto-regeneration ability is limited, such as sever and large volume bone defects caused by trauma, infection, tumor, skeletal abnormalities, or bone diseases [68, 69]. Due to these burdens in which the natural process of bone healing is either restricted or insufficient, there are currently a number of treatment methods available in the clinic, which can be used to overcome and management of these significant situations [70].It should be noted that bone is the second most transplanted tissue in humans after blood. Standard approaches widely used in clinics to aid natural bone regeneration process include a number of different bone grafting methods [67, 71]. The roles of bone grafts are to provide mechanical or structural support, fill defective gaps, and induce bone tissue healing process [72, 73]. They are widely applied in orthopedic and dental surgery. The grafts not only replace missing bone but also help the body to restore its own lost bone tissue. By this method, bone healing time is reduced and new bone formation supports the defective site by bridging grafts with surrounding tissue [74].

Autogenic bone grafting [75-79] is a method in which bone tissue is taken from one site to another site in the same individual. Bone can be taken from non-essential bones, often from the iliac crest. This process is the most preferred because there is less risk of the rejection because the graft isolated from the patient's own body. However, autograft is the gold standard for treatment of bone defects; donor site morbidity and additional surgical operation are complex problems. However, *Allogenic* and *xenogenic bone grafts* [76, 80] are alternatives to autografts, they are expensive, and suffer from potential risks such as disease transmission and adverse host immune response.

Synthetic bone grafts or *biomaterials* have also been developed as alternatives to autologous bone grafts [80-85]. A wide range of biomaterials is currently used as bone substitutes or scaffolds including natural or synthetic materials such as, titanium,

collagen, HA, tricalcium phosphate, other calcium phosphates, and glass ceramics [83, 84].

1.2.2 Challenges and limitations of bone regeneration

Most of the current applied techniques for the treatment of bone defects or diseases exhibit relatively satisfactory and sufficient results [86-90]. However, there are a number of queries concerning the benefits of their usage, availability and cost-effectiveness as well as even controversial biological outcomes about their efficacy [89, 90]. To date, it is clear that the features of synthetic bone grafts or biomaterials are still away from even coming close to the desirable physical, chemical and biological characteristics of natural bone. Therefore, there is a necessity to develop novel biomaterials and treatment approaches as alternatives to the current methods used for bone healing and as a new direction to overcome these obstacles which had been a challenge for many decades [86].

Currently, advances made in cellular and molecular biology have introduce more detailed information about *in vitro* and *in vivo* performances of osteogenic or bone-forming cells and identification of a number of genes and proteins involved in the process of bone fracture repair [63, 91]. As a result trends are turned to isolate these cells from a patient to grow them on a temporary matrix under controlled *in vitro* culture conditions and deliver them to the damaged site in the patient's body with the aim to guide and direct new tissue formation into the matrix that will be degraded over time [53, 92].

1.2.3 Emerging of tissue engineering

Regenerative medicine is a fast growing medical field that aims to fabricate biological active implants or living tissues *in vitro* to restore and regenerate damaged or malfunctioning tissues and organs *in vivo* [15, 18, 93]. This approach has the potential to replace organ transplants. It is also called tissue engineering because regenerative medicine generates tissues or organs using engineering technology to build up the

template structure of the target tissue or organ before transplantation. To make regenerative medicine successful, three components are required: stem cells, scaffolds and growth factors [72, 93]. Translational research, which takes results from the laboratory and translates them to the clinics, and industry-academic collaborations also play important roles in making regenerative medicine suitable for practical use.

Tissue engineering is an interdisciplinary field of research that applies the principles of engineering and the life sciences towards the development of biological or living substitutes for restoring, maintaining or improving a damaged tissue, which fails to heal spontaneously or regenerate [74, 94]. This field aims at a fundamental understanding of structure–function relationships in normal and pathological tissue, as a route to generate new functional tissues, rather than just to close up the gap by non-living implant [72]. Tissue engineering approach would be able to overcome the limitations of current therapies, by combining the principles of orthopaedic surgery with knowledge from biology, materials science and engineering and its clinical application offers great potential [95, 96].

1.2.4 Biomaterials in bone regeneration

In an attempt to solve a critical issue, poor tissue regeneration capacity after severe or large mass defects, tissue engineering has been introduced as a potential therapeutic treatment to induce natural regeneration mechanisms that require during wound healing process and tissue developments [11, 98]. Thus, a combination between scaffold, specific cell types and growth factors is supposed to promote regeneration or replacement of degenerated tissue or organs [15, 97]. Therefore, tissue engineered materials have to mimic a certain extent the chemical, physical and biological properties of natural extracellular matrix of the target tissue to help in the restoration of the full structure and functionality of the tissue [72, 99].

In tissue engineering, biomaterials are used in two or three dimensions (3D) form and usually described as matrices or scaffolds. The basic role of scaffolds is to provide a temporary template for guiding newly formed tissue and regeneration process [100-

102]. The scaffold also plays a critical role in providing the appropriate chemical, morphological and structural cues to direct the cells towards a targeted functional outcome. Since, there is no final conclusion about the use of definite type of scaffolding materials (ceramics, polymers or their composites)in tissue regeneration and due to native extracellular matrix is complex, dynamic and highly specific, the characteristics of the scaffold materials are based on tissue or organ type [103, 104].

For instance, bone has a complex 3D form and cells do not grow in this fashion *in vitro*. Hence, a 3D scaffold or supporting material must be used so that new tissue can be grown in a 3D manner [105]. In general, tissue engineering scaffolds should have the following characteristics [106-108] : {a} 2 or 3D structure configuration; {b} High porosity with an interconnected pore network for cell growth and flow transport of nutrients and metabolic waste; {c} Gradually degrade while the new tissue is formed; {d} appropriate physical and chemical composition as well as topography for cell attachment, migration, proliferation, and differentiation; {e} Adequate mechanical strength to support and maintain the initial space of the defect site during regeneration process. Moreover, scaffolds should also mimic the reactivity of natural target tissue, sterilizable without chemical or physical modifications and for clinical use the design and fabrication methods must be easy, reproducible, economical and scalable [86, 89].

Recently, development of biomaterials has become one of the central themes in bone tissue regeneration due to the material composition of the scaffold plays an important role in guiding cell behavior [10, 89]. Over the past decades, several biomaterials have been developed and successfully used for replacement soft and hart tissues. They are commonly made of metals, ceramics, polymers, and their composites. In most of the cases, metals (e.g., stainless steel and titanium alloys) [75, 77] and ceramics (e.g., alumina, zirconia, HA and bioglass) are used in hard tissue replacements [26, 29, 103], whilst polymers (poly(methyl methacrylate), collagen, gelatin and poly(α-hydroxy esters)) in soft tissue applications. Composites (e.g., HA/collagen and HA/ poly(α-hydroxy esters)) are widely used in both the applications[101, 102]. Although there are

numerous types of biomaterials from natural or synthetic origin, tissue engineering requires the use of bioresorbable or biodegradable ones in the fabrication of template scaffold or matrices for initial cell attachment and subsequent tissue formation both *in vitro* and *in* vivo[89, 98].

1.3 Polyphosphate: an inorganic biopolymer

Organic polymers are characteristically hydrocarbon chains that by their extreme length provide entangled materials with unique properties. On the other hand, the most obvious definition for an inorganic polymer is a polymer which has inorganic repeating units in the backbone. Among the inorganic polymers, polyP which is formed of phosphate groups linked together by bridging oxygen atoms is currently getting a great attention in biomedical application [109].

1.3.1 Biological importance of phosphate

Phosphate is the naturally occurring form of phosphorus element and found in many salts or minerals. Phosphorus is estimated to have the ninth largest total concentration in igneous rocks (rocks formed from cooled magma), without oxygen and nitrogen. Most naturally occurring phosphates on our Earth are found in the apatite phosphate mineral [110, 111].Phosphates move quickly through plants and animals, however the processes that move them through the soil or ocean are very slow [111].

Phosphate is assumed to be one of the fundamental anions for living organisms. Phosphate-containing compounds have important roles in cell structure (maintenance of cell membrane integrity and nucleic acids), cellular metabolism, regulation of subcellular processes (cell signaling through protein phosphorylation of key enzymes), maintenance of acid–base homeostasis (urinary buffering), and bone mineralization [112-116]. The primary biological importance of phosphates is as a component of nucleotides, which serve as energy storage within cells (ATP) or when linked together, form the nucleic acids DNA and RNA [113].

In our human body, phosphate is the most abundant anion and comprises upto 1 % of total body weight [113]. It is a predominantly intracellular anion where its concentration is 100-fold higher than that in the plasma. The majority of phosphate is present in skeleton bone (60 to 70%) and teeth (90 %), with the remainder distributed between other tissues (14 %) and extracellular fluid (1 %) [114]. In human body skeleton, phosphate is primarily bound to calcium in the form of HA crystals, the remaining phosphate appears as amorphous calcium phosphate [115]. In soft tissue and cell membranes, phosphorus exists mainly as phosphate esters and to a lesser extent as phosphoproteins and free phosphate ions. In the extracellular fluid, about one-tenth of the phosphorus content is bind to proteins, one-third is compound to sodium, calcium, and magnesium, and the rest is present as inorganic phosphate [117]. Serum phosphate concentration varies with age with the highest concentration being in infants [normal range 4.5–8.3 mg/dL] and concentrations declining towards adult [normal range 2.5–4.5 mg/dL [118].

1.3.2 Phosphate forms in biological systems

Phosphates can be found in different forms: free inorganic phosphate, phosphate conjugates of organic molecules, and inorganic polyP. Inorganic polyP is a structurally very simple polymer, consisting of linear chain of orthophosphate linked by high-energy phosphoanhydride bonds [109, 119]. According to the chain length of polyP, two types of those polymers are distinguished [120, 121]: (i) very long-chain polyPs, ranging from hundreds to thousands of Pi units, existing in microorganisms and (ii) short-chain polyPs that are abundant in mammalians.

1.3.3 Chemistry of polyphosphate or condensed phosphate

The chemistry of polyPs has received considerable attention as a biopolymer used in numerous biomedical and industrial applications [122-126].PolyP is an inorganic polymer arises by polymerization of monomeric phosphate or phosphoric acid derivatives [110]. The process starts with two phosphate units coming together in a condensation reaction and proceeds under release of water; during this process

phosphoanhydride (P-O-P) bonds are formed [127]. This process occurs in the absence of enzymes at high temperature [128] or enzymatically under physiological environments [109, 128]. In contrast to silica formation via polycondensation that results in the formation of three-dimensional networks, the condensation products of phosphate could be adapted to linear or cyclic molecules [122, 124]. Even though the monomers within the polyP polymer are linked via energy-rich phosphoanhydride bonds, the degradation of the polymer *in vitro* at physiological conditions and neutral pH and in absence of catalysts (enzymes) is consider to be slow [123, 128].

Inorganic PolyPs are also termed as condensed phosphates or traditionally as metaphosphates [129, 130, 131]. Condensed phosphates, the general term applied to all pentavalent phosphorus compounds in which various numbers of phosphate groups are connected together by oxygen bridges. They are classified into three types [132-134]: cyclophosphates (metaphosphates), linear polyPs or ultraphosphates (cages, sheets or 3D structures).

Cyclophosphates or metaphosphates have been incorrectly assigned to the whole group of condensed phosphates, i.e. $(MPO_3)_n$, where (M) could be hydrogen or monovalent ions and (n) is number of repeating phosphate units and can be any value [135]. These compounds are built up from cyclic or ring structure. The best known metaphosphates are trimetaphosphate, tetrametaphosphate and hexametaphosphate as shown in **Fig. 1.3.**

Linear polyPs have the general formula $M_{(n+2)}P_nO_{(3n+1)}$[136]. Their anions are composed of chains in which each phosphorus atom is linked to its neighbours through two oxygen atoms, thus forming a linear, unbranched structure which may be represented schematically as shown in **Fig. 1.3.** The degree of polymerization, n, can take values from 2 to 10^6[135].

Ultra-polyPs occur in certain melts at high temperature [128, 137]. Unlike the linear polyPs, contain branching points, i.e. phosphorus atoms which are linked to three rather

than two neighbour phosphorus atoms, are known as cross-linked or branched polyPs. Such polyphosphates have a branched structure, a fragment of which is shown in **Fig. 1.3.** Although branched phosphates have not yet been found in living organisms (perhaps as a consequence of their unusually fast hydrolysis in aqueous environments, irrespective of pH, even at room temperature), it is believed that their presence in biological materials cannot be excluded [118, 121].

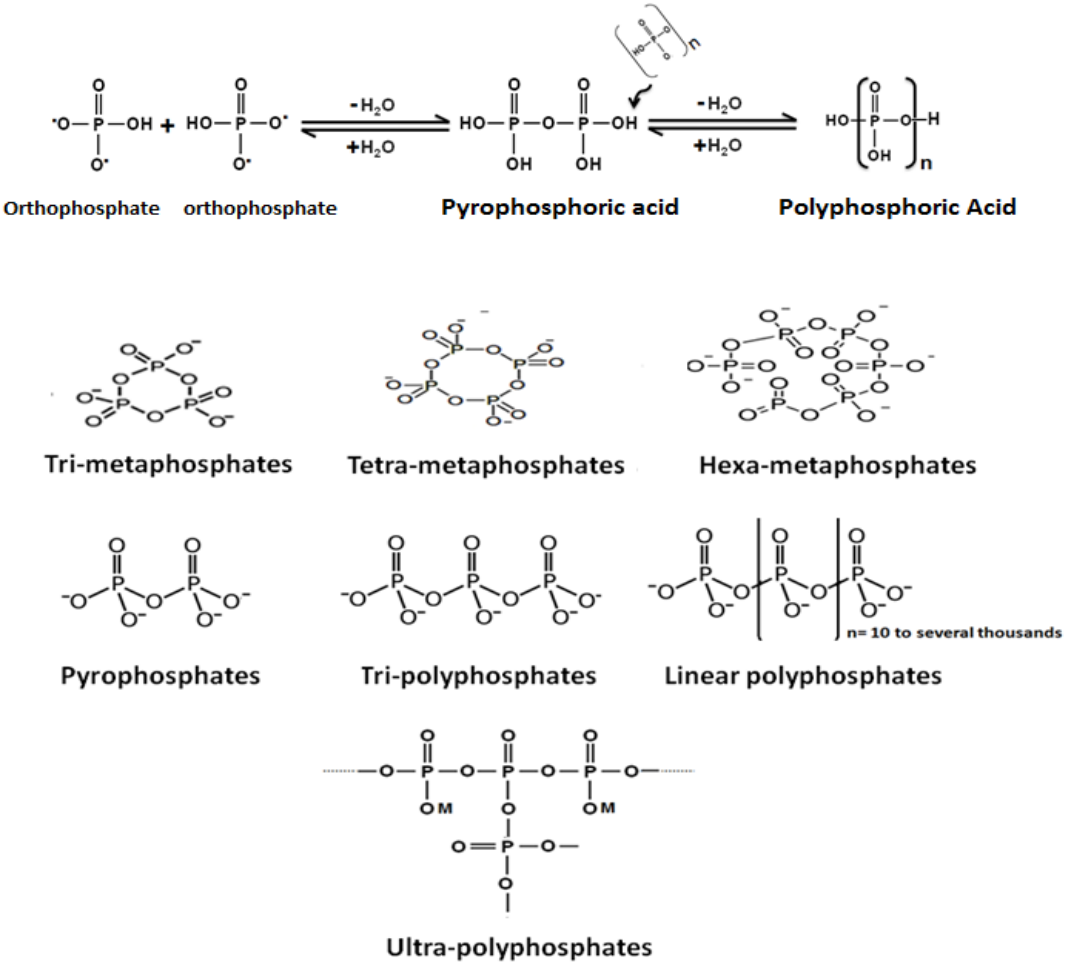

Figure 1.3.
Formation of polyPs by condensation reactions and their current classification. PolyPs or condensed phosphates are divided into three groups: metaphosphates, linear polyP and ultra-polyP.

1.3.4 Biochemical roles of polyphosphate: an old player

PolyP is one of the most ancient and well-conserved molecules and is widespread in all living beings. In fact, polyP is found in all mammalian cells, forming chains of different lengths and performing a broad range of functions [130, 138]. The biological history of polyP is back to 1888, when Liebermann [139] found inorganic polyPs in the nuclei of yeast. After that, Kossel and Ascoli showed that polyPs form a part of plasminic acids and extracted by the partial hydrolysis of yeast nucleic acids [140, 141]. These macromolecules are linear inorganic polymers containing from a few to several hundred residues of orthophosphates [138, 109]. Previously, it was considered either as "*molecular fossil*" or as only a phosphorus and energy source providing the survival of microorganisms under extreme conditions [142-145]. These compounds are now known to have regulatory roles and to occur in representatives of all kingdoms of living organisms, participating in metabolic correction and control on both genetic and enzymatic levels [146, 147]. The biochemical roles of polyPs continue to be discovered; inorganic polyP plays a significant role in increasing cell resistance to unfavorable environmental conditions and in regulating different biochemical processes [130, 148]. The functions of polyPs could be summarized as following [149-152]: reservation of phosphate and energy, sequestration and storage of cations, formation of membrane channels, participation in phosphate transport, involvement in cell envelope formation and function, control of gene activity, and regulation of enzyme activities. As a result, polyP plays an important role in stress response and stationary-phase adaptation [136].

1.3.5 Polyphosphate in animal cells and tissues

PolyP has been most extensively examined in prokaryotes and unicellular eukaryotes, but roles for polyP in mammalians are rapidly emerging [127, 152, 153]. It is particularly abundant in bacteria and yeast, where it is present in the millimolar range as a long polymer material that can reach hundreds of phosphates repeating units in length [123, 154]. By contrast, in mammalian, polyP chains are short and exist in the micromolar range [137]. It has been described in various tissues, cells and other organelles

components. For example, polyP polymer of different chains length are found both extracellularly, in the diverse body fluids (e.g., synovial and blood), and intracellularly in mammalian cells (predominantly in platelets, mononuclear cells, fibroblasts, and osteoblasts) [109, 150, 153]. Within the mammalian cells, polyP is found in nuclei, mitochondria, and also in the plasma membrane [152]. A series of functions have been attributed or proposed to polyPs [130, 138]. Among those is their potential role as molecular chaperone[153], as control molecule of mitochondrial function and membrane depolarization [151], as balancing polymers in the cell energy metabolism [159], as signaling molecule in the brain [159], as control polyanion during blood coagulation [160, 161], as well as during inflammation [162].Recently, other functions has been added to the biochemical roles of polyP in mammalian cells such as, cell growth, angiogenesis, apoptosis, proliferation and differentiation of osteoblast, energy metabolism and tumor metastasis [163-167].

The total amount of cellular polyP is highly dynamic and depends on type of human tissues or cells. For example, in normal osteoblast-like cells, the total concentration of polyP was shown to be around 500 µM (evaluated as orthophosphate residues) [160, 168], while in human blood plasma cells, it is 10-folds lower and in gingival cells, erythrocytes, and peripheral blood mononuclear cells is identified to be between 3 and 6 times lower [161, 166]. On the other hand, in platelets the concentration of polyP is supposed to be within the millimolar range [168]. Generally, in mammalian organelles polyP is estimated to be within the µM range, usually between ten and several hundred µM [156, 160]. Regarding the physiological functions of polyP, it has been previously demonstrated that polyP is known to promote intracellular calcification [169, 170]. In addition to induction of alkaline phosphatase (*ALP*) activity in mouse osteoblastic MC3T3-E1 cells, polyP up-regulates osteoblastic marker genes such as osteopontin and osteocalcin [171]. Therefore, polyP is thought to play an important role in the maturation of bone-related immature cells, which might lead to the formation of bone tissues by osteoblasts [167, 172].

1.3.6 Biological synthesis of inorganic polyphosphate

An understanding of the enzymes involved in the metabolism of polyPs is essential to the determination of their functions and a better comprehension of the pathways modulating their levels. The most studied enzyme involved in the synthesis of inorganic polyPs is polyP kinase 1 [173, 174]. Such studies led first to the source of inorganic pyrophosphate and then to a remark about how the many more phosphoanhydride-linked residues in polyP were assembled [175-177]. The only pathway for the synthesis of polyP that has been established is the polymerization of the terminal phosphate of ATP through the action of polyP kinase in *Escherichia coli* [174]. The gene encoding the kinase is part of an operon in which the gene for exopolyphosphatase is located immediately downstream [109, 154]. Interruption of the operon produces mutants which, for lack of long-chain polyP, are defective in survival in the stationary phase [166, 130]. How the said operon is regulated to balance two counteracting enzymes that are roughly equal in activity has yet to be explained. Although a polyP Kinase activity has been purified from other bacteria [178, 179] and reported in yeast [154], such an enzyme action has yet to be proven in animal systems. While PPK as the device to produce long chains of polyP (ca. 750 residues) has been validated in *E. coli* by genetic studies, mutants lacking this enzyme can still make short poly P chains, about 60 residues long, by an undefined pathway [174].

Several other reasonable mechanisms for the biological synthesis of poly P need to be considered. These are from ADP by reversal of an AMP phosphotransferase [149, 176] and of special interest, by proton motive forces, known to fix Phosphate in inorganic pyrophosphate as well as in ATP [180].

1.3.7 Inorganic polyphosphate biological degradation

However, the phosphoanhydride bond linkage that is characteristic for polyPs is under hydrolytic degradation, the kinetics of polyP hydrolytic degradation are slow at neutral pH and ambient temperatures [123, 128, 148]. This tendency suggests that the bond is an excellent substrate for enzymatic control. The stability of polyP in aqueous solutions

containing living organisms had been observed to be extremely fast due to the enzymatic degradation of polyP [109, 153, 166]. Since then, many polyphosphatase enzymes have been identified to break down polyPs by either transferring an orthophosphate residue to another molecule, cleaving a free orthophosphate residue from the end of the chain (exopolyphosphatase) [181], or hydrolyzing the polyP chain within the middle of the chain, producing shorter polyP chains (endopolyphosphatase) [182] as shown in **Fig.1.4.**

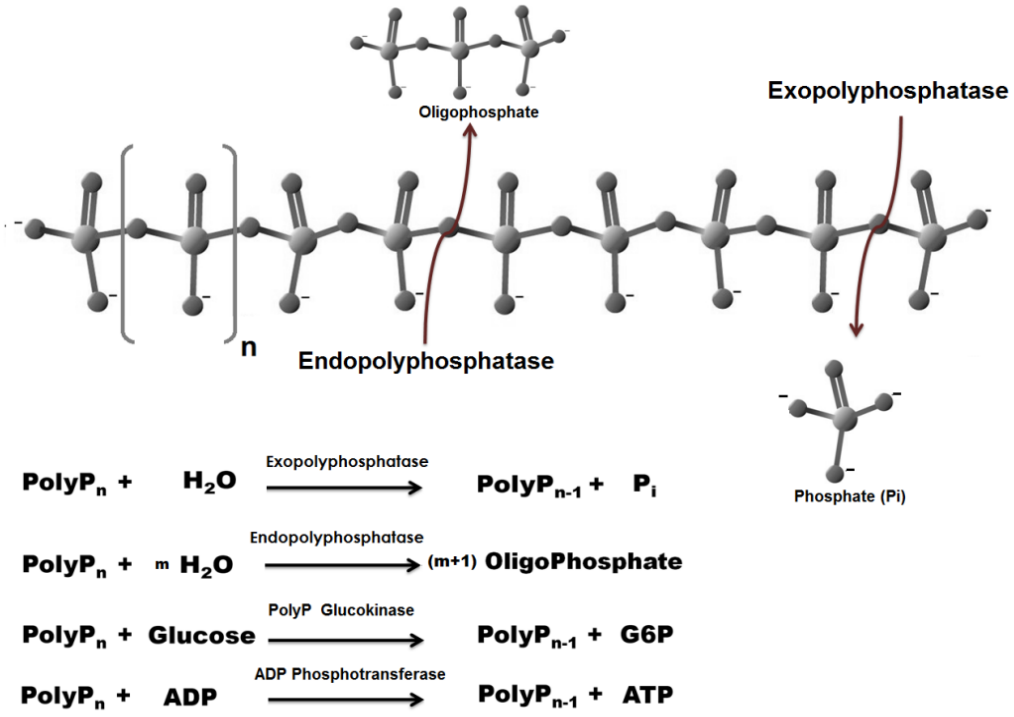

Figure 1.4.
PolyP can be degraded *via*: endopolyphosphatases (which cleave within the polyP chain) and exopolyphosphatases (which sequentially remove terminal phosphates from polyP). There are variety of hydrolases and phosphotransferases known to utilize polyP as a substrate [152].

Exopolyphosphatase is an exophosphatase, which means that it begins at the ends of the polyP chains to release orthophosphate as it moves along the polyP molecule [166, 167,173]. it has several characteristics which distinguish it from other known polyphosphatases, namely that it does not work on ATP, has a strong preference for

long chain polyP and has a very low affinity for polyP molecules with less than 15 phosphate monomers [156, 184]. In general, exopolyphosphatase plays an important role in the metabolism of phosphate and energy in all living organisms [109, 123]. It is of particular important for maintenance of appropriate levels of intracellular polyP, which has been implicated in a numerous cellular activities including response to stressors such as deficiencies in amino acids, orthophosphate, or nitrogen, changes in pH, nutrient downshift, and high salt, and as an inorganic molecular chaperone[153, 176].On the other hand, endopolyphosphatase is an enzyme that catalyzes the interaction between polyP and water molecule, whereas its product is oligophosphate. This enzyme belongs to the family of hydrolases, specifically those acting on acid anhydrides in phosphorus-containing anhydrides.

The first enzyme shown to be involved in mammalian polyP metabolism had been the *ALP*. Mammalian *ALP* is a potent exopolyphosphatase. Among the family of *ALP*, it is the tissue-non-specific alkaline phosphatase (*TN-ALP*) isoenzyme that is highest expressed in liver, kidney, and bone tissues [166, 167]. Initially, it had been proposed that the *ALP* controls the concentration and the homeostasis of P_i, required as one substrate for HA formation [167]. A further human exopolyphosphatase has been described, the DHH super family human protein h-prune, a binding partner of the metastasis suppressor nm23-H1 protein [184]. This enzyme degrades polyPs of all chain lengths. Finally, it is important to mention that polyP is break down not only by exopolyphosphatases but also by endopolyphosphatases as shown by cell culture studies between polyP and bone forming cells osteoblasts [185, 186].

1.4 Booming time for polyphosphate based biomaterials

In the last two decades, there was a dramatic shift from inert to biodegradable (hydrolytically or enzymatically degradable) biomaterials for biomedical and related applications [17, 29, 187]. The current trend shows that in the next years, the applied permanent medical devices and tools will be replaced by biodegradable ones [188, 189]. Thus, the damaged part of the body will heal or regenerate without the need for second

additional operation to remove the tool [29, 189]. The major driving force being the long-term biocompatibility for the permanent implants and technical issues associated with revision surgeries [190].

PolyPs are an important family of inorganic polymers with excellent biocompatibility and biodegradability as well as similar structure to nucleic acids. Some reports that have been published in the recent decade compel us to take a fresh look at the biological role of polyP in animal and human cells. One of the examples of polyP activities in animals is enhancing the proliferation of fibroblasts [191] and stimulating mammalian TOR, a kinase involved in the proliferation of mammary cancer cells [164]. The most impressive results were obtained recently on the role of polyP in bone tissue [186] and blood [160, 161]. Therefore, the applications of polyPs have attracted considerable attention in biomedical fields, including bone tissue engineering, wound healing, bioactive surface coats, controlled drug release and gene delivery.

1.4.1 Calcium polyphosphate as a bone material

As large polyanions, polyPs have a high affinity for calcium and other divalent cations and can produce an amorphous and almost charge-neutral complex [143]. The chemical composition of the Ca-polyP complex is a function of the polyP chain length, but the Ca: P ratio of these complexes is always less than 1.0 [192]. This complex represents a concentrated store of Ca^{2+} and PO_4^{3-} ions, which could be used for bone mineralization process. The theory of polyPs as an intrinsic source for Ca^{2+} and P_i for mineralization is strengthened by the observation that osteoblast cells contain higher amounts of polyP compared to soft tissue cells [186, 193]. However, the biological effect of polyP on bone formation is still a matter of controversy: in some cases exogenous polyP is reported to stimulate bone mineralization [169, 170, 194] while other authors report the inhibition of mineralization [195, 196]. The above conflicts could be attributed to high solubility of sodium polyP and the ability of polyP to react with calcium or other cations which leads to decrease concentration of these ions in the surrounding medium [197, 198]. It is well known that these cations are of great important for different biological process in the

cells. Hence, fine tune the solubility of polyP and composition will be of a great interest for introducing polyP as bone stimulating materials not only as a source for phosphate ions, but also as a morphogenetic active material able to activate different biological process intracellular base on the numerous biochemical roles of polyp [199, 200].

1.4.2 Polyphosphate: from blood coagulation to wound healing

Skin wounds heal spontaneously via auto-regeneration capacity leaving a scar which will become less noticeable with time. However, sever wounds need a stimulus to induce the healing process [201, 202]. Due to wound healing without scar formation has not yet been achieved and since doctors are dealing daily with numerous wounds with different types and levels of severity, novel treatment methods to assist and improve wound healing are needed and many of these treatments use biomaterials as a support matrix for promoting damaged tissue regeneration process [203, 204].

In fact, the wound healing process starts at the damaged place where platelets adhere to the exposed subendothelium of the injured blood vessel and provide a suitable surface for blood clotting, leading to thrombin generation and fibrin formation [205]. The fibrin net stabilizes the initial platelet plug and creates a matrix for the next step of healing process [162]. In this context, inorganic polyP exhibits prohemostatic, prothrombotic, and proinflammatory effects *in vivo* [160, 161]. The importance of polyP in blood clotting suggests that polyP may play an important role in the wound healing [160, 205]. Moreover, a number of studies have been demonstrated the ability of polyP dressings to sequester various proteinases within the wound sites and promote healing of chronic wounds though the inhibition of proteases, in turn maintaining a robust extracellular matrix [206, 207]. In this context, our group has developed PLA fiber mats containing retinol and polyP as morphogenetic active matrices for healing of chronic wounds [208].

1.4.3 Pharmaceutical carriers: subcellular targeting

A drug delivery/carrier system is defined as a formulation or a device that enables the uptake of a therapeutic molecule in the body and improves its efficacy in a safe way by controlling the rate, time, and site of release the drug in the body [209]. The term drug substance also refers to genes or proteins that will increase synthesis of specific active agent in *vivo*. Hence, gene therapy can fit in the basic and broad definition of a drug delivery system [210]. The components of drug delivery system are [210- 212]: (a) drug or active molecule (b) target place and (c) pharmaceutical carrier or vehicle used to multiply the number of drug molecules per single targeting moiety. Various pharmaceutical carriers including liposome, polymer, silica, metal oxide and magnetic nanoparticles, have been used as carriers in drug delivery systems [209].The ability of a pharmacologically active molecule to find the target site is closely linked with its potential as a successful therapeutic drug. It has become increasingly evident that there are several active molecules that exert their action on a specific molecular organelle inside cell [210, 211]. Subcellular or organelle-specific targeting has been emerged as a new direction for drug delivery [212]. In general, the delivery carriers have to be biocompatible and biodegradable. Both properties are fulfiled by inorganic polymer polyP [125, 159,213]. Beside, cells use phosphate or polyP as enzyme substrates, second messengers, membrane structural components and vital energy reservoirs [214].

1.4.4 Surface modifications of bone implants

Metallic alloys are commonly used as orthopedic implants to replenish bone defects, owing to their high fracture toughness and high tensile strength when compared to those of other bone substitute materials such as ceramics or polymeric materials [215]. Stainless steel, titanium and titanium alloys are widely used to manufacture these metallic medical prostheses [216, 217]. They have favorable properties, such as corrosion-resistance, biocompatibility with human body, and mechanical strength in order to function as orthopedic or dental implants. However surface modification is usually required to avoid corrosion, improve bioactivity and increase osteointegration

with host bone tissue [218]. It has been described that polyPs promote bone-forming cell differentiation via increase *ALP* gene expression and modulate biomineralization process [169, 170, 194]. In addition, exogenous polyP has attracted considerable attention as an antimicrobial agent [219, 220]. Thus, polyP seems to be a promising material for surface modification of metal implants.

1.5 References

1. Marks S. C. Jr. & Odgren P. R. (2002). In: Bilezikian J. P., Raisz L. G., Rodan G. A., editors. Principles of Bone Biology. 2nd ed. Academic Press. New York. 3-15.

2. Rho J. Y., Kuhn-Spearing L. & Zioupos P. (1998). Med Eng Phys. 20: 92-102.

3. Martin R. B. (1999). Mater Sci Forum. 293: 5-16.

4. Rho J. Y., Tsui T. Y. & Pharr G. M. (1997). Biomater. 18: 1325-1330.

5. Klein-Nulend J., Bacabac R. G. & Mullender M. G. (2005). Pathol Biol (Paris). 53: 576-580.

6. Cooper D. M., Matyas J. R., Katzenberg M. A. & Hallgrimsson B. (2004). Calcif Tissue Int. 74: 437-447.

7. Weiner S. & Wagner H. D. (1998). Ann Rev Mater Sci. 28: 271-298.

8. Liu Q., Huang S., Matinlinna J. P., Chen Z. & Pan H. (2013). BioMed Research Int. 2013: 929748.

9. Palmer L. C., Newcomb C. J., Kaltz S. R., Spoerke E. D. & Samuel I. (2009). NIH Public Access 108: 4754-4783.

10. Salgado A. J., Coutinho O. P. & Reis R. L. (2004). Macromol Biosci. 4: 743-765.

11. Vallet-Regí M. & Arcos Navarrete D. (2015). Royal Society of Chemistry: Cambridge, UK.

12. Traub W., Arad T. & Weiner S. (1989). Proc Natl Acad Sci USA. 86: 9822-9826.

13. Mann S. (2001). Oxford University Press; Oxford, UK.

14. Rho J. Y., Kuhn-Spearing L. & Zioupos P. (1998). Med Eng Phys. 20: 92-102.

15. Zimmermann E. A., Busse B. & Ritchie R. O. (2015). Bone key Rep. 4: 743.

16. Barrère F., Mahmood T. A., De Groot K. & van Blitterswijk C. A. (2008). Mat Sci Eng R. 59: 38-71.

17. Komatsu D. E. & Warden S. J. (2010). J Cell Biochem. 109: 302-311.

18. Giannoudis P. V., Einhorn T. A. & Marsh D. (2007). Injury 38:S3-6.

19. Aizenberg, J. &Fratzl, P. (2009). Adv Mater. 21: 387-388.

20. Prockop D. J. & Kivirikko K. I. (1995). Annu Rev Biochem. 64: 403-434.

21. Cui F. Z., Li Y. & Ge J. (2007). Mater Sci Eng R Reports. 57: 1-27.

22. Kadler K. E., Holmes D. F., Trotter J. A. & Chapman J. A. (1996). Biochem J. 316: 1-11.

23. Jäger I. & Fratzl P. (2000). Biophys J. 79: 1737-1746.

24. Boskey A. L. (2007). Elements 3: 385-391.

25. Glimcher M. J. (1987). Instr Course Lect. 36: 49-69.

26. Bonjour J. P. (2011). J Am Coll Nutr. 30: 438s-448s.

27. Burton. (2007). John Wiley & Sons, Inc., Biological Anthropology of the Human Skeleton. 443-460.

28. Barralet J., Best S. & Bonfield W. J. (1998). Biomed Mater Res. 41: 79.

29. Dorozhkin S. V. (2010). Biomater. 31: 1465-1485.

30. Mann S., Webb J. & Williams R. J. P. (1989). VCH, Weinheim, Germany.

31. Lees S. (2003). Biophys J. 85: 204-207.

32. Rey C., Combes C., Drouet C. & Glimcher M. J. (2009). Osteoporosis Intern. 20: 1013-1021.

33. Fratzl P., Fratzl-Zelman N. & Klaushofer K. (1993). Biophys J. 64: 260-266.

34. Hodge A.J. & Petruska J.A. (1963). Academic New York 289-300.

35. Glimcher M. J. (2006). Rev Mineral Geochem. 64: 223-282.

36. Eyre D. R. & Ann Weis M. (2013). Calcif Tissue Int. 93: 338-347.

37. Hudson D. M., Kim L. S., Weis M., Cohn D. H. & Eyre D. R. (2012). Biochem. 51: 2417-2424.

38. Amos F. F., Olszta M. J., Khan S. R. & Gower L. B. (2006). In: Königsberger E., Königsberger L., editors. West Sussex, England: John Wiley & Sons, Ltd. 125-217.

39. Olszta J., Douglas E. P. & Gower L. B. (2003). Calcif Tissue Int. 72: 583-591.

40. Schumacher M. A., Mizuno K. & Bächinger H. P. (2006). J Biol Chem. 28: 27566-27574.

41. Borowitzka M. A. (1989). Williams, VCH, Weinheim, Germany 63–94.

42. Perry C. C. (1989). Chemical VCH, Weinheim, Germany 223-256.

43. Deshpande A. S. & Beniash E. (2008). Growth Des. 8: 3084-3090.

44. Lowenstam H. A. & Weiner S. Oxford University Press (1989).

45. Habraken W., Habibovic P., Epple M. & Bohner M. (2016). Mater Today. 19: 69-86

46. Suzuki O. (2010). Acta Biomater. 6: 3379-3387.

47. Suzuki, O. (2013). Jpn Dent Sci Rev. 49: 58-71.

48. Christoffersen J., Christoffersen M. R., Kibalczyc W. & Andersen F. A. (1989). J Cryst Growth. 94: 767-777.

49. Beniash E., Metzler R. A., Lam R. S. & Gilbert P. U. (2009). J Struct Biol. 166: 133-143.

50. Combes C. & Rey C. (2010). Acta Biomater. 6: 3362- 3378.

51. Olszta M. J., Odom D. J., Douglas E. P. & Gower L.B. (2003). Connect Tissue Res. 44: 326-334.

52. Grynpas M. D., Bonar L. C. & Glimcher M. J. (1984). Calcif Tissue Int. 36: 291-301.

53. Urist M. R. (1965). Clin Orthop. 395: 4-10.

54. Ehrlich P. J. & Lanyon L. E. (2002). Osteoporosis Int. 13: 688-700.

55. Matsuo K. & Irie N. (2008). Arch Biochem Biophys. 473: 201-209.

56. Xing L. & Boyce B.F. (2005). Biochem Biophys Res Comm. 328: 709-720.

57. Ducy P., Schinke T. & Karsenty G. (2000). Sci. 289: 1501-1504.

58. Rosenberg N., Rosenberg O., & Soudry M. (2012). Rambam Maimonides Med J. 3: e0013.

59. Aarden E. M., Nijweide P. J. & Burger E. H. (1994). J Cell Biochem. 55: 287-299.

60. Buenzli R. P. & Sims N. A. (2015). Bone. 75: 144 - 150

61. Galli C., Passeri G. & Macaluso G.M. (2010). J Dent Res. 89: 331-343.

62. Negishi-Koga T., Shinohara M., Komatsu N., Bito H., Kodama T., Friedel R. H. &Takayanagi H. (2011). Nature Med. 17: 1473-1480.

63. Long F. (2012). NPG. 13: 27–38.

64. Jimi E., Hirata S., Osawa K., Terashita M., Kitamura C., & Fukushima H. (2012). Int J Dent. 2012. 148261.

65. Gurtner G. C., Callaghan M. J. & Longaker M. T. (2007). Annu Rev Med. 58: 299-312.

66. Sahrmann P., Attin T. & Schmidlin P. R. (2011). Clin Implant Dent Relat Res. 13: 46- 57.

67. Bates P. & Ramachandran M. (2007). The Stanmore Guide. Edited by: Ramachandran M. London: Hodder Arnold. 123- 134.

68. Komatsu D. E & Warden S. J. (2010). J Cell Biochem. 109: 302- 311.

69. Dimitriou R., Tsiridis E. & Giannoudis P. V. (2005). Injury 36: 1392-1404.

70. Henkel J., Woodruff M. A., Epari D. R., Steck R., Glatt V., Dickinson I. C. & Hutmacher D. W. (2013). Bone Res. 1: 216-248.

71. Smith J. O., Aarvold A., Tayton E. R., Dunlop D. G. & Oreffo R.O. (2011). Tissue Eng Part B Rev. 17: 307-320

72. Langer R. & Vacanti J. P. (1993). Science 260: 920- 926.

73. Kolk A., Handschel J., Drescher W., Rothamel D., Kloss F., Blessmann M., Heiland M., Wolff K. D & Smeets R. (2012). J Craniomaxillofac Surg. 40: 706-718.

74. Belthur M. V., Conway J. D., Jindal G., Ranade A. & Herzenberg J. E. (2008). Clin Orthop Relat Res. 466: 2973- 2980.

75. Dinopoulos H., Dimitriou R. & Giannoudis P. V. (2012). Surgeon 10: 230- 239.

76. De Long W. G. Jr., Einhorn T. A., Koval K., McKee M., Smith W., Sanders R. & Watson T. (2007). J Bone Joint Surg Am. 89: 649-658.

77. Giannoudis P. V., Dinopoulos H. & Tsiridis E. (2005). Injury 36: S20-27.

78. Chau, A. M. T., & Mobbs, R. J. (2009). Eur Spine J. 18: 449-464.

79. Banwart J. C., Asher M. A. & Hassanein R. S. (1995). Spine 20: 1055-1060.

80. Younger E. M. & Chapman M. W. (1989). J Orthop Trauma 3: 192-5.

81. Wakitani S., Okabe T., Horibe S., Mitsuoka T., Saito M., Koyama T., Nawata M., Tensho K., Kato H., Uematsu K., Kuroda R., Kurosaka M., Yoshiya S., Hattori K. & Ohgushi H. (2011). J Tissue Eng Regen Med. 5: 146-150

82. Arrington E. D., Smith W. J., Chambers H. G., Bucknell A. L. & Davino N. A. (1996). Clin Orthop. 329: 300-9.

83. Ladd A. L. & Pliam N. B. (1999). J Amer Acad Orthop Surg.7: 279- 290.

84. Hofmann G. O., Kirschner M. H., Wangemann T., Falk C., Mempel W. & Hammer C. (1995). Arch Orthop Trauma Surg. 114: 159-66.

85. Bohner M. (2010). Mater Today. 13: 24-30.

86. Chen, F., & Liu, X. (2016). Prog Polym Sci. 53: 86-168.

87. Shrivats, A. R., Mcdermott M. C. & Hollinger J. O. (2014). Drug Discov Today. 19: 781-786.

88. Gurtner G.C., Werner S., Barrandon Y. & Longaker M.T. (2008). Nature 453: 314-321.

89. Stevens M. M. (2008). Materials Today 11: 18-25.

90. Meyers M. A., Chen P. Y., Lin A-Y. M. & Seki Y. (2008). Prog Mater Sci. 53: 1-206.

91. McMahon R. E, Wang L., Skoracki R. & Mathur A.B. (2013). Biomed Mater Res B Appl Biomater.101: 387–397.

92. Lee S.H. & Shin H. (2007). Adv Drug Deliv Rev. 59: 339-359.

93. Fernandez-yague, M. A., Akogwu, S., Mcnamara, L., Zeugolis, D. I., Pandit, A., & Biggs, M. J. (2015). Adv Drug Deliv Rev. 84: 1-29.

94. Gong T., Xie J., Liao J., Zhang T., Lin S. & Lin Y. (2015). Bone Res. 3: 15029.

95. Sommerdijk N. A. J. M. & Cölfen H. (2011). MRS Bull. 35: 116- 121.

96. Watt F. M. & Huck W. T. S. (2013). Nat Rev Mol Cell Biol. 14: 467-473.

97. Komatsu D. E., Warden S. J. (2010). J Cell Biochem. 109: 302-311.

98. Murphy W. L., McDevitt T. C. & Engler A. J. (2014). Nat Mater. 13: 547-557.

99. Hong S. J., Yu H. S. & Kim H. W. (2009). Macromol Biosci. 9: 639-645.

100. Obrien F. J. (2011). Mater Today. 14: 88-95.

101. Rezwan K., Chen Q. Z., Blaker J. J. & Boccaccini A. R. (2006). Biomater. 27: 3413-3431.

102. Okamoto M. & John B. (2013). Prog Polym Sci. 38: 1487-1503.

103. Wang P., Zhao L., Liu J., Weir M. D., Zhou X. & Xu H. H. K. (2014). Bone Res. 2: 14017.

104. Ramiro-Gutiérrez M. L., Will J., Boccaccini A. R. & Díaz-Cuenca A. (2014). J Biomed Mater Res A. 102: 2982-2992.

105. Smith I. O., Liu X. H., Smith L. A. & Ma P. X. (2009). Wiley Interdiscip Rev Nanomed Nanobiotechnol. 1: 226-236.

106. Tadic D. & Epple M. (2004). Biomater. 25: 987-994.

107. Hollister S. J. (2005). Nat Mater. 4: 518-24.

108. Dutta R. C. & Dutta A. K. (2009). Biotechnol Adv. 27: 334–9.

109. Kornberg A., Rao N. N. & Ault-Riché D. (1999). Ann Rev Biochem. 68: 89-125.

110. Hughes J. M. & Rakovan J. (2002). In Reviews in Mineralogy and Geochemistry, Vol. 48 (Kohn M. J., Rakovan J. &Hughes J. M., Eds.), Mineralogical Society of America: Washington, DC.

111. Piccoli P. M. & Candela P. A. (2002). Rev Mineral Geochem. 48: 255-292.

112. Takeda E., Taketani Y., Sawada N., Sato T. & Yamamoto H. (2004). Biofactors 21: 345-355.

113. Tenenhouse H. S. (2005). Annu Rev Nutr. 25:197-214

114. Farrow E. G. & White K. E. (2010). Nat Rev Nephrol. 6: 207-217.

115. Alizadeh Naderi A. S. & Reilly R. F. (2010). Nat Rev Nephrol. 6: 657-665.

116. Bergwitz C. & Huppner H. (2010). Annu Rev Med. 61: 91-104.

117. Penido M. G. M. G. & Alon U. S. (2012). Pediatric Nephrology (Berlin, Germany) 27: 2039-2048.

118. Noegel A. & Gotschlich E. C. (1983). J Exp Med. 157: 2049.

119. Tammenkoski M., Koivula K., Cusanelli E., Zollo M., Steegborn C., Baykov A. A. & Lahti R. (2008). Biochem. 47: 9707.

120. Clark J. E. & Wood H. G. (1987). Anal Biochem. 161: 280-290.

121. Kulakovskaya T. V., Vagabov V. M. & Kulaev I. S. (2012). Biochem. 47:1-10.

122. Urman K. & Otaigbe J. U. (2007). Polym Sci. 32: 1462-1498.

123. Rao N. N., Gómez-García M. R. & Kornberg A. (2009). Ann Rev Biochem. 78: 605-647.

124. Rashchi F. & Finch J.A. (2000). Miner Eng, 13:1019-1035.

125. Chaubal M. V., Gupta A. S., Lopina S. T. & Bruley D. F. (2003). Crit Rev Ther Drug Carrier Syst. 20: 295–315.

126. E. J. Griffith. (1995). Phosphate Fibers. Plenum Press. New York.

127. Kulaev I. S., Vagabov V. & Kulakovskaya T. (2004). John Wiley JT & Sons. Inc., New York.

128. Graham T. (1834). Ann Phys-Berlin. 108: 33-76.

129. Graham T. (1833). Research Philos Trans R Soc Lond. 123: 253-356

130. Thilo E. (1965). Angew Chem Int Ed Engl. 4: 1061-1071.

131. Kornberg A. (1995). J Bacteriol. 177: 491-496.

132. Clark T. (1827). Edinb J Sci. 7: 298.

133. Cini N. & Ball V. (2014). Adv Colloid Interface Sci. 209: 84-97.

134. Van Wazer J. R. (1950). J Am Chem Soc. 72: 644-647.

135. Mehrotra R. C. (1975). Pure Appl Chem. 44: 201-220.

136. Kumble K. D. & Kornberg A. (1995). J Biol Chem. 270: 5818-5822.

137. Kroll A. V. (1912). Z Anorg Chem. 76: 387-418.

138. Pavlov E., Aschar-Sobbi R., Campanella M., Turner R. J., Gomez-Garcia M. R. & Abramov A.Y. (2010). J Biol Chem. 285: 9420- 9428.

139. Lieberman L. (1888). Ber Chem-Ges. 21: 598- 607.

140. Kossel A. (1893). Arch Anat Physiol. 23: 157-160.

141. Ascoli A. (1899). Z Physiol Chem. 28: 426-431.

142. Clark T. (1827).Edinburgh J Sci. 7: 298.

143. Waehneldt T. V. & Fox S. (1967). Biochim Biophys Acta. 134: 9-16.

144. Yamagata Y., Watanabe H., Saitoh M. & Namba T. (1991). Nature 352: 516-519.

145. Wood H. G., Clark J. E. (1988). Annu Rev Biochem. 57: 235-260.

146. Ault-Riché D., Fraley C. D., Tzeng C. M. & Kornberg A. (1998). J Bacteriol. 180:1841-1847.

147. Saiardi A. (2012). Subcell Biochem. 59: 413-443.

148. Kulaev I., Vagabov V. & Kulakovskaya T. (1999). J Biosci Bioeng. 88: 111-129.

149. Brown M. R. & Kornberg A. (2004) Proc. Natl Acad Sci USA. 101: 16085–16087.

150. Dedkova E. N. & Blatter L. A. (2014). Front Physiol. 5: 260.

151. Seidlmayer L. K., Gomez-Garcia, M. R., Blatter L. A., Pavlov E. & Dedkova E. N. (2012). J Gen Physiol. 139: 321-331.

152. Azevedo C. & Saiardi A. (2014). Biochem Soc Trans. 42:98-102.

153. Gray M. J., Wholey W.-Y., Wagner N. O., Cremers C. M., Mueller-Schickert A., Hock N. T. & Jakob U. (2014). Molecular Cell 53: 689-699.

154. Lichko L., Kulakovskaya T., Pestov N. & Kulaev I. (2006). Biosci Rep. 26: 45-54.

155. Huang G., Ulrich P. N., Storey M., Johnson D., Tischer J., Tovar J. A. & Docampo R. (2014). PLoS Pathogens 10: e1004555.

156. Moreno S. N. J. & Docampo R. (2013). PLoS Pathogens. 9: e1003230.

157. Livermore T. M., Chubb J. R. & Saiardi A. (2016). Proc Natl Acad Sci USA. 113: 996-1001.

158. Lander N., Ulrich P. N. & Docampo R. (2013). J Biol Chem. 288: 34205-34216.

159. Holmstrom K. M., Marina N., Baev A. Y., Wood N. W., Gourine A. V. & Abramov A. Y.(2013). Nat Commun. 4: 1362.

160. Morrissey J. H., Choi S. H. & Smith S. A. (2012). Blood 119: 5972-5979.

161. Smith S. A., Mutch N. J., Baskar D., Rohloff P., Docampo R. & Morrissey J. H. (2006). Proc Natl Acad Sci USA. 103: 903-908.

162. Müller F., Mutch N. J., Schenk W. A., Smith S. A., Esterl L., Spronk H. M., Schmidbauer S., Gahl W. A., Morrissey J. H. & Renné T. (2009). Cell 139: 1143-1156.

163. Shiba T., Nishimura D., Kawazoe Y., Onodera Y., Tsutsumi K., Nakamura R. &Ohshiro M. (2003). J Biol Chem. 278: 26788-26792.

164. Wang L., Fraley C. D., Faridi J., Kornberg A. & Roth R.A. (2003). Proc Natl Acad Sci USA. 100: 11249-11254.

165. Jimenez-Nunez M. D., Moreno-Sanchez D., Hernandez-Ruiz L., Benitez-Rondan A., Ramos-Amaya A., Rodriguez-Bayona B., Medina F., Brieva J. A. & Ruiz F. A. (2012). Haematologica 97: 1264-1271.

166. Lorenz B. & Schröder H. C. (2001). Biochim Biophys Acta. 1547: 254-261.

167. Leyhausen G., Lorenz B., Zhu H., Geurtsen W., Bohnensack R., Müller W. E. G. & Schröder H. C. (1998). J Bone Miner Res. 13:803-812.

168. Moreno-Sanchez D., Hernandez-Ruiz L., Ruiz F. A. & Docampo R. (2012). J Biol Chem. 287: 28435-28444.

169. Hacchou Y., Uematsu T., Ueda O., Usui Y., Uematsu S., Takahashi M., Uchihashi T., Kawazoe Y., Shiba T. & Kurihara S. (2007). J Dent Res. 86: 893-897.

170. Müller W. E. G.,Wang X., Diehl-Seifert B., Kropf K., Schlossmacher U., Lieberwirth I., Glasser G., Wiens M. & Schröder H. C. (2011). Acta Biomater. 7: 2661-2671.

171. Kawazoe Y., Shiba T., Nakamura R., Mizuno A., Tsutsumi K., Uematsu T., Yamaoka M., Shindoh M. & Kohgo T.(2004). J Dent Res. 83:613-618.

172. Tsutsumi K., Saito N., Kawazoe Y., Ooi H. K. & Shiba T. (2014). PLoS One 9: e86834.

173. Wurst H. & Kornberg A. (1994). J Biol Chem. 269: 10996-11001.

174. Ahn K. & Kornberg A. (1990). J Biol Chem. 265: 11734-11739.

175. Szymona M. (1962). Acta Biochim Pol. 9: 165-181.

176. Szymona M. & Ostrowski W. (1964). Biochim Biophys Acta. 85: 283-295.

177. Rashid M. H., Rao N. N. & Kornberg A. (2000). J Bacteriol. 182: 225-227.

178. Fraley C. D., Rashid M. H., Lee S. S., Gottschalk R., Harrison J., Wood P. J., Brown M. R. & Kornberg A. (2007). Proc Natl Acad Sci USA. 104: 3526-3531.

179. Zhang H., Ishige K. & Kornberg A. (2002). Proc Natl Acad Sci USA. 99: 16678-16683.

180. Nocek B., Kochinyan S., Proudfoot M., Brown G., Evdokimova E., Osipiuk J., Edwards A. M., Savchenko A., Joachimiak A. & Yakunin A. F. (2008). Proc Natl Acad Sci USA. 105: 17730-17735.

181. Rashid M. H. & Kornberg A. (2000). Proc Natl Acad Sci USA. 97: 4885-4890.

182. Lonetti A., Szijgyarto Z., Bosh D., Loss O., Azevedo C. & Saiardi A. (2011). J Biol Chem. 286: 31966-31974

183. Kumble K. D. & Kornberg A. (1996). J Biol Chem. 271: 27146-27151.

184. Tammenkoski M., Koivula K., Cusanelli E., Zollo M., Steegborn C., Baykov A. A. & Lahti R. (2008). Biochem. 47: 9707-9713.

185. Lorenz B., Leuck J., Kohl D., Müller W. E. G. & Schröder H. C. (1997). J Acquir Immune Defic Syndr Hum Retrovirol 14:110-8.

186. Schröder H. C., Kurz L., Müller W. E. G. & Lorenz B. (2000). Biochem (Mosc.) 65:296-303.

187. Chaudhury K., Kumar V., Kandasamy J. & RoyChoudhury S. (2014). Int J Nanomed. 9: 4153-4167.

188. Nelson T. J., Behfar A. & Terzic A. (2008). Clin Transl Sci. 1: 168-171.

189. Mason C. & Dunnill P. (2008). Regen Med. 3: 1-5.

190. Dvir T., Timko B. P., Kohane D. S. & Langer R. (2011). Nat Nanotechnol. 6: 13-22.

191. Kawazoe Y., Katoh S., Onodera Y., Kohgo T., Shindoh M. & Shiba T. (2008). Int J Biol Sci. 4: 37-47.

192. Landis W. J. & Glimcher M. J. (1978). J Ultrastruct Mol Struct Res. 63:188-223.

193. Ariganello M. B., Omelon S., Variola F., Wazen R. M., Moffatt P. & Nanci A. (2014). J. Cell Biochem. 115: 2089-2102.

194. Usui Y., Uematsu T., Uchihashi T., Takahashi M., Takahashi M., Ishizuka M., Doto R., Tanaka H., Komazaki Y., Osawa M., Yamada K., Yamaoka M. & Furusawa K. (2010). J Dent Res. 89: 504-509.

195. Hoac B., Kiffer-Moreira T., Millán J. L. & McKee M. D. (2013). Bone 53:478-486.

196. Schibler D. & Fleisch H. (1966). Cell Mol Life Sci. 22:367-369.

197. Omelon S., Georgiou J., Henneman Z. J., Wise L. M., Sukhu B., Hunt T., Wynnyckyj C., Holmyard D., Bielecki R. & Grynpas M. D. (2009). PLoS ONE 4: e5634.

198. Ding Y. L., Chen, Y. W., Qin Y. J., Shi, G. Q. Yu X. X. & Wan C. X. (2008). J Mater Sci Mater Med. 19: 1291-1295.

199. Wang X. H., Schröder H. C., Schlossmacher U., Neufurth M., Feng Q, Diehl-Seifert B. & Müller W.E.G. (2014). Calcif Tissue Int. 94: 495-509.

200. Schröder H. C., Wang X. H., Wiens M., Diehl-Seifert B., Kropf K., Schloßmacher U. & Müller W.E.G. (2012). J Cell Biochem. 113: 3197-3206.

201. Guo S. & Dipietro L. A. (2010). J Dent Res. 89: 219-229.

202. Shaw T. J. & Martin P. (2009). J Cell Sci. 122: 3209-3213.

203. Abrigo M., McArthur S. L. & Kingshott P. (2014). Macromol Biosci. 14: 772-792

204. Nurden A. T., Nurden P., Sanchez M., Andia I. & Anitua E. (2008). Front Biosci. 13: 3532-3548

205. Cullen B., Smith R., Mcculloch E., Silcock D. & Morrison L. (2002). Wound Repair Regen. 10:16-25.

206. Ravanti L. & Kahari V. (2000). Int J mol med. 6: 391-407.

207. Edwards J. V. & Howley P. S. (2007). J Biomed Mater Res A. 83:446-54.

208. Müller W. E. G., Tolba E., Schröder H. C., Diehl-Seifert B. & Wang X. H. (2015). Biochem Biophys Rep. 3: 150-160.

209. Tiwari G., Tiwari R., Sriwastawa B., Bhati L., Pandey S., Pandey P. & Bannerjee S. K. (2012). Int. J Pharm Investig. 2: 2-11.

210. Park K. (2014). J Control Release. 190: 3-8.

211. Mossalam M., Dixon A. S. & Lim C. S. (2010). Ther Deliv. 1: 169-193.

212. Gullotti, E. & Yeo, Y. (2009). Mol Pharm. 6: 1041-1051.

213. Galmarini C. M., Warren G., Kohli E., Zeman A., Mitin A. & Vinogradov S. V. (2008). Mol Cancer Ther. 7: 3373-3380.

214. Müller W. E. G., Tolba E., Schröder H. C., Diehl-Seifert B. & Wang X. H. (2015). Eur J Pharm Biopharm. 93: 214-223.

215. Oshida Y., Tuna E. B., Aktören O. & Gençay K. (2010). Int J Mol Sci. 11: 1580-1678.

216. Förster Y., Rentsch C., Schneiders W., Bernhardt R., Simon J. C., Worch H. & Rammelt S. (2012). Biomatter. 2: 149-157.

217. Zhang B. G. X., Myers D. E., Wallace G. G., Brandt M. & Choong, P. F. M. (2014). Int. J Mol Sci. 15:11878-11921.

218. Lewallen E. A., Riester S. M., Bonin C. A., Kremers H. M., Dudakovic A., Kakar S., Cohen R. C., Westendorf J. J., Lewallen D. G. & van Wijnen A. J. (2015). Tissue Eng B Rev. 21: 218-230.

219. Moon J-H., Park J-H. & Lee J-Y. (2011). Antimicrob Agents Chemother. 55: 806–812.

220. Lee R. M., Hartman P. A., Stahr H. M., Olson D. G. & Williams F. D. (1994). J Food Prot. 57: 289-294.

Chapter 2:

Structure and properties of calcium polyphosphate material with morphogenetic activity

2.1 Introduction

Advances in bone tissue engineering approach demand design and development of multifunctional biomaterials that will not only replace bone tissue but also induce regeneration of damaged tissue [1-5]. For tissue regeneration, the initial interaction between tissue-forming cells and biomaterials is the core task in the regulation and formation of new tissue [4]. The regeneration process is highly dependent on the acceptance of the materials by the surrounding tissues and their ability to promote specific cellular responses as well as on the biomechanical properties and biodegradation rate of the used materials. There is, therefore, a great need for developing new biomaterials for bone tissue regeneration that are designed to be: *osteoconductive* (i.e., serve as a framework upon which bone cells spread and generate new bone tissue), *osteoinductive and osteogenesis* (i.e., promote the proliferation and differentiation of osteoblasts cells or bone marrow mesenchymal stem cells) as well as able to integrate with surrounding tissues (*osteointegration*) [3, 6].

Because of its excellent biocompatibility, biological activity, and strong affinity to divalent cations, polyphosphate (polyP), a phosphate inorganic polymer found in various subcellular compartment of mammalian cells, i.e. nuclei, mitochondria, lysosomes and plasma membranes. PolyP has been introduced with tissue engineering to enhance bone regeneration as an intrinsic source for phosphate for mineralization is strengthened by the observation that osteoblast cells contain higher amounts of polyP compared to soft tissue cells [7-12]. It has been also described that polyP has an inductive effect on osteoblasts, mainly as an anabolic polymer that stimulates differentiation of bone cells and mineralization [13-15]. Interesting, polyP induces the enzyme alkaline phosphatase [*ALP*] [16, 17], an enzyme that degrades polyP [18]. These findings suggest that polyP can be expected to promote and control bone regeneration.

However, the biological effect of polyP on bone formation is still a matter of controversy: in some cases exogenous polyP is reported to stimulate bone mineralization, while other authors report the inhibition of mineralization [19].

The above conflicts could be attributed to high solubility of sodium polyP and the ability of polyP to react with calcium or other cations which leads to decrease concentration of these ions in the surrounding medium. Thus, fine tune the solubility of polyP and composition will be of a great interest for introducing polyP as a bone stimulating material not only as a source for phosphate ions, but also as a morphogenetic active material able to activate different biological process intracellular base on the numerous biochemical roles of polyP. The chemical structure of polyP is very simple and consists of linearly arranged orthophosphate units, linked by high-energy phosphoanhydride bonds. As large negatively charged macromolecules, polyPs have a great affinity for calcium and other divalent cations and can produce an amorphous and charge-neutral Ca-polyP complex [9, 13]. The chemical composition of the Ca-polyP complex is a function of the polyP chain length, but the Ca: P molar ratio of these complexes is always less than 1.0 [13, 20].

This chapter describes the synthesis of Ca-polyP nanoparticles via a simple chemical precipitation method and influence of calcium ion concentration on the chemical as well as physical properties of polyP were evaluated using X-ray Diffractometry (XRD), Fourier Transform Infrared Spectroscopy (FTIR), Scanning Electron Microscope (SEM) with Energy Dispersive X-ray (EDX) and Transmission Electron Microscopy (TEM). Moreover, the proliferation, osteogenic differentiation and deposition of a mineralized extracellular matrix of the sarcoma osteogenic (SaOS-2) cell line (osteoblast-like cells) following exposure to Ca-polyP nanoparticles were also investigated.

2.2 Material and methods

2.2.1 Preparation of calcium polyphosphate nanoparticles

Unless otherwise stated, all chemicals were analytical grade reagents and used without further purification. Calcium polyphosphate (Ca-polyP) nanoparticles were synthesized by a wet chemical precipitation method from calcium chloride dihydrate ($CaCl_2 \cdot 2H_2O$; Sigma-Aldrich, Taufkirchen; Germany) as Ca^{2+}source, and sodium polyphosphate(Na-polyP) with an average chain length of approximately 40 phosphate units (Chemische Fabrik Budenheim; Germany) was used as polyP source.

According to our preliminary study, the Ca-polyP particles were prepared by slow addition, at room temperature, of a fixed volume of sodium polyP solution (4 mol L^{-1}) to different volume of calcium chloride stock solution (4 mol L^{-1}) in order to maintain the same amount of polyP in the mixture and clarify the influence of calcium ions concentration on structure and morphology of polyP. The obtained Ca-polyP particles contain under different calcium/phosphate molar ratio 1:1 and 2:1 were named as “Ca-polyP1” and “Ca-polyP2”, respectively. The experimental procedure is shown in the schematic drawing **Fig. 2.1**. In the first step, the pH of the Na-polyP and calcium chloride solutions was adjusted at 10 by 0.2 M sodium hydroxide (NaOH) solution and left under stirring for 1 h. Then, polyP solution was added drop-wise to the calcium solution at room temperature. The pH of the mixed solution/suspension was increased to 10 and maintained at this value by adding the required amounts of 1 M NaOH solution. The reaction was performed at room temperature for 24 h under constant stirring conditions. The precipitated slurries were poured out from the reactor and the solid particles were separated by vacuum filtration through a Nalgene Filter Units (pore size 0.45 µm; Cole-Parmer, Kehl/Rhein; Germany) and washed three times with ethanol to remove the non-bound Ca^{2+} and the other by products. The obtained gel was re-dispersed in 100ml of ethanol to prevent agglomeration and dried at 60 °C overnight. Finally, the dried cakes were ground to fine powders, sieved through a 100 µm mesh, and used for characterization studies.

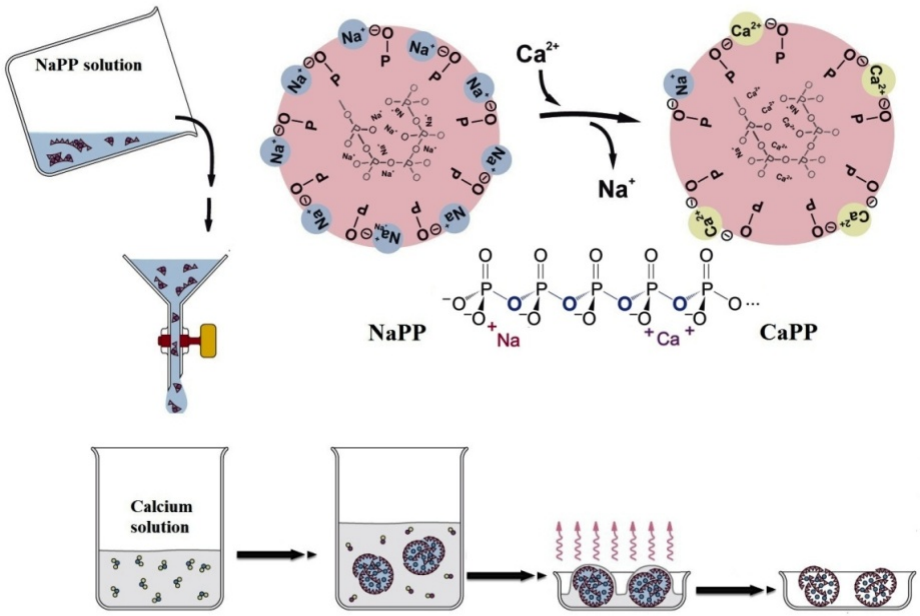

Figure 2.1.
Scheme represents preparation process of Ca-polyP nanospheres via wet chemical precipitation method.

2.3 Material characterization

2.3.1 X-ray diffraction analyses

The patterns of obtained Ca-polyP powders were registered on a Philips PW 1820 diffractometer with $Cu_{K\alpha}$ radiation (λ = 1.5418 Å, 40 kV, 30 mA) in the range 2θ = 5–65° (Δ2θ = 0.02, Δt = 5 s).

2.3.2 Fourier transformed infrared spectroscopy

Fourier transformed infrared spectroscopic (FTIR) analyses were performed with micro-milled (agate mortar and pestle) mineral powder in an ATR (attenuated total reflectance)-FTIR spectroscope/Varian 660-IR spectrometer (Agilent, Santa Clara; CA), fitted with a Golden Gate ATR unit (Specac, Orpington; UK). The spectra given represent the average of 100 scans with a spectral resolution of 4 cm^{-1}(typically 550-4000 cm^{-1}). The baseline correction, smoothing, and analysis of the spectra were achieved with the Varian 660-IR software package 5.2.0 (Agilent). Graphical display and annotation of the spectra were performed with Origin Pro (version 8.5.1; OriginLab, Northampton, MA).

2.3.3 Microscopic analyses

Scanning electron microscopic (SEM) analyses were performed with an SU 8000 instrument (Hitachi High-Technologies Europe, Krefeld, Germany), at low voltage (1 kV) and Transmission electron microscopic (TEM) analyses the TemCam-F416 (4 × 4 K) CCD camera (TVIPS, Gauting; Germany), operated on a Tecnai 12 transmission electron microscope (FEI, Eindhoven; The Netherlands) at an accelerating voltage of 120 kV, was used. The equipment was connected with a particle size analyzer (ImageJ); 25–50 crystals/spheres were evaluated.

2.3.4 Elemental analyses

Energy dispersive X-ray (EDX) spectroscopy was also performed with an EDAX Genesis EDX System attached to a scanning electron microscope (Nova 600 Nanolab; FEI, Eindhoven, the Netherlands) operating at 10 kV with a collection time of 30–45 s. Areas of approximately 10 μm^2 were analyzed.

2.3.5 Cultivation of SaOS-2 cells

SaOS-2 cells (human osteogenic sarcoma cells), were cultured in McCoy's medium (Biochrom-Seromed, Berlin; Germany), supplemented with 2 mM L-glutamine, 10% heat-inactivated fetal calf serum (FCS) and 100 units/ml penicillin/100 µg/ml streptomycin [21]. The cells were incubated in 25 cm^2 flasks or in six-well plates (surface area 9.46 cm^2; Orange Scientifique, Brainel, Alleud, Belgium) in a humidified incubator at 37°C. The cultures were started with $1x10^4$cells/well in a total volume of 3 ml. After an initial incubation period of 3 d the cultures were continued to be incubated for 5 d in the absence or presence of the mineralization activation cocktail (MAC), composed of 5 mM β-glycerophosphate, 50 mM ascorbic acid and 10 nM dexamethasone to induce biomineralization [21, 22].

2.3.6 Cell growth assay

SaOS-2 cells were seeded into the 24-well plates at a density of 1×10^4 cells per well and cultured for 3 d in McCoy's medium/15% FCS. The Ca-polyP samples were added to the

cultures at concentrations 0, 100, 200 and 300 µg/mL. After a 3 d incubation period, the cells were incubated with fresh medium containing 200 µL of 3-[4,5-dimethyl thiazole-2-yl]-2,5-diphenyl tetrazolium (MTT; Sigma M2128) for 4 h in the dark. Then the remaining MTT dye was aspirated and 200 µL of DMSO were added to solubilize the formazan crystals. Finally, the optical density (OD) was determined at 570 nm using an ELISA reader/spectrophotometer [23]. Ten parallel experiments each were performed.

2.3.7 Mineralization by SaOS-2 cells in-vitro

For the assessment of mineral deposited by SaOS-2 cells, the Alizarin red staining (ARS) procedure was applied. The SaOS-2 cells were cultured in 12 well culture plates. After an initial incubation period of 3 days in the absence of the MAC, the cultures were transferred into medium/FBS supplemented with MAC and then incubated for additional 5 days. Subsequently, the cells were fixed with 4% PFA and 500 µL of 1% Alizarin red staining solution for 20 min. After washing and complete removal of excess stain, the intensity of red stain was quantitatively assessed by dissolving calcium-bound AR-S complex in 10% hexadecylpyridinium chloride monohydrate (HDPC; Fluka) prepared in sodium phosphate buffer (10 mM, pH 7.0) for 1 h. The absorbance was measured at 562 nm [24].

2.3.8 Quantitative real-time polymerase chain reaction: *ALP* expression

The SaOS-2 cells were pre-cultivated for 3 d in medium/serum. Then the cultures were split and incubated without any polyP particles (control) or with50 µg/mL of Na-polyP or Ca-polyP and the cultivation were continued for an additional 7 d in the absence or presence of MAC. Subsequently, the cells were harvested, RNA extracted and subjected for quantitative real-time RT [reverse transcription]-polymerase chain reaction (qRT-PCR) as described [25, 26].

2.3.9 Response of SaOS-2 cells and translocation of the *ALP* after incubation with Ca-polyP nanoparticles

The SaOS-2 cells were incubated as described above. At first, the cells were incubated for a period of 3 days in the absence of the MAC, the MAC was then added and the cells were incubated for a further 4 days in the absence or presence of 30 µg/ml a Ca-polyP nanoparticles. Subsequently, the cells were harvested, sliced and analyzed by using TEM**.** The methods and techniques applied for TEM had been recently published [27]. The cells were fixed in paraformaldehyde and glutaraldehyde, embedded in agarose and then in LR-White resin (62661 Sigma). After polymerization, ultrathin sections (80 nm) were cut (Microsystems, Wetzlar; Germany). Moreover, for immunogold labeling in TEM analyses, the cells were incubated with a monoclonal IgG antibody against human alkaline phosphatase (produced in mouse, no. A2064, Sigma-Aldrich) and then with a secondary anti-mouse antibody coupled to 10-nm gold particles (1:50 diluted with water, Sigma-Aldrich). The samples were enhanced with silver [28], and contrasted with uranyl acetate and lead citrate. The slices were inspected with a TemCam-F416 (4K×4K) CCD camera (TVIPS, Gauting, Germany) operated on a Tecnai 12 transmission electron microscope (FEI, Eindhoven, The Netherlands) at an accelerating voltage of 120 kV. In the controls, the antibodies were omitted during the procedure.

2.3.10 Statistical analysis

The results were statistically evaluated using paired Student's t-test [29].

2.4 Results

2.4.1 Chemical and phase characterization of Ca-polyP particles

The chemical functional groups for Na-polyP and Ca-polyP nanoparticles were investigated using FTIR spectroscopy. The complete spectra between 4000 and 600 cm^{-1} are shown in **Fig. 2.2A**, while segments between 1400 and 600 cm^{-1} are given in **Fig. 2.2B**. In general, the spectra of obtained particles have two main sets of IR absorption bands in the low and high frequency regions due to phosphate group and OH molecule. On the basis of literature data available [30-33], the bands were attributed to the vibrations of the following structural units:

(i) The peaks at ~ 3400 and 1627 cm^{-1} are mainly assigned to the OH stretching and bending vibrations of absorbed water, respectively.

(ii) The band near 1250 cm^{-1} designate to the asymmetric stretching of the doubly bonded oxygen vibration, i.e. $\nu_{as}(PO_2)^-$.

(iii) The weak band at 1190 cm^{-1} is the PO_2 symmetric stretching mode $\nu_s(PO_2)^-$ [30].

(iv) The absorption bands close to 1083 and 999 cm^{-1} are assigned to the asymmetric and symmetric stretching modes of chain-terminating (PO_3) groups $\nu_{as}(PO_3)^{2-}$ and $\nu_s(PO_3)^{2-}$ [32].

(v) The absorption band near 864 cm^{-1} is assigned to the asymmetric stretching modes of the P–O–P linkages, ν_{as}(P–O–P) and the partially split band centered around 763 cm^{-1} is assigned to the symmetric stretching modes of these linkages, ν_s(P–O–P).

The comparison of the spectra of Na-polyP and Ca-polyP indicate that the polyP features are seen in the 1300-600 cm^{-1} region. For all three samples this pattern is observed, reflecting that the polyP chain backbones are not broken down during the reaction with the Ca^{2+} ions. However, these peaks shifted in the Ca-polyP1 and Ca-polyP2 samples if compared the Na-polyP spectrum. These changes in phosphate structures appear because of calcium ions, which generally provide ionic cross-linking

between non-bridging oxygen of phosphate groups. In conclusion, the modification in polyP structures can be understood further because of change in terminal charge density at the anionic site, i.e. formation of P-O-M (where M is Ca^{2+}). Hence, the IR spectra confirm the interaction between Ca^{2+} and polyP and the formation of Ca-polyP.

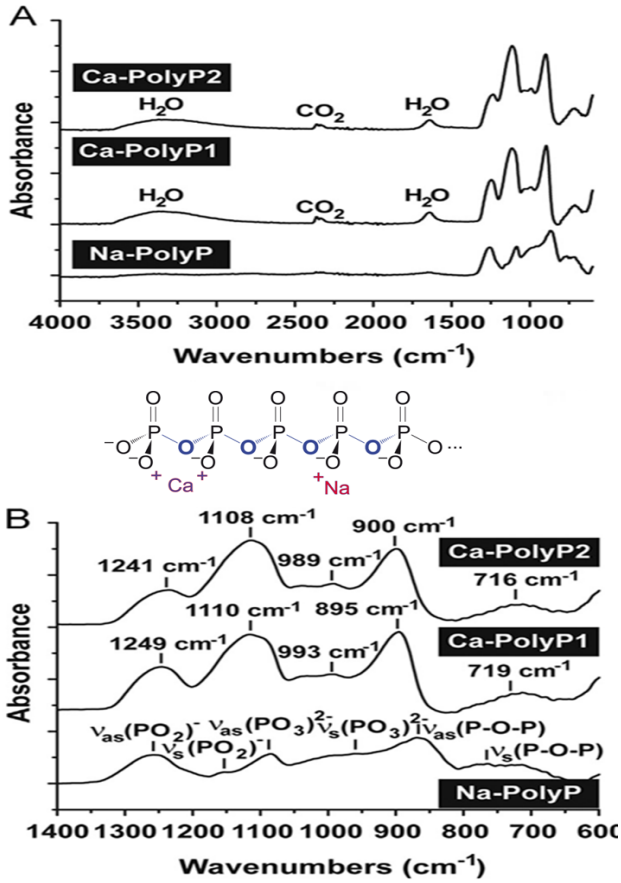

Figure 2.2.
FTIR spectra of Na-polyP, Ca-polyP1 and Ca-polyP2; (**A**) Wavenumber 4000–600 $cm^{-1}$and (**B**) Wavenumber 1400–600 cm^{-1}.

Fig.2.3 shows the XRD patterns of Na-polyP, Ca-polyP1 and Ca-polyP2 powder samples. These samples have been obtained after drying at 60°C for 24 h. The absence of any sharp peak confirms the non-existence of crystalline phase and reveals the amorphous nature of the synthesized materials [34]. The XRD patterns for Na-polyP, Ca-polyP1 and Ca-polyP2, shown in **Fig. 2.3**, indicate a clear amorphous phase, with a broad peak from 20° to 40° for Na-polyP and centered around 30° for Ca-polyP1 and 2.

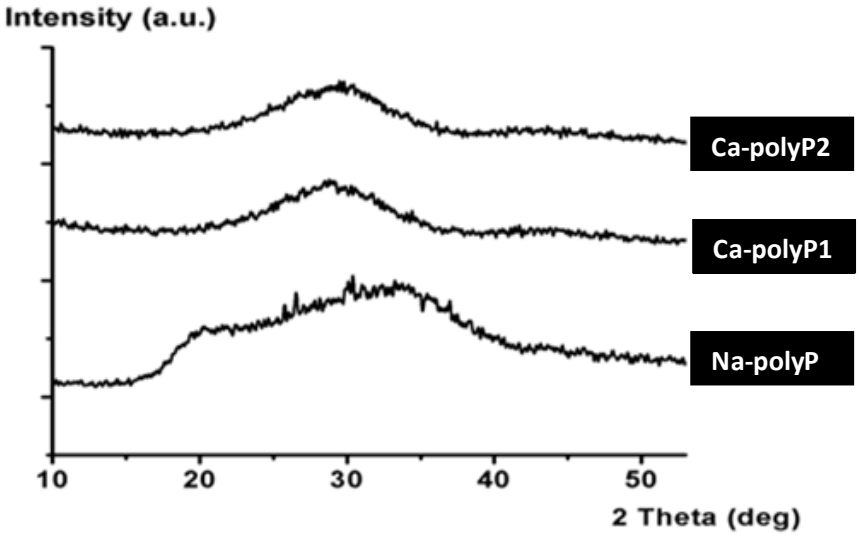

Figure 2.3.
X-ray diffraction patterns for Na-polyP, Ca-polyP1 and Ca-polyP2.

2.4.2 Morphological observations and elemental analyses

SEM and TEM studies have been made for micro- and nano-structural analysis. **Fig. 2.4** shows the SEM morphology of Na-polyP and Ca-polyP1 samples. The Na-polyP particles, of a non-regular shapes, often show a tapered morphology (**Fig. 2.4 A**, **B**). The sizes of the particles vary between 1 and 100 µm. Likewise, non-regular shapes show the Ca-polyP1 particles (**Fig. 2.4 C, D**). They are smaller than the Na-polyP particles with an average diameter of ≈4 µm. On the other hand, **Fig. 2.5** represents the SEM and TEM micrograph of Ca-polyP2 particles at two different magnifications. The particles morphology was completely different from the Na-polyP and Ca-polyP1. It appears that nanosize spherical particles are formed. Ca-polyP2 particles exhibit spherical particles of nano-size from 200 to 500nm. The Ca-polyP nanoparticles formed were highly agglomerated as indicated from SEM and TEM micrographs.

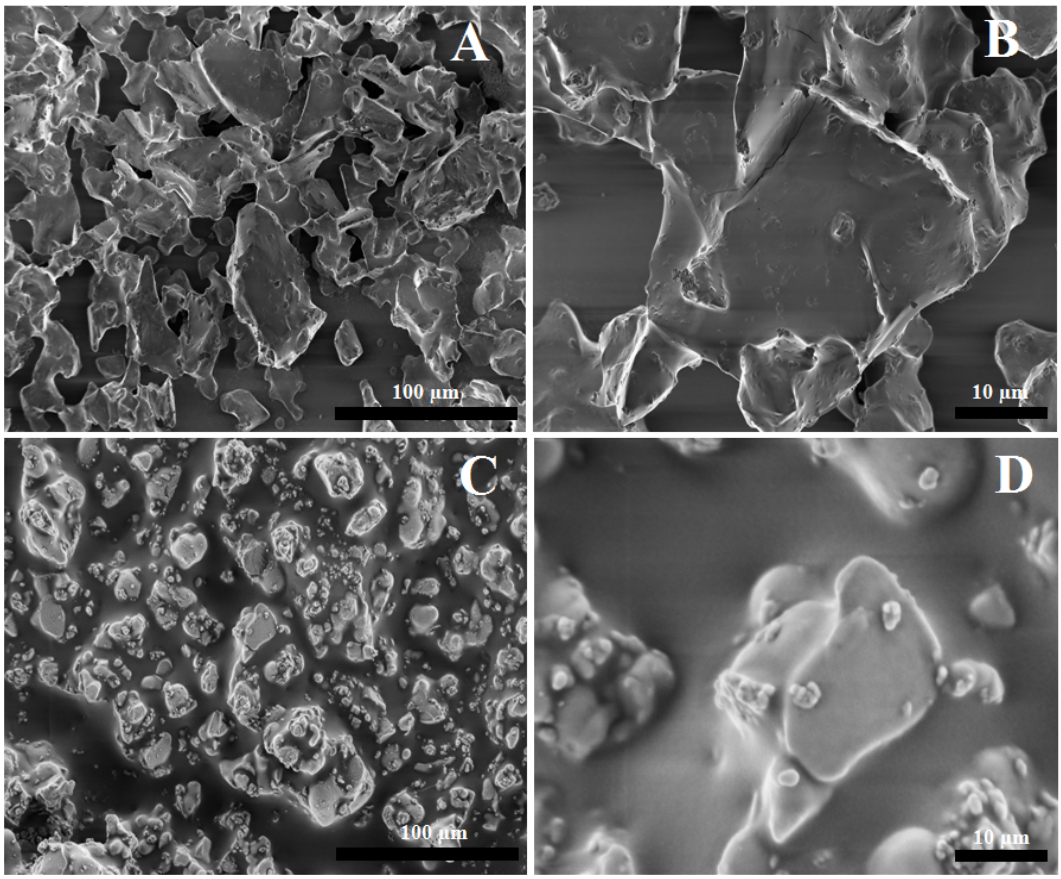

Figure 2.4.

SEM images of Na-polyP and Ca-polyP powders. (**A, B**) Na-polyP and (**C**, **D**) Ca-polyP1.

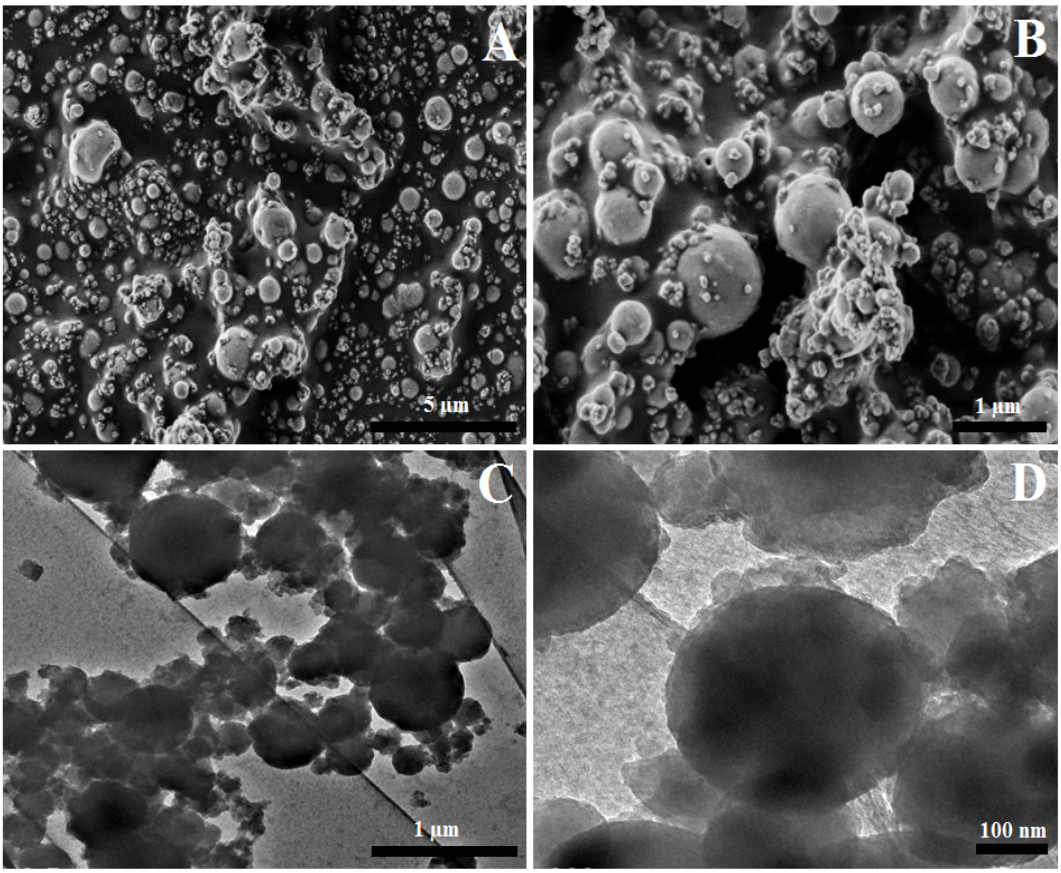

Figure 2.5.
SEM and TEM micrographs for Ca-PolyP nanospheres particle sample named Ca-polyP2.

The elemental analysis for Na-polyP, Ca-polyP1 and Ca-polyP2 samples was performed by Energy dispersive X-ray (EDX) spectroscopy and given in **Fig. 2.6.** The obtained EDX spectra represent the elemental contents of Na, Ca, P, O and C in all powder. The atomic weight ratio between Na: P for Na-polyP was 1.08± 0.07. On the other hand, the ratio between Ca: P for Ca-polyP1 was 0.60± 0.05 and increased to 0.84± 0.09 for Ca-polyP2. However, The EDX spectra of Ca-polyP particles indicate formation of Ca-polyP phase with different Ca/P ratio. There was a small peak for sodium reflecting the residual Na^+ that originates from the raw Na-polyP material, used for the conversion to the insoluble Ca-polyP.

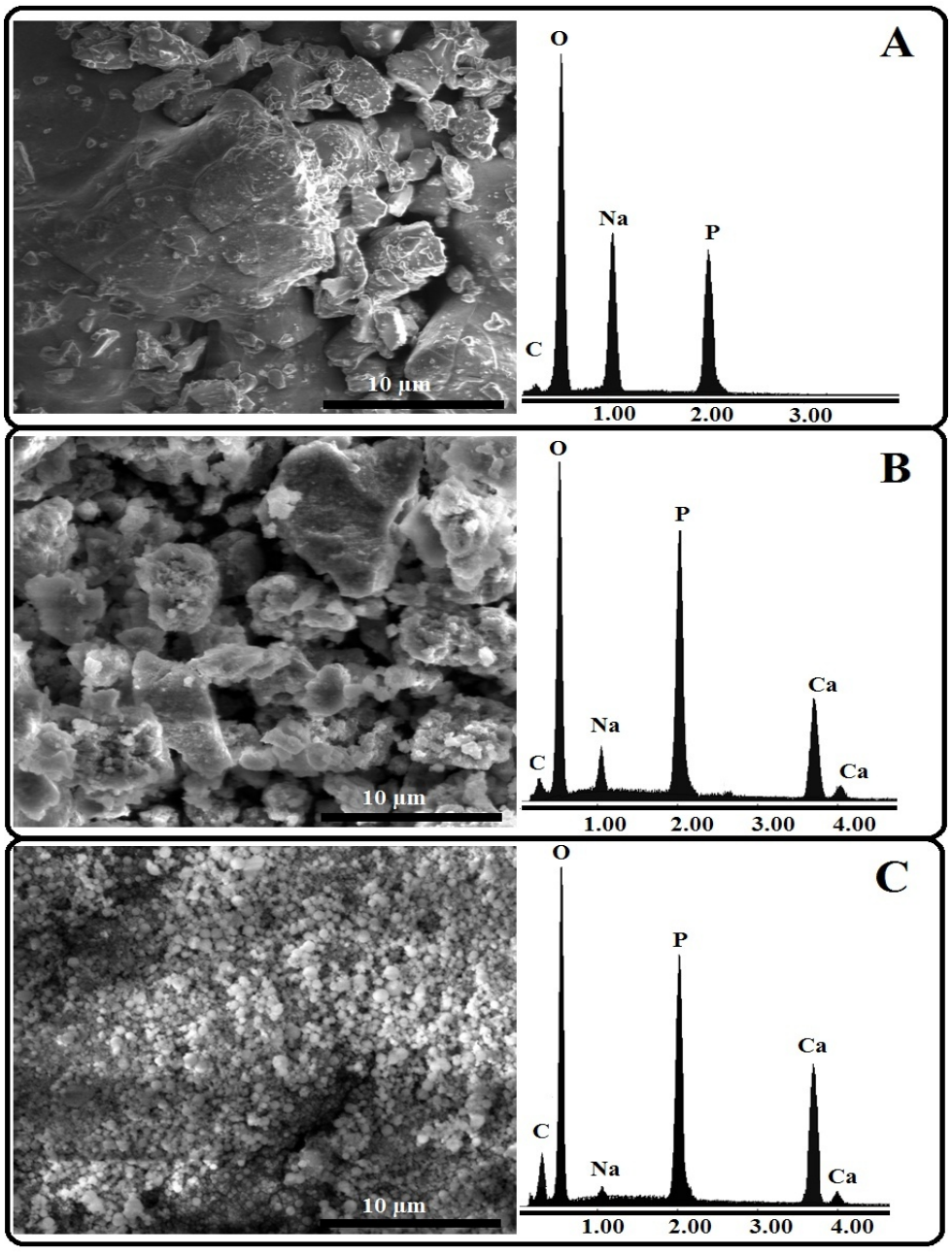

Figure 2.6.

SEM micrographs and Energy dispersive X-ray (EDX) spectra for (**A**) Na-polyP, (**B**)Ca-polyP1 and (**C**)Ca-polyP2.

2.4.3 SaOS-2 cell growth

The cell viability of SaOS-2 cells was tested by applying the MTT assay for Na-polyP, Ca-polyP1 and Ca-polyP2 particles (**Fig. 2.7**). The results revealed that the absorbance value for cells in absence of particles (zero conc.) was 0.65± 0.12 after an incubation period of SaOS-2 cells for 3 d. However, a significant and strong increase in cell number is seen in the assays with 10 µg/mL Na-polyP (0.93± 0.18), a decrease in the absorbance values to 0.7± 0.20 and 0.53± 0.21 are measured in assays with 100 µg/mL and 200 µg/mL of Na-polyP, respectively. On other hand, an increase in the absorbance values is measured for Ca-polyP1 and Ca-polyP2 particles. For instance, a stimulatory response was seen for 100 µg/mL Ca-polyP1 (1± 0.17), as well as of 100 µg/mL Ca-polyP2 (0.82± 0.13), if compared to the values determined for cultures incubated with 100 µg/mL Na-polyP (0.7± 0.20). At all the Ca-polyP concentrations, cell viability was almost equal or above the control value. Finally, a significant difference was observed among the different samples, suggesting that the low concentration of polyP in the medium and Ca-polyP did not affect the cell growth.

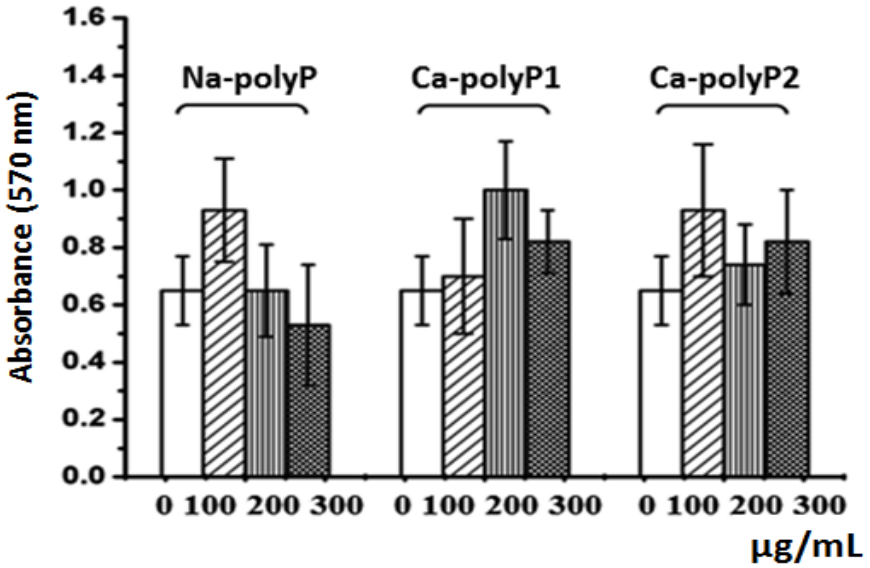

Figure 2.7.
Cell growth for SaOS-2 cells. The cells were cultured at different conc. 0 100, 200 and 300 µg/mL for Na-polyP, Ca-polyP1 and Ca-polyP2 samples. After terminating the cultivation at 3 day, the assays were subjected to the MTT assay and the absorbance at 570 nm was determined.

2.4.4 Mineralization in SaOS-2 cells

The influence of prepared ca-polyP particles on the extent of mineralization of SaOS-2 cells was determined *in vitro* using McCoy's medium/10% FCS and applying Alizarin Red S as a dye to monitor HA formation as shown in **Fig. 2.8**. The medium was changed every 2 days. According to MTT assay, mentioned above, the concentrations of Na-polyP, Ca-polyP1 and Ca-polyP2 powders were set to 100 µg/mL. In absence of MAC, the extent of biomineralization of control (SaOS-2 cells) was low, amounting to only 0.16± 0.007 nmol μg^{-1}, with addition of MAC an increase in the intensity was observed, which is reflected by an enhancement to 0.28± 0.01 nmol μg^{-1} after 5 d and 0.38± 0.006 for 8 d. In comparison, when Na-polyP was added, the intensity of the staining first decreased compared with control (0.15± 0.005) and then increased to 0.29± 0.02 and 0.40±0.008 nmol μg^{-1}. In this sequence, the addition of Ca-polyP resulted in a pronounced increase in the red staining and likewise an increase in the amount of dye bound to the cells up to 0.42± 0.02 nmol μg^{-1} for Ca-polyP1 and 0.52± 0.02 nmol μg^{-1} by the end of incubation time. However, this experimental part from this study indicates that biominerization process is quite complex and many factors could alter the results, we could conclude that the polyP can be used at low concentration or in Ca-polyP form to modulate biomineralization.

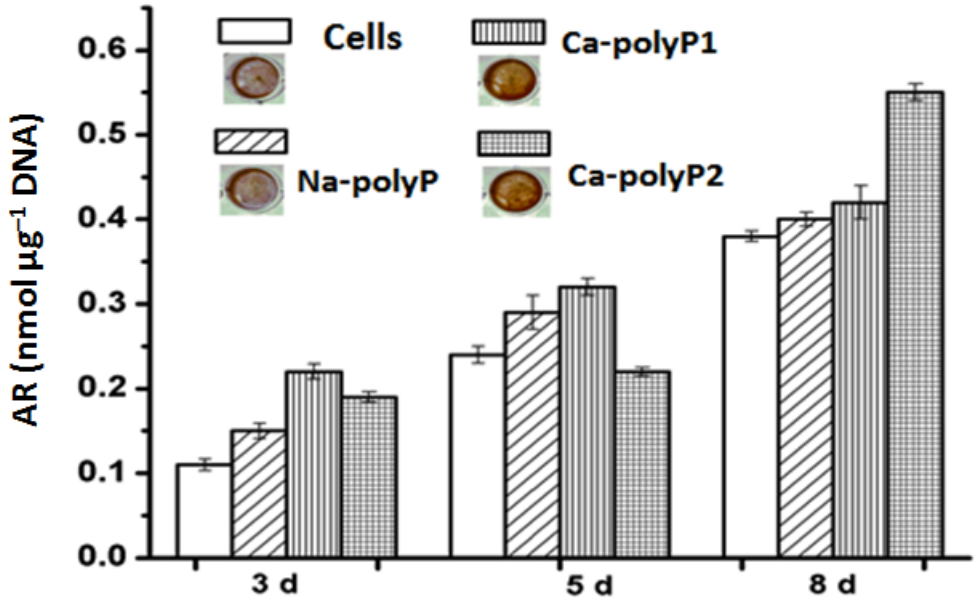

Figure 2.8.

Influence of Na-polyP, Ca-polyP1 and Ca-polyP2 samples on HA mineralization *in vitro*. The SaOS-2 cells were incubated in the presence of the activation cocktail (MAC) for 8 d. After incubation, the cell assays were stained with Alizarin Red S. To determine quantitatively the degree of the mineralization, the cultures were assayed at the end of the incubation with Alizarin Red S, using the spectrophotometric assay. Standard errors of the means are shown (*n* = 5 experiments per time point). In separate experiment, the cover slips onto which the cells had been cultivated were removed and stained with Alizarin Red S. Eye-inspection revealed that the intensity of the color reaction is highest for Ca-polyP1 and for Ca-polyP2. The degree of color reaction is lower for Na-polyP; the intensities of those samples are only slightly higher, compared to the control.

2.4.5 Expression level of *ALP* in response to Ca-polyP particles

The expression level of *ALP* in SaOS-2 cells was quantified by qRT-PCR [25]. However, the data revealed that at day 1 the expression level of *ALP* is statistically not different between the different polyP samples, Ca-polyP2 nano-particles show a slight increase. After an incubation period of 7 d the expression levels of *ALP* in the cells exposed to Ca-polyP1 and Ca-polyP2 are significantly higher than those measured for Na-polyP (**Fig. 2.9)**.

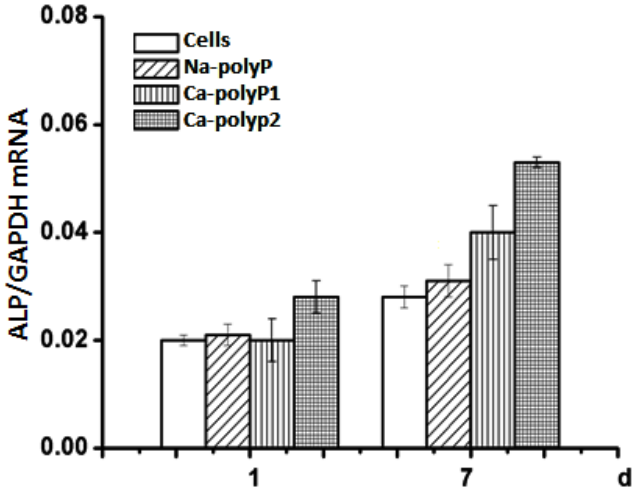

Figure 2.9.
Steady-state expression levels of the genes for alkaline phosphatase (*ALP*) in SaOS-2 cells.

2.4.6 Mitochondria abundance in SaOS-2 cells after incubation with Ca-polyP particles

The SaOS-2 cells were incubated as described before. At first, the cells were incubated for a period of 3 days in the absence of the cocktail (MAC), the cocktail was then added and the cells were incubated for a further 4 days in the absence or presence of 30 µg/ml of Ca-polyP nanoparticles. Subsequently, the cells were harvested, sliced and analyzed by using TEM (**Fig. 2.10 A, B, D, E**). The thin sections revealed that the osteoblast-like SaOS-2 cells [35, 36] from untreated cells contained only a low number of mitochondria (**Fig. 2.10 A, B**), whereas those cells that had been exposed to Ca-polyP contained dense

clusters of mitochondria (**Fig. 2.10 D, E**). The overall cell morphology was identical in both cultures.

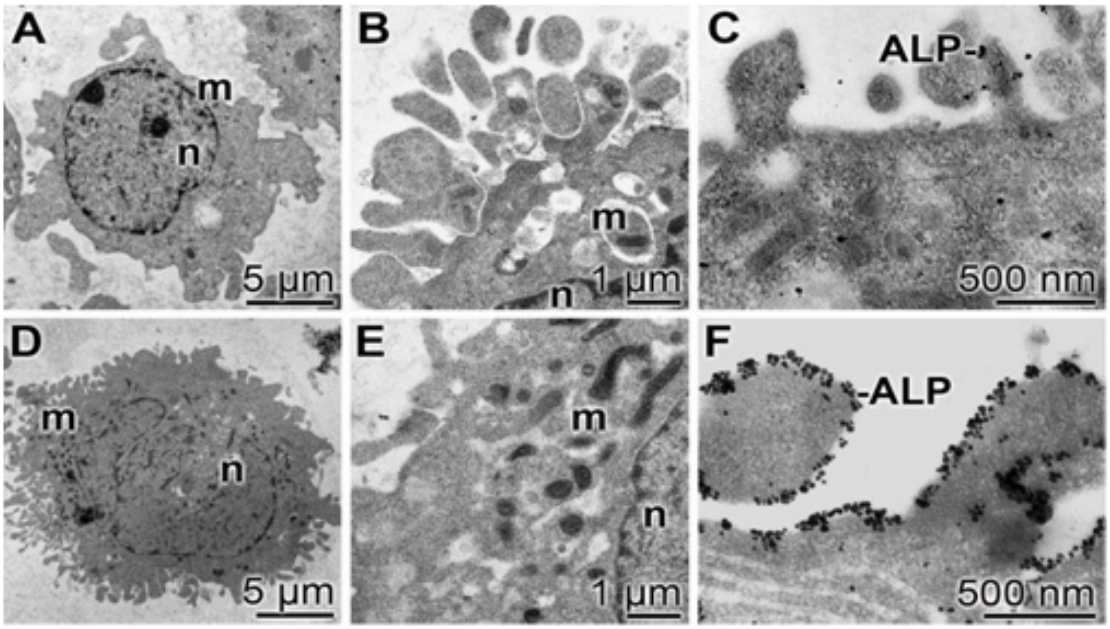

Figure 2.10.

Abundance of mitochondria in SaOS-2 cells and localization of the *ALP* in dependence of exposure to Ca-polyP nanoparticles. The cells have been treated for 3 d with the cocktail, in the absence of Ca-polyP (**A** to **C**) or presence of 30 µg/mL of Ca-polyP2 (**D** to **F**); TEM and immune-TEM images. (**A** and **B**) The abundance of mitochondria (**m**) within SaOS-2 cells, not treated with polyP is low, while (**D** and **E**) cells exposed for 3d with aCa-polyP2 the mitochondria (**m**) are abundantly present; nucleus (n). Also the localization of the *ALP* is drastically different; while the enzyme (**C**) in untreated cells is present in a scattered pattern within the cells, (**F**) almost all *ALP*-gold-intensified immunocomplexes are clustered at the cell surface.

2.4.7 Translocation of the alkaline phosphatase in response to polyP

The *ALP* is a marker protein for mature osteoblasts [37]. In addition, it has been described that the enzyme has, in dependence of the intra- or extracellular localization as well as during bone disease development, an altered pattern of glycosylation [38]. Furthermore, light microscopic studies to localize the *ALP* by enzyme histochemistry suggested that after activation of the osteoblasts the *ALP* translocates to the membrane region [39].

To elucidate if the enzyme changes its localization after exposure to Ca-polyP nanoparticles immunogold TEM-localization of the enzyme has been performed. Again cells have been incubated for an initial period of 3 d, and then transferred for 3 d in the presence of MAC and additionally either in the absence (**Fig. 2.10 C**) or presence of 30 µg/mL Ca-polyP nanoparticles (**Fig. 2.10 F**). After labeling with gold the *ALP* molecules in cells not treated with the nanoparticles are present in a scattered pattern and are not frequently seen (**Fig. 2.10 C**). In contrast, the enzyme in cells exposed to Ca-polyP nanoparticles has been abundantly, and almost exclusively, detected in association with the cell membrane (**Fig. 2.10 F**). Very often the grains appeared in clusters. In the controls, omitting the antibodies from the staining procedure no gold grains could be detected (data not shown).

2.5 Discussion

Amongst many other biological functions, phosphate has long been known to be important in hard tissue mineralization, where orthophosphate (PO_4^{3-}) and calcium ions (Ca^{2+}) combine to form the biological apatite mineral phase found in bones and teeth [40, 41]. Phosphate can also be found as inorganic linear polyPs – its chemical structure is very simple and comprises linearly arranged phosphate units that are linked through high-energy phosphoanhydride bonds. In a physiological pH environment, each internal P_i of the polymer exposes a monovalent negative charge, rendering polyP as an intensely anionic polymer. With cations, polyP forms salts [7, 8]. Although polyPs are now known to be ubiquitous in mammalian cells and tissue fluids, they have been reported to exist in particularly high amounts in human osteoblast-like cells, suggesting a potential role in bone biology [11, 12]. Early work has demonstrated that polyPs bind to HA, supporting the notion that inhibition of calcification by polyP may occur through adsorption of the inorganic polymer to growth sites of the crystals with equal or better potency than pyrophosphate (PP_i) [42, 43].The key role that PP_i plays in regulating physiologic and pathologic mineralization has now been well studied both in animal models and in humans, where the P/ PP_i ratio is known to be a critical determinant in allowing the progression of mineralization [43, 44]..

Despite abundant data showing mineralization inhibition in various systems, it has also been proposed by these authors that if bone mineralization proceeds, enzymes such as tissue-nonspecific *ALP* release the ions from the polyP-calcium complex to be used in HA crystal formation and growth [9, 45]. Despite this possible scenario that occurs outside the bone cells in the extracellular matrix, it is not yet known how polyP granules observed intracellularly are exported or formed in the extracellular matrix where mineralization occurs. Given that polyPs are found at relatively high concentrations in osteoblast-like cells [12], it can be assumed that they potently inhibit HA formation intracellularly [46].

In addition to our previous studies and other reports, it was found that a relatively low concentration of polyP (0.1 mM) induces ALP expression and leads to cellular proliferation [9, 47]. Furthermore, treatment ofNa-polyP with calcium chloride resulted in further increase in *ALP* expression and delays of the inhibitory action of polyP at high concentration [23].Consequently, a new strategy has been developed in the frame of this PhD work to prepare Ca-polyP through direct addition of calcium ions to polyP solution and find out the chemical and physical properties for obtained Ca-polyP nanoparticles. As a result, Ca-polyP particles with different Ca/P molar ratios were successfully synthesized *via* a simple method at room temperature. The complex formation was performed at pH 10. Analyzing the final Ca-polyP product, it has been clarified by X-ray diffraction analysis that the Ca-polyP powders did not show any sign of crystallinity. The SEM and TEM analyses of the "Ca-polyP2" grains shows that they are composed of globular amorphous structures with an average diameter of 200–500 nm.

Based on the view that Ca-polyP nanoparticles can be considered as nanoscopic mineral entities of bone, it has been tempting to study the biological effect of Ca-polyP nanoparticles ("Ca-polyP2") on SaOS-2 cell *in vitro*. In the first series of experiments for the said nanoparticles, the presence of the *ALP* and the site of localization of this enzyme within the SaOS-2 cells were determined by immunogold electron microscopy of cross-sections through the cells using human anti-*ALP* antibodies. Interesting enough, the *ALP*-reacting sites are exclusively found in close areas of the cells membrane. This finding is taken as first evidence that the SaOS-2 cells become strongly activated after exposure to the "Ca-polyP2" particles. In an earlier study, it could be demonstrated that in activated osteoblasts the *ALP* is abundantly localized along the osteoidal region of osteoblast membranes [48].In addition, the authors reported that *ALP* enzymatic activity along the osteoidal surface of osteoblasts can be increased by both Mg^{2+} and Ca^{2+}; the enzyme could be inhibited by vanadate but is resistant to levamisole, implying the close relationship of this enzyme with the plasma membrane Ca^{2+} transport ATPase. However, it remained totally unclear by which mechanism polyP is anabolically affecting both the gene expression and activity of the *ALP*.

Moreover, the data revealed that after treatment of the cells with Na-polyP, a very few mitochondria could be detected in the cells. In contrast, those cells that have been treated with "Ca-polyP2" showed areas with densely packed mitochondria. Because the ATP level within the cells is coupled to the number of mitochondria, these findings might be taken as an indication that the ATP level in the cells of these two assays is different. Consequently, it appears to be obvious that polyP which is accumulated in cells surrounding bone growth areas, e.g., osteoblasts and platelets [49, 50], might act as a potential energy source, as a metabolic fuel, for bone synthesis.

2.6 Conclusion

- The Ca-polyP particles with different Ca/P molar ratios were successfully synthesized via a simple wet chemical precipitation method at room temperature.
- A full structural determination by different techniques – such as X-ray diffraction, FTIR, SEM and TEM– has shown a unique structure and morphology when compared to that of other calcium phosphate phases.
- The Ca/P molar ratio was found to influence not only physical and chemical properties of Ca-polyP particles but also the biological behavior during *in vitro* study.
- The study further highlights, Ca-polyP nanoparticles represent not only a concentrated store of $Ca^{2+}$and PO_4^{3-}, which could be used during bone tissue mineralization but also a stimulator of morphogenetic processes, providing a favorable biochemical environment for bone formation.
- It is nonetheless important that new therapeutic directions could be suggested, particularly with regard to the control of mineralization.

2.7 References

1. Amini A. R., Laurencin C. T. & Nukavarapu S. P. (2012). Critical reviews in biomedical engineering 40, 363-408.

2. Ikada Y. (2006). Journal of the Royal Society Interface 3, 589- 601.

3. Gurtner G. C., Callaghan M. J. & Longaker M. T. (2007). Annual Review of Medicine 58, 299-312.

4. Sahrmann P., Attin T. & Schmidlin P. R. (2011). Clinical Implant Dentistry and Related Research 13, 46- 57.

5. Komatsu D. E. & Warden S. J., (2010). The J Cell Biochem. 109, 302-311.

6. Henkel J., Woodruff M. A., Epari D. R., Steck R., Glatt V., Dickinson I. C. & Hutmacher D. W. (2013). Bone Research 1, 216- 248.

7. Kornberg A., Rao N. N. & Ault-Riché, D. (1999). Annu Rev Biochem. 68, 89-125.

8. Morrissey J. H., Choi S. H. & Smith S. A. (2012). Blood 119, 5972-5979.

9. Müller W. E. G., Wang X. H., Diehl-Seifert B., Kropf K., Schloßmacher U., Lieberwirth I., Glasser G., Wiens M. & Schröder H. C. (2011). Acta Biomater. 7, 2661-2671.

10. Hacchou Y., Uematsu T., Ueda O., Usui Y., Uematsu S., Takahashi M., Uchihashi T., Kawazoe Y., Shiba T. & Kurihara S. (2007). J Dent Res. 86, 893-897.

11. Leyhausen G., Lorenz B., Zhu H., Geurtsen W., Bohnensack R., Müller W. E. G. & Schröder, H. C. (1998). J Bone Mineral Res. 13, 803-812.

12. Schröder, H. C., Kurz L., Müller W. E. G. & Lorenz, B. (2000). Biochemistry (Mosc.) 65, 296-303.

13. Ariganello M. B., Omelon S., Variola F., Wazen R. M., Moffatt P. & Nanci A. (2014). J Cell Biochem. 115, 2089-2102.

14. Usui Y., Uematsu T., Uchihashi T., Takahashi M., Takahashi M., Ishizuka M., Doto R., Tanaka H., Komazaki Y., Osawa M., Yamada K., Yamaoka M. & Furusawa, K. (2010). J Dent Res. 89, 504-509.

15. Tsutsumi K., Saito N., Kawazoe Y., Ooi H. K. & Shiba T. (2014). PLoS One. 9, e86834.

16. Lorenz B. & Schröder H. C. (2001). Biochim Biophys Acta. 1547, 254-261.

17. Magnusson P., Larsson L., Magnusson M., Davie M. W. & Sharp C. A. (1999). J Bone Miner Res. 14, 1926-1933.

18. Lorenz B., Müller W. E. G., Kulaev I. S. & Schröder H. C. (1994). J Biol Chem. 269, 22198-22204.

19. Addison W. N., Azari F., Sørensen E. S., Kaartinen M. T. & McKee M. D. (2007). J Biol Chem. 282, 15872-15883.

20. Ding Y. L., Chen Y. W., Qin Y. J., Shi G. Q., Yu X. X. & Wan C. X. (2008). J Mater Sci Mater Med. 19, 1291-1295.

21. Wiens M.,Wang X., Schröder H. C., Kolb U., Schlossmacher U., Ushijima H. & Müller W. E. G. (2010a). Biomater. 31, 7716-7725.

22. Wiens M., Wang X., Schlossmacher U., Lieberwirth I., Glasser G., Ushijima H., Schröder H. C. & Müller W. E. G. (2010b). Calcif Tissue Int. 87, 513-524.

23. Wang X.H., Schröder H.C., Schlossmacher U., Neufurth M,. Feng Q, Diehl-Seifert B. & Müller W.E.G. (2014). Calcif Tissue Int. 94: 495-509.

24. Schröder H.C., Wang X.H., Wiens M., Diehl-Seifert B., Kropf K., Schloßmacher U., Müller W.E.G. (2012). J Cell Biochem. 113, 3197-3206

25. Schröder H. C., Borejko A., Krasko A., Reiber A., Schwertner H. & Müller W. E. G. (2005). J Biomed Mater Res B Appl Biomater. 75, 387-392.

26. Wang X., Schröder H. C., Diehl-Seifert B., Kropf K., Schlossmacher U., Wiens M. & Müller W. E. G. (2013). J Tissue Eng Regen Med. 7, 767–776.

27. Kokkinopoulou M., Güler M. A., Lieb B., Barbeck M., Ghanaati S., Markl J. (2014). PLoS ONE. 9, e101078.

28. Danscher G. (1981). Histochemistry 71, 81-88.

29. Sachs L. (1984). Angewandte Statistik. Springer-Verlag: Berlin, Germany.242.

30. Szumera M. (2014). Spectrochim Acta A Mol Biomol Spectrosc.130, 1-6.

31. Pavic L., Milankovic A.M., Rao P.R., Santic A., Kumar V. R. & Veeraiah N. (2014). J Alloy Compd. 604, 352–362.

32. He Z., Honeycutt C. W., Xing B., McDowell R. W., Pellechia P. J. & Zhang T. (2007) Soil Sci. 172 (7), 501–515.

33. Chahine A., Et-tabirou M. & Pascal J. L. (2004). Mater Lett. 58, 2776-2778.

34. Fischer V., Lieberwirth I., Jakob G., Landfester K. & Muñoz-Espí R.(2013). Adv Funct Mater. 23, 451–466.

35. Guranowski A. (2004). Front Biosci. 9, 1398-1411.

36. Baxter L. C., Frauchiger V., Textor M., ap Gwynn I. & Richards R.G. (2002). Eur Cell Mater. 30, 1-17.

37. Wang X. H., Schröder H. C., Wiens M., Ushijima H. & Müller W. E. G. (2012). Current Opinion Biotechnol. 23, 570–578.

38. Langlois M. R., Delanghe J. R., Kaufman J. M., De Buyzere M. L., Van Hoecke M. J. & Leroux-Roels G. G. (1994). Eur J Clin Chem Clin Biochem. 32, 675-680.

39. Nakano Y., Beertsen W., van den Bos T., Kawamoto T., Oda, K. & Takano Y. (2004). Bone 35, 1077-1085.

40. Tenenbaum H. C. (1981). J Dent Res. 60, 1586-1589.

41. Penido M. G. M. G. & Alon, U. S. (2012). Pediatric Nephrology Berlin Germany 27, 2039-2048.

42. Fleisch H. & Neuman W. F. (1961). Am J Physiol. 200, 1296-300.

43. Francis M. D. (1969). Calcif Tissue Res. 3, 151-62.

44. Fleisch H., Russell R. G. & Straumann F. (1966). Nat. 212, 901- 903.

45. Omelon S., Georgiou J., Henneman Z. J., Wise L. M., Sukhu B., Hunt T., Wynnyckyj C., Holmyard D., Bielecki R. & Grynpas M. D. (2009). PLoS One. 4, e5634.

46. Hoac B., Kiffer-Moreira T., Millán J. L. & McKee M. D. (2013). Bone 53, 478–486.

47. Kawazoe Y., Shiba T., Nakamura R., Mizuno A., Tsutsumi K., Uematsu T., Yamaoka M., Shindoh M.&Kohgo T.(2004). J Dent Res. 83, 613-618.

48. Miyazaki T., Iwasawa M., Nakashima T., Mori S., Shigemoto K., Nakamura H., Kata giri H., Takayanagi H. & Tanaka S. (2012). J Biol Chem. 287, 37808-37823.

49. Kumble K. D. & Kornberg A. (1995). J Biol Chem. 270, 5818-5822.

50. Müller F., Mutch N. J., Schenk W. A., Smith S. A., Esterl L., Spronk H. M., Schmidbauer S., Gahl W. A., Morrissey J. H. & Renné T. (2009). Cell 139, 1143-1156.

Chapter 3:

Amorphous polyphosphate–hydroxyapatite: A morphogenetically active substrate for bone-related SaOS-2 cells *in vitro*.

3.1 Introduction

Two main stages of bone formation (ossification) are distinguished [1]. First, during the primary phase, the endochondral ossification, the epiphysial cartilage, a combination of ground substance and loosely interconnected fibril bundles of collagen, interspersed with a large number of matrix vesicles, allows a relatively rapid mineralization process (reviewed in: [2]). The mineralized, ‘‘woven’” bone microstructures comprise collagen type-I, which exists in rat cartilage to ≈17%. The crystals formed are not closely associated with collagen; the clusters of hydroxyapatite (HA) crystals are deposited into the collagen-surrounding proteoglycan matrix [3]. While during primary ossification phase collagen does not markedly direct the mineralization deposits, during the subsequent secondary phase of bone formation the primary woven bone is remodeled into an organized tissue comprising concentric lamellae that make up the osteons [4]. The nanoscopic HA platelets become oriented and aligned within the self-assembled collagen fibrils and are arranged concentrically around blood vessels [5]. The cells that form the mineral deposits within bone are the osteoblasts. In a tightly controlled process, the collagen fibrils undergo a progressive mineralization starting with poorly crystalline carbonated apatite (see: [6]).

Three main mechanisms have been proposed to explain the initial bone mineral deposition. *First:* a cell-independent process, whereby charged non-collagenous proteins facilitate mineral nucleation from ions in solution [7]. Second: a cell-controlled mechanism during which vesicles are budding off from the cellular plasma membrane. In these matrix vesicles, and supported by phosphatases including the alkaline phosphatase (ALP), as well as by Ca-binding molecules, initial calcium phosphate (CaP) mineral crystals are formed. Subsequently the matrix vesicles break down at the cell membrane, releasing the mineral deposits into the extracellular space [8]. *Third:* more

recently an alternative route has been proposed in which amorphous mineral precursors are transiently produced. They are deposited within the collagen fibrils where they transform into crystalline apatite platelets [9]. However, the origin of the proposed amorphous CaP remained still to be elucidated. Experimental evidence has been presented that revealed that osteoblasts contain intracellularly localized CaPcontaining vesicles which are potential candidates for the extracellular mineralization process [10]. Element analyses suggested that the intracellular mineral granules consist of a highly metastable phase and, in addition, a potential precursor stage of carbonated HA. Moreover, experimental evidence indicates that initially, on the surface of osteoblasts, Ca-carbonate deposits are synthesized in concert with the carbonic anhydrase that act as bio-seeds for the biomineralization process [11, 12]. It is reasonable to assume that those Ca-carbonate deposits are amorphous, since this material is unstable and readily processes to other states of Ca-carbonate [13, 14]. This proposition is supported by the finding that Ca-carbonate is converted to CaP by exposure to external orthophosphate [15]. In addition, during the evolution of the animals first Ca-carbonate-based skeletons, e.g. in sponges or corals, developed while later CaP skeletons are dominating [16]. The analytical demonstration that Ca-carbonate exists in vertebrate bone goes back to Pellegrino and Biltz [17]; and, to mention, that in the vestibular labyrinth of the vertebrate ear the otoliths predominantly consist of Ca-carbonate [18].

Bone, being a composite material, forms the inorganic deposits around the collagen fibrils. Evidence has been presented indicating that the uniaxially oriented apatite crystals are formed within the periodic 67 nm cross-striated pattern of the collagen fibril at the less dense 40 nm long gap zone [19]. It is proposed that the positive net charge at the C-termini of the collagen molecules initiates and promotes the infiltration of the fibrils with amorphous CaP (ACP). The latter discovery was supported by the finding that during bone and teeth formation the development of the apatite crystals starts from an ACP precursor phase [20, 21] at the prenucleation clusters. Those amorphous clusters have also been demonstrated for amorphous $CaCO_3$ (ACC) [22, 23]. The transition from

ACP to crystalline HA in those clusters is a fast process that is decelerated when a size is reached at which the increasing surface energy is counter-balanced by the reduction of bulk energy, originating from the process of crystal lattice formation. The resulting primary critical-sized crystal nuclei grow further, driven by the associated reduction of the Gibbs free energy. The basic building blocks, as in tooth crowns, are dense arrays of needle-shaped carbonated apatite crystals (≈50 nm in diameter and tens of μm long), with crystalline c-axes, arranged along the rods [24]. Interesting is the finding that in-vitro collagen-mediated mineralization is decelerated by substituting the spacing of non-collagenous proteins either with polyaspartic acid or with fetuin; both of them are inhibitors of HA crystallization [2, 25, 26]. Those additional components added during *in-vitro* HA synthesis are considered as structure forming elements during the intrafibrillar formation of oriented HA crystals.

HA is a naturally occurring mineral with the formula $Ca_5(PO_4)_3(OH)$ [or: $Ca_{10}(PO_4)_6(OH)_2$ to signify that the HA crystal unit cell comprises two entities]. Natural bone HA elicits biological activity, at least bone conducting properties [27]. In turn, natural HA, a bio-ceramic which is crystalline to different scale has been used as a biomaterial to fabricate scaffolds for in situ bone regeneration and other tissue engineering purposes (reviewed in:[28–30]). While natural HA shows pronounced mineralization promoting activity *in vivo*, synthetic apatite is much less effective. In general, although HA is bioactive, its interaction and biocompatibility with existing bone tissue is low. These properties have been attributed to a minimal degradability in the physiological environment as observable by the lack of resorption via the surrounding intact tissue [31]. Recent advances in nanotechnology allowed the synthesis of nano-hydroxyapatite of various morphologies with a reasonable biocompatibility [32]. Moreover, it has been demonstrated that ACP has a better osteoconductivity and biodegradability than tricalcium phosphate and HA *in vivo* [33].

In the present study we introduce a new CaP fabrication technology, starting from calcium chloride and dibasic ammonium phosphate [34]. Besides of the preparation of

HA, with the characteristic Ca/P molar ratio of 10:6, we prepared CaP mixed with various amounts of polyphosphate (polyP). While the CaP/HA samples were found to consist of a crystalline phase, those CaP preparations that contained >10% by weight of polyP (with respect to the modified HA deposits) are amorphous. All those polyP-supplemented CaP samples were found to support the growth of bone cell related SaOS-2 cells [35] as well as human mesenchymal stem cells (hMSC). Surprisingly, only the CaP preparation, containing 10 weight percent (wt.%) of polyP, elicits strong morphogenetic activity, as measured by gene expression analysis and using the marker genes alkaline phosphatase (*ALP*) and collagen type I (*COL-I*) for differentiation of bone and bone-related cells [36]. These results let us to conclude that polyP/HA-based material might be beneficial for application as bone substitute implant.

3.2 Material and methods

3.2.1 Materials

Sodium polyphosphate (Na–polyP) with an average chain length of 40 phosphate units was obtained from Chemische Fabrik Budenheim (Budenheim, Germany).

3.2.2 In situ synthesis of HA and polyphosphate–hydroxyapatite

Hydroxyapatite (HA) nanoparticles were synthesized by a wet chemical precipitation method from calcium chloride ($CaCl_2$; Sigma–Aldrich, Taufkirchen; Germany) as Ca^{2+} source, and ammonium phosphate dibasic ($(NH_4)_2HPO_4$; Sigma–Aldrich 215996) as phosphate source [34]. To precipitate stoichiometric HA ($Ca_{10}(PO_4)_6(OH)_2$; Ca/P ratio of 1.667), 100 mL of 0.3 M aqueous solution of $(NH_4)_2HPO_4$ was dropwise added to 100 mL 0.5 M aqueous solution of $CaCl_2$. The amount of reagents was calculated in order to obtain the Ca/P molar ratio for HA of 10:6. The pH of the reaction was maintained at 10 with the addition of sodium hydroxide solution.

In order to prepare polyP-substituted HA nanoparticles of various polyP content, the starting components ($CaCl_2$ and $(NH_4)_2HPO_4$) were additionally supplemented with 2.5, 5 or 10 wt.% of Na–polyP (referred to HA, or the respective CaP preparation) as follows. The respective amount of Na–polyP, 0.12 g [‘‘HA(2.5)polyP”], 0.25 g [‘‘HA(5)polyP”] or 0.50 g [‘‘aCaP(10)polyP”], was added to the aqueous solution of (NH4)2HPO4; then this solution was added to the dissolved $CaCl_2$. The pH was kept at 10. The resulting precipitates were left at room temperature for 24 h. Then the precipitates were filtered, washed 3-times with distilled water before being dried in a hot air oven at 60 _C for 24 h. The final powders were termed ‘‘HA”, ‘‘HA(2.5)polyP”, ‘‘HA(5)polyP” and ‘‘aCaP(10)polyP”.

For comparative functional/biological studies amorphous Ca–polyP nanoparticles were prepared as described [37]. In brief, 2.8 g of CaCl2 in 30 mL distilled water were added dropwise to 1 g of Na–polyP, dissolved in 50 mL distilled water at a pH of 10.0. The amorphous Ca–polyP nanoparticles formed were washed in water and then dried at 50

^{o}C; the preparation is termed ''aCa–polyP-NP''. The average diameter of the spherical particles was 96±28 nm and they have an amorphous state [38].

3.3 Materials characterizations

3.3.1 X-ray diffraction analyses

The X-ray diffraction (XRD) experiments were performed as described previously [39]. The patterns of dried powders were registered on a Philips PW 1820 diffractometer with $Cu_{K\alpha}$ radiation (λ = 1.5418 Å, 40 kV, 30 mA) in the range $2\theta = 5^{o}$- 65^{o} (Δ 2θ= 0.02, Δ t = 5 s). The HA crystals were identified as described [40].

3.3.2 Fourier transformed infrared spectroscopy

The Fourier transformed infrared (FTIR) spectroscopic analyses were performed by using micro-milled (agate mortar and pestle) mineral powder in an ATR-FTIR spectroscope/Varian 660-IR spectrometer (Agilent), equipped with a Golden Gate ATR unit (Specac, Orpington; UK) [15]. Each spectrum represents the average of 100 scans with a spectral resolution of 4 cm^{-1}. Baseline correction, smoothing, and analysis of the spectra were achieved with the Varian 660-IR software package 5.2.0 (Agilent). Graphical display and annotation of the spectra were performed with Origin Pro (version 8.5.1; OriginLab, Northampton; MA).

3.3.3 Electron microscopy studies

For the transmission electron microscopic (TEM) analyses the TemCam-F416 (4x4 K) CCD camera (TVIPS, Gauting; Germany), operated on a Tecnai 12 transmission electron microscope (FEI, Eindhoven; The Netherlands) at an accelerating voltage of 120 kV, was used. The equipment was connected with a particle size analyzer (ImageJ); 25–50 crystals/spheres were evaluated.

The scanning electron microscopic (SEM) analyses were performed with an SU 8000 instrument (Hitachi High-Technologies Europe, Krefeld; Germany), employed at low voltage (1 kV) as described [41]. For these studies the cells were grown in the 6-well plates onto CaP preparations that had been pressed to 1 mm thick disks, with a

diameter of 34mm, for 3d. The cells, growing on the CaP substrates were fixed with 4% paraformaldehyde.

3.3.4 Cultivation of SaOS-2 and human mesenchymal stem cells

The human osteogenic sarcoma cells SaOS-2 were cultured in McCoy's medium (Biochrom-Seromed, Berlin, Germany) supplemented with 2 mM l-glutamine, 15% heat-inactivated fetal calf serum (FCS), 100 units/mL penicillin and 100 µg/mL streptomycin [42]. The cells were incubated in 25 cm2 flasks or in 6-well plates (surface area 9.46 cm2; Orange Scientifique, Brainel'Alleud; Belgium) at 37 oC. Routinely, the cultures were started with 1x 104cells per well in a total volume of 3 mL. Where indicated, the cultures were first incubated for a period of 3 d in the absence the mineralization-activating cocktail (MAC), comprising 5 mM b-glycerophosphate, 50 mM ascorbic acid and 10 nM dexamethasone to induce biomineralization [43]. Then the cultures were continued to be incubated for additional 7 d in the absence or presence of the MAC. The HA/polyP mineral samples (100 µg/mL [HA, CaP] or 10 µg/mL ["aCa–polyP-NP"]), were added to each well at the beginning of the experiments. Every third day the culture medium was replaced by fresh medium/serum and, where indicated, also with MAC. The human mesenchymal stem cells (hMSCs) were isolated using the previously described method; the experiments had been approved from the ethics committee [44]. Briefly, the cells were cultivated in α-minimum essential medium (α-MEM; cat. No. F0915; Biochrom, Berlin; Germany), supplemented with 20% FCS, as well as with 0.5 mg/mL of gentamycin, 100 units penicillin, 100 µg/mL of streptomycin and 1 mM pyruvate Sigma–Aldrich P2256). After the initial incubation for 3 d the non-adherent cells were discarded, and the adherent cells were continued to be incubated with α-MEM/FCS.

3.3.5 Cell growth assay

SaOS-2 cells were seeded into the 6-well plates at a density of $1x10^4$ cells per well and cultured for 3 d in McCoy's medium/15% FCS. 300µg (in 3 mL assays) of the respective CaP preparation were added per well. Parallel with those samples, polyP as nanoparticles, ''aCa–polyP-NP'', was tested at a concentration of 10 µg/mL. After a 2 or

3 d incubation period, the cells were incubated with fresh medium containing 200 µL of 3-[4,5-dimethyl thiazole-2-yl]-2,5- diphenyl tetrazolium (MTT; Sigma M2128) for 4 h in the dark. Then the remaining MTT dye was aspirated and 200 µL of DMSO were added to solubilize the formazan crystals. Finally, the optical density (OD) was determined at 560 nm using an ELISA reader/ spectrophotometer [45]. Ten parallel experiments each were performed.

In a parallel series of experiments hMSCs were incubated with 10 µg/mL of ‘‘aCa–polyP-NP’’, or 100 µg/mL each of HA, ‘‘HA(2.5) polyP”, ‘‘HA(5)polyP” or ‘‘aCaP(10)polyP”. Then the cultures were subjected to the MTT assay.

3.3.6 Quantitative real-time polymerase chain reaction

The SaOS-2 cells were initially cultivated for 3 d in medium/serum. Then the cultures were supplemented with either 300 µg (in 3 mL) of the respective CaP preparation, “HA”, “HA(2.5)polyP”, “HA(5)polyP” or “aCaP(10)polyP”, or with 10 µg/mL of the polyP nanoparticles, ‘‘aCa–polyP-NP’’, and the cultivation was continued for 7 d in the absence or presence of MAC. Subsequently, the cells were analyzed for gene expression. Applying the technique of quantitative real-time RT [reverse transcription]-polymerase chain reaction (qRT-PCR) the levels of transcription of the two genes, *ALP* and *COL-I* were quantified in SaOS-2 cells, as described [46]. Applying the technique of quantitative real-time RT [reverse transcription]-polymerase chain reaction (qRT-PCR) the levels of transcription of the two genes, *ALP* and *COL-I* were quantified in SaOS-2 cells, as described [46]. The following primer pairs were used: *ALP* [alkaline phosphatase; NM_000478.4] Fwd: 5′-TGCAGTACGAGCTGAACAGGAACA-3′ [nt_{1141} to nt_{1164}] and Rev: 5′-TCCACCAAATGTGAAGACGTGGGA-3′ [nt_{1418} to nt_{1395}; 278 bp] and *COL-I* [collagen type I; NM_000088.3] Fwd: 5′-GACTGCCAAAGAAGCCTTGCC-3′ [nt_{5073} to nt_{5093}] and Rev: 5′-TTCCTGACTCTCCTCCGAACCC-3′ [nt_{51196} to nt_{5175}] (124 bp). As the reference the expression of *GAPDH* [glyceraldehyde 3-phosphate dehydrogenase; NM_002046.3] Fwd: 5′-CCGTCTAGAAAAACCTGCC-3′ [nt_{929} to nt_{947}] and Rev: 5′-GCCAAATTCGTTGTCATACC-3′ [nt_{1145} to nt_{1126}; 199 bp] was determined. After incubation the cells were harvested and

the RNA was extracted, which was used for the qRT-PCR determinations, using an iCycler (Bio-Rad, Hercules, CA, USA). The mean C_t values and efficiencies were calculated by iCycler software (Bio-Rad); the estimated PCR efficiencies were in the range of 93–103%.

3.3.7 Statistical analysis

After finding that the values follow a standard normal Gaussian distribution, the results were statistically evaluated using paired Student's *t*-test [47].

3.4 Results

3.4.1 XRD analyses

The phase identification of the ‘‘HA” as well as the polyP-HA particles was performed by applying the powder X-ray diffraction (XRD) method (**Fig. 3.1**). While for pure Na–polyP no distinct diffraction signals can be resolved, indicating an amorphous phase, pure ‘‘HA” as well as ‘‘HA(2.5)polyP” and ‘‘HA(5)polyP” exhibit broad diffraction peaks indicating formation of HA with low crystallinity; no other crystalline phase was detected (JCPDS [http://www.icdd. com/] #09-0432) [48,49]. However, when the amount of polyp increases to 10 wt.%, as in ‘‘aCaP(10)polyP”, no signs of crystallinity are seen in the XRD pattern (**Fig. 3.1**). These results show that the degree of crystallinity of the prepared HA sample progressively decreases with the increase in polyP content.

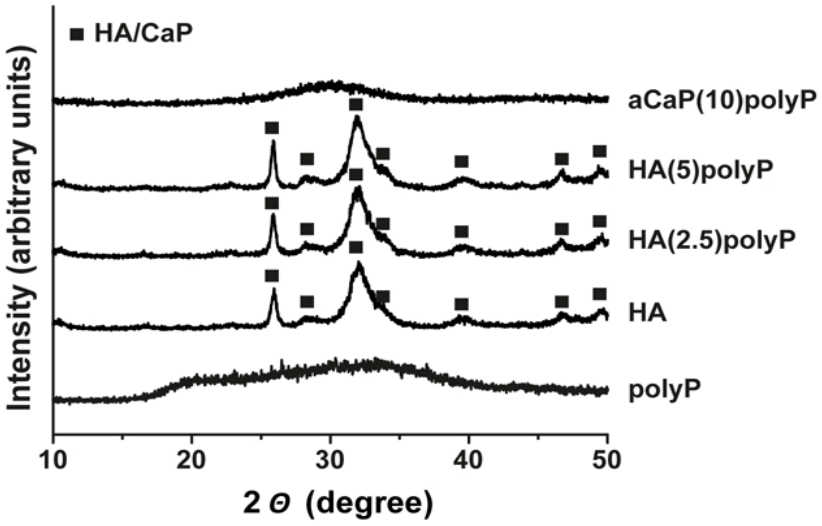

Figure 3.1.

Diffraction patterns taken from pure Na–polyP ‘‘polyP” and pure ‘‘HA”, as well as from HA, prepared in the presence of different amounts of Na–polyP, 2.5 wt.% as in ‘‘HA(2.5)polyP”, 5 wt.% in ‘‘HA(5)polyP”, and 10 wt.% in ‘‘aCaP(10)polyP”. The respective patterns are given from the bottom to the top. No diffraction signals are seen for ‘‘polyP” and ‘‘aCaP(10)polyP”. The diffraction peaks characteristic for HA or crystalline CaP are highlighted (■).

3.4.2 FTIR spectral analysis

All the spectra for CaP recorded here, like pure "HA", as well as "HA(2.5)polyP" and "HA(5)polyP", showed the HA bandings (**Fig. 3.2A, B**), except for "aCaP(10)polyP". As expected, the absorption bands of HA with high intensity are recorded at 1090 cm^{-1}, 1015 cm^{-1} and 960 cm^{-1}, with the symmetric v_1 (PO_4^{3-}) and the asymmetric v_3 (PO_4^{3-}) stretching vibrations. In addition, the peaks at 556 cm^{-1} and 604 cm^{-1} are characteristic bending v_4 (PO_4^{3-}) vibrations. In contrast, the spectrum for "aCaP(10)polyP" shows a distinct shift of the phosphate absorption band for the symmetric v_1 (PO_4^{3-}) and asymmetric v_3 (PO_4^{3-}) stretching vibrations in the region between 1100-900 cm^{-1} and also the v_4 (PO_4^{3-}) harmonics of P = O bending vibrations, which appeared as one peak centered around 610 cm^{-1}. In addition, a wide absorption band within the range from ~3600 cm^{-1} up to 3100 cm^{-1} points on v_3 and v_1 with H_2O molecules bonded with hydrogen for stretching modes. The absorption band at 1629 cm^{-1} is attributed to the deformation mode v_2 of H_2O molecules, proving the presence of physically adsorbed water in the synthesized samples. It has been reported that the vibration bands around 556 cm^{-1} and 604 cm^{-1} in the FTIR spectra of CaP reflect the characteristic bending signals of the harmonic vibration for crystalline PO_4^{3-}[48] and [49]; shifting of the two peaks indicate the transformation from crystalline to amorphous phase. This shift is clearly seen in the pattern of "aCaP(10)polyP", where the two peaks now show up as one peak, indicating the amorphous nature of this sample. This finding is also in agreement with the reported XRD pattern **Fig. 3.1**. For comparison, the spectrum of polyP is also included in the CaP tracings (**Fig. 3.2**). It is apparent that for polyP a peak near 1261 cm^{-1} appears that is assigned to the asymmetric stretching mode of (O–P= O), characteristics for polyP [50]. The absorption bands close to 1090 cm^{-1} and 960 cm^{-1} are assigned to the asymmetric and symmetric stretching modes of (O–P–O), respectively. These signals further confirm the presence of polyP. In addition, the absorption band near 864 cm^{-1} is indicative for the asymmetric stretching modes of the P–O–P linkages and the partially split band centered around 763 cm^{-1} should be attributed to the symmetric stretching modes of these linkages.

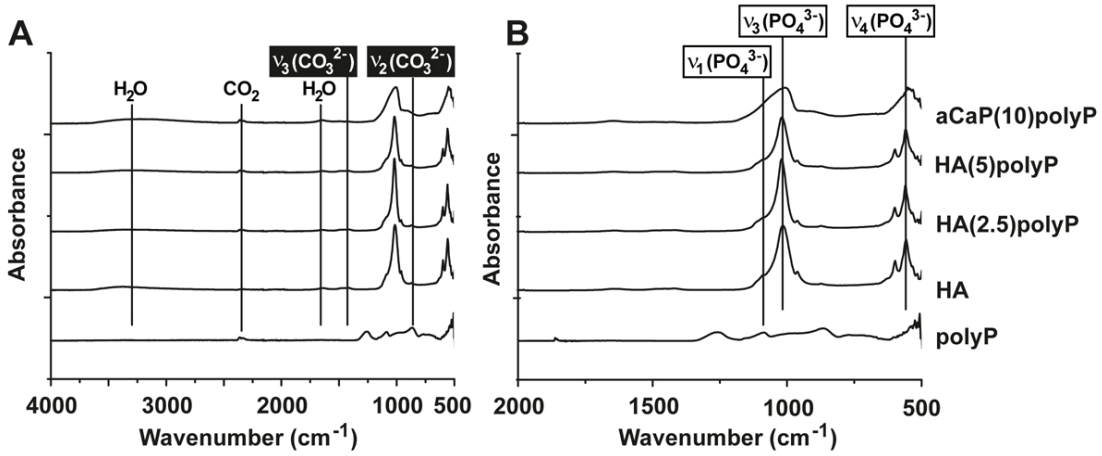

Figure 3.2.

FTIR spectra for "polyP" and "HA", as well as for CaP samples, in which ortho-phosphate has been partially substituted by polyP, "HA(2.5)polyP", "HA(5)polyP" and "aCaP(10)polyP". Some vibration bands for CO_3^{2-} and PO_4^{3-} are marked; in addition, the regions for the H_2O and CO_2 bands are indicated. (A) Wavenumber between 4000 and 500 cm^{-1}; (B) Enlargement of the segment 2000–500 cm^{-1}.

3.4.3 TEM and particle size distribution results

The morphologies of the CaP samples were analyzed by TEM. The ''HA" sample showed needle-like nano-crystals with an average length of 39±8 nm and a width of 14±4 nm (n = 25); **Fig. 3.3A**. Almost the same dimensions were visualized in ''HA(2.5) polyP" samples with a length of 42±10 nm and a width of 9±5 nm (n = 25); **Fig. 3.3B**. Slightly longer are the crystals present in the ''HA(5)polyP" preparation with 56±12 and 6±3 nm in width (n = 25); **Fig. 3.3 C**. In contrast, the CaP preparation, containing the highest proportion of polyP, ''aCaP(10)polyP", showed particles with different morphologies (**Fig. 3.3D**). Instead of needle-like structure spherical particles with a diameter of 70–120 nm (96±15 nm; n=25) are resolved. Those particles have the tendency to agglomerate to larger entities. In both samples, ''HA(5)polyP" and ''aCaP (10)polyP" the percentage of ACP is, as a rough estimation, smaller than 20%.

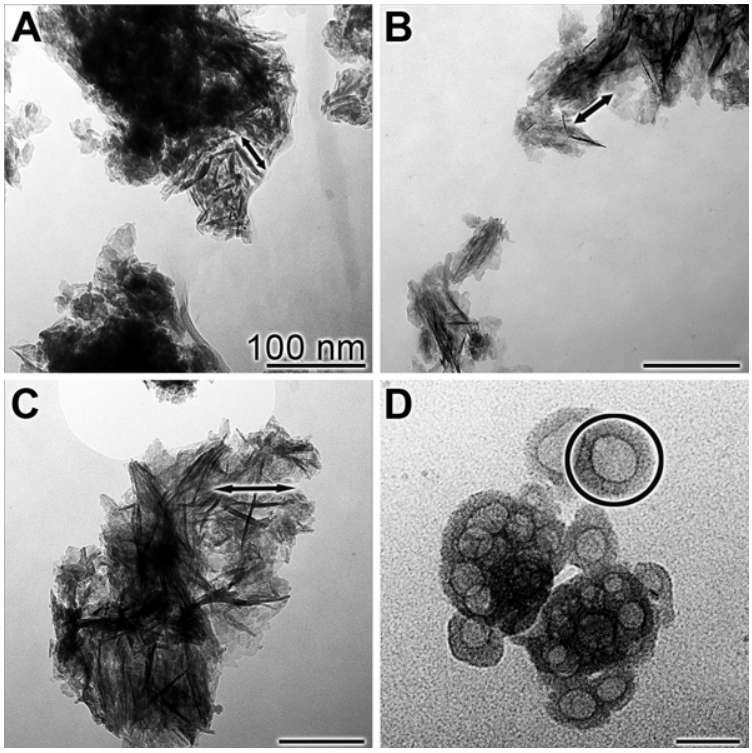

Figure 3.3.

TEM micrographs of the polyP and CaP particles. (**A**) ‘‘HA” crystals; (**B** and **C**) ‘‘HA(2.5)polyP” and ‘‘HA(5)polyP” crystals; and (**D**) ‘‘aCaP(10)polyP” amorphous spherical particles.

3.4.4 Effect of CaP samples and of Ca–polyP nanoparticles on cell growth

The cell viability (metabolic activity) of either SaOS-2 cells (**Fig. 3.4 A**) or hMSCs (**Fig. 3.4 B**), growing onto the CaP samples, were tested by applying the MTT assay. Those samples were added at a concentration of 100 μg/mL to the cells. In parallel, an incubation was performed with 10 μg/mL of Ca–polyP nanoparticles, ‘‘aCa–polyP-NP’’, a sample which has been proven to increase the growth rate of the cells and to cause an increased gene expression of *ALP* and *COL-I* [37, 38]. The results revealed that, after an incubation period of SaOS-2 cells for 2 d no significant differences in the growth of the cells on the different substrates are seen (**Fig. 3.4 A**). The absorbance values at time 0 are 1.15±0.19. However, after an incubation period of 3 d a significant increase, with respect to the metabolic activity of HA-exposed cells (1.98±0.21 absorbance units), is seen for SaOS-2 cells, growing in the presence of ‘‘aCa–polyP-NP’’ (2.45±0.20

absorbance units), as well as of ‘‘aCaP(10)polyP” (2.31±0.25). A similar stimulatory response is also seen for hMSCs after a 3 d incubation period for ‘‘aCa–polyP-NP’’ (2.43±0.35 absorbance units), as well as of ‘‘aCaP(10)polyP” (2.59±0.31), if compared to the values determined for cultures incubated with HA (1.35±0.21); **Fig. 3.4B**. Under these incubation conditions also an increase of the metabolic activity is seen for cells exposed to ‘‘aCaP(2.5)polyP” (2.08±0.29); **Fig. 3.4 B**. At time 0 the absorbance values are 1.23±0.18.

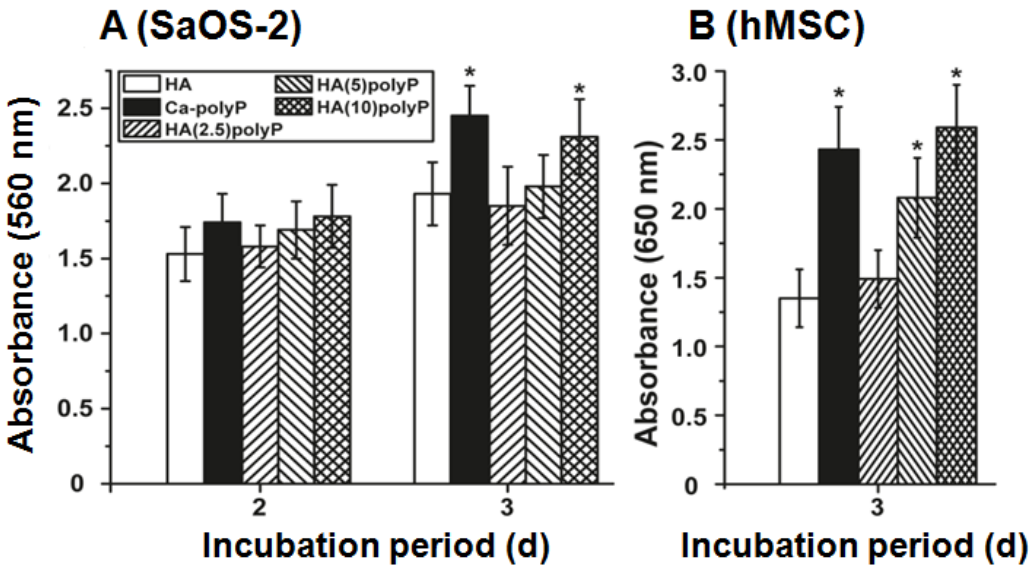

Figure 3.4.

Cell growth response (based on the metabolic activity) of (A) SaOS-2 cells or of (B) hMSCs, cultured onto the different CaP substrates or in the presence of polyP nanoparticles. The assays contained either 10 µg/1 mL of polyP nanoparticles ‘‘aCa–polyP-NP’’ (filled bars), or 100 µg/mL of ‘‘HA” (open bars), ‘‘HA(2.5)polyP” (right hatched bars), ‘‘HA(5)polyP” (left hatched bars) or ‘‘aCaP(10)polyP” (cross-hatched bars). After terminating the cultivation at day 2 (SaOS-2 cells) or day 3 (SaOS-2 cells and hMSCs), the assays were subjected to the MTT assay and the absorbance at 650 nm was determined. Data represent means ± SD of ten independent experiments ($P < 0.01$); the significant correlations have been determined for the values, measured for the respective CaP assays, compared to the HA-exposed cells.

3.4.5 SEM analyses

Cells were cultivated onto either pure ‘‘HA” or onto ‘‘aCaP(10) polyP” disks for 3 d. Then the samples were fixed with paraformaldehyde and inspected by SEM (**Fig. 3.5**). It is

seen that in both assays the cells firmly attach to the substrate both for the ‘‘HA” (**Fig. 3.5A**, **B**) and the ‘‘aCaP(10)polyP” cultures (**Fig. 3.5C, D**). At higher magnification the property of the cells for spreading becomes obvious (**Fig. 3.5B, D**).

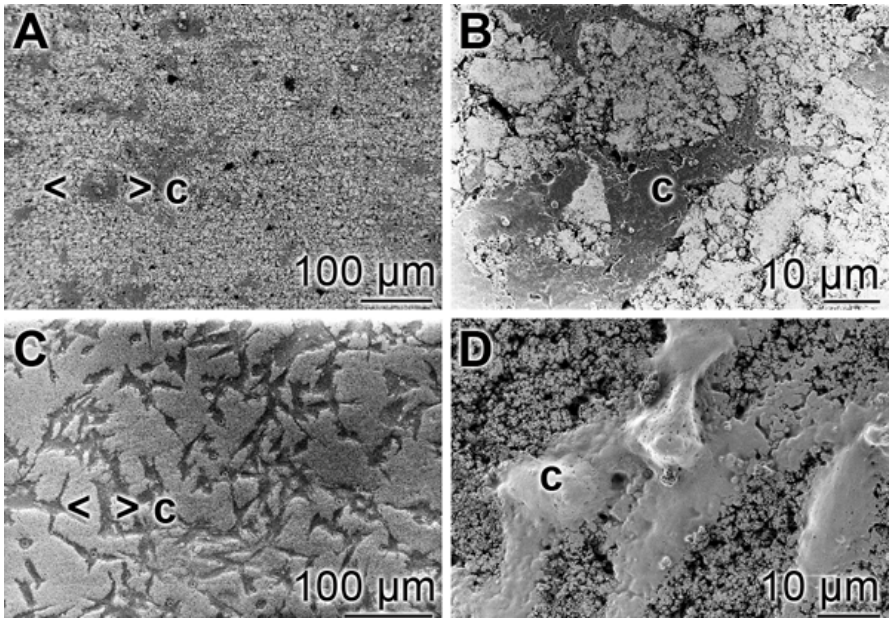

Figure 3.5.
Growth of SaOS-2 cells onto ‘‘HA”(**A** and **B**)or onto CaP, containing 10% polyP,‘‘aCaP(10)polyP” (**C and D**)**.** The cells (**c**) are densely covering the material and show the phenomenon of spreading.

3.4.6 Gene expression propensity of SaOS-2 cells on CaP

The bone-related SaOS-2 cells were cultivated initially for 3 d and then transferred into new medium, lacking or supplemented with MAC and containing also the CaP samples (100 µg/mL) or the polyP nanoparticles (10 µg/mL). Then the incubation was continued for 7 d prior to qRT-PCR analyses to determine the steady state level of transcripts for *COL*-I or *ALP* (**Fig. 3.6**). The determinations revealed that the expression of *COL*-I at the time of seeding the cells is low with 0.26±0.07 expression units, related to the expression of GAPDH. In the absence of MAC and the 7 d presence of the CaP samples or the polyP nanoparticles the expression level significantly increased after incubation with ‘‘HA(2.5)polyP” (to 0.35±0.05), ‘‘HA(5)polyP” (to 0.43±0.05), as well as ‘‘aCaP(10)polyP” (to 0.52±0.06), and, as expected, also for polyP ‘‘aCa–polyP-NP’’ (to

0.63±0.07). With respect to the expression values, measured for the HA-exposed cultures (0.31±0.045), a significant higher steady-state expression level is seen for the ‘‘aCa–polyP-NP’’ (0.63±0.07), as well as for the ‘‘HA (5)polyP” (to 0.43±0.05) and the ‘‘aCaP(10)polyP” series of experiments (to 0.52±0.07); **Fig. 3.6A**. After stimulation of the cells with MAC and exposure to all CaP preparations, the steady-state expression levels of *COL*-I increased significantly, if correlated to the level measured for HA-exposed cultures (0.41±0.05); **Fig. 3.6A**. Strongest upregulation is seen in cells exposed to ‘‘aCaP(10)polyP” (1.38±0.16) or to ‘‘aCaP(10) polyP” (1.03±0.11). A comparable inducing expression pattern is recorded for the *ALP* gene, if correlated to the reference gene GAPDH. Again, in the absence of MAC the *ALP* expression level is lower compared to the values measured for cells incubated for 7 d in the presence of MAC (**Fig. 3.6B**). In the assays without the MAC, but supplemented with polyP nanoparticles (0.17±0.01), or the ‘‘aCaP(10)polyP” sample (0.15±0.03), the increase of the expression level of *ALP*, with respect to the level measured in HA-exposed cultures (0.15±0.03), is significant. However, after exposure to MAC the expression levels for all polyP-containing CaP-preparations are significantly higher than the one seen during the seeding of the cells. The elevated values, for the polyP nanoparticles (1.37±0.15), HA (5)polyP” (0.28±0.03) and for the ‘‘aCaP(10)polyP” sample (0.89±0.09) are statistically significantly if compared to the expression level seen for HA-treated cultures (**Fig. 3.6B**).

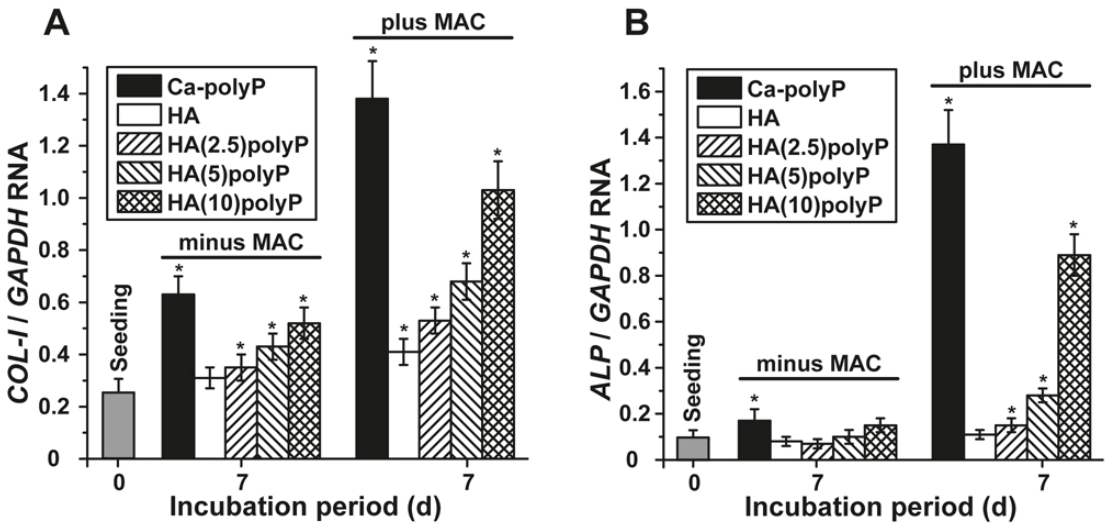

Figure 3.6.

Steady-state expression levels of the genes, encoding (**A**) for collagen type I (*COL-I*) or (**B**) for alkaline phosphatase (*ALP*) in SaOS-2 cells.The cells are exposed to 10 µg/ 1 mL polyP nanoparticles ‘‘aCa–polyP-NP’’ (filled bars), or to 100 mg/mL of ‘‘HA” (open bars), ‘‘HA(2.5)polyP” (right hatched bars), ‘‘HA(5)polyP” (left hatched bars) or ‘‘aCaP (10)polyP” (cross-hatched bars). After the initial incubation for 3 d in the standard medium/serum, the cells were transferred to culture medium/serum lacking (minus MAC) or containing MAC (plus MAC). After the 7 d incubation period the cells were harvested, the RNA extracted and subsequently used for qRT-PCR analyses. The expression values are given as ratios to the reference gene GAPDH. The results are means from 5 parallel experiments; $P < 0.01$. The significance relationship was calculated with respect to the values from HA-exposed cultures.

3.5 Discussion

The major inorganic bone scaffold is HA. Following the concept of biomineralization, physiological macromolecules display important control functions during the nucleation and subsequent growth of the biomaterial, e.g. of HA. In the past, primarily organic macromolecules have been considered as regulators of these processes [50, 51]. The studies focused mainly on the following three aspects, concerning recognition sites of the inorganic–organic interfaces between the template and the inorganic biomaterial: (i) the electrostatic accumulation of cations, (ii) the structure-giving elements, and (iii) the stereochemical requirements of the templates for the controlled biomineralization. It turned out that the surface charge is crucial for seed formation. Focusing on HA,

negatively charged surfaces are always favorable for a heterogeneous nucleation of HA in a supersaturated solution, like in ‘‘simulated body fluid’’, or Kokubo solution [52], while positive surfaces inhibit nucleation [53, 54]. One major reason for this selection is that the Ca^{2+} ions accumulate at those negatively charged surface spots with the result that the adjusting process of supersaturation triggers the bio-seed formation. This view is supported by the finding that bone sialoprotein, rich in poly-carboxylate (glutamic acid) groups, and poly(glutamic acid) induces nucleation of HA [55]. However, the initial transformation reaction(s), resulting in the formation of nuclei for HA/bone formation is/are still unclear [56]. Those data suggest that HA nucleus formation, preceding HA crystal growth is the rate limiting step during bone mineralization. HA crystal growth is driven by the supply of Ca^{2+} and PO_4^{3-} ions. Growing evidence is available indicating that the initial CaP mineral deposit during bone formation is ACP [19]. In turn, ACP is transformed *via* a heterogeneous nucleation pathway to HA [57]. Subsequently, a nucleation-growth-agglomeration process of the HA particles takes place around the fibrillar scaffold during bone formation. By analyzing the presented results and according to other studies, the addition of polyP restricts growth along the side faces by Ca-polyP particles while activating growth along the end direction (c-axis), resulting in a high aspect ratio of the growth of HA nanorods [58]. When the concentration of polyP increased, spherical particles were obtained with hollow porous structure. This could be due to an encapsulation of ACP by polyP, resulting in an inhibition of a transformation to HA [59]. Here we need further studies on the growth kinetics.

In the recent years it became overt that besides of organic polymers, the physiological inorganic polymer, polyP (reviewed in: [60]), might play a decisive role during the initiation, growth and maintenance of biominerals [61, 62]. PolyP was found to supply ortho-phosphate units to the formation of ACP and subsequently also to the transition of ACP to HA [60]. This polymer, polyP, is metabolically produced in blood platelets in the vicinity of bone defects (reviewed in: [61, 62]). In view of earlier findings, showing that additives, e.g. silica and zirconia, can stabilize the transformation of ACP to HA [63], we asked if also polyP has this potential. If so, then it is feasible that this polymer will

cause this delaying effect only in the amorphous phase. Therefore, we introduced a recently developed method to fabricate nanoparticles/nanospheres from polyP and Ca^{2+} [37, 38]. This particles display morphogenetic activity, e.g. induction of genes, encoding for a series of collagens and for *ALP*, as well as an induction of ATP generation in bone cells [37, 64]. In the present study Na–polyP was added together with $CaCl_2$ and $(NH_4)_2HPO_4$, the substrates for HA formation in aqueous solution, during the precipitation procedure. It is well known that Na–polyP is readily chelating Ca^{2+} und forms insoluble precipitates. In turn, addition of Na–polyP to $CaCl_2$ and $(NH_4)_2HPO_4$, added in different ratios, will result in a co-precipitation of CaP/polyP mineral deposits. In the present study it is shown that a content of 10 wt.% polyP prevents the formation of crystalline HA under simultaneous fabrication of amorphous polyP/HA hybrid ≈100 nm sized particles.

The application of crystalline HA, even though being biocompatible, is currently limited to powders, coatings and porous bodies, and non-load-bearing implants due to the adverse physical (low solubility) and mechanical properties (brittleness) [65]. Those two disadvantages can be circumvented if CaP, also in the hybrid form, can be synthesized in an amorphous phase. It has been proven that implants, coated with thin ACP layers, show an improved implant fixation, combined with an accelerated bone response [66]. The data presented here revealed that polyphosphated CaP shows, in combination with cell growth promoting activity a distinct morphogenetic activity. The latter property has been deduced from the observation that polyP/CaP ("aCaP(10)polyP"), causes a strong upregulation of the two marker genes for bone formation, *collagen type I* and *ALP*. Interestingly enough the potency of "aCaP(10)polyP" is comparable to Ca–polyP, at least under the experimental conditions used and using the bone-related SaOS-2 cells. The essential role of *COL-I*, as matrix and template, during bone formation is well established [67]. The importance of *ALP* as an enzyme providing ortho-phosphate to the osteoblasts for the formation of biomineral is proven [68]. In addition, both *COL-I* and *ALP* gene expression is a reliable marker for differentiation and proliferation [69]. It is interesting to note that crystalline/sintered HA elicits morphogenetic activity, e.g.

by inducing the genes *COL-I* and *ALP*, primarily in those scaffolds containing growth factors, like bone morphogenic protein-2 [70].

The addition of polyP to the substrates for HA particle formation, to $CaCl_2$ and $(NH_4)_2HPO_4$, causes a change in the morphology of the deposits. While the synthesized HA crystals have dimensions of 39±8 nm to 14±4 nm, similar to those in the literature[71] and [72], the CaP samples enriched with polyP grow to larger sizes, 42 ± 10 nm to 9 ± 5 nm for "HA(2.5)polyP", and 56±12 to 6±3 nm for "HA(5)polyP". This increase in accordance with published data revealing that additives to HA usually result in an increase in the size of the crystal deposits [73]. HA crystals expose ionic phosphate groups at their surfaces [74] allowing Ca^{2+} to bind and very likely to form also bridges to the phosphate groups within the polyP chain. This would imply that polyP accumulates at the surface of the CaP deposits, crystals and spheres. In line with this assumption we assign the rim of the spherical CaP–polyP ("aCaP(10)polyP") particles (**Fig. 3.3D**) to polyP. The data recently published suggest that polyP and/or ortho phosphate have the potential to "fuse" with the HA surfaces [75].

In conclusion, we interpret the data gathered here through the following reactions/interactions (**Fig. 3.7**). In the presence of the substrates for the CaP deposit formation, Ca^{2+} and PO_4^{3-} ions, HA is formed, starting from ACP in a temperature-dependent transformation reaction [76]; at 37 °C this process would last 60 min at pH 8.0. In the presence of polyP, with a final content of <10 wt.% polyP, "HA(2.5)polyP" and "HA(5)polyP", still crystal-like structures are formed that turn to become spherical if the polyP concentration is ⩾10 wt.% polyP, "aCaP(10)polyP". The data suggest that around the CaP crystals, the polyP is linked *via* Ca^{2+} to the ionic phosphate groups to CaP. Since the amorphous CaP, polyP–CaP, elicits morphogenetic activity this material is a promising candidate to be used as artificial bone implant, fabricated from physiological metabolites/polymers.

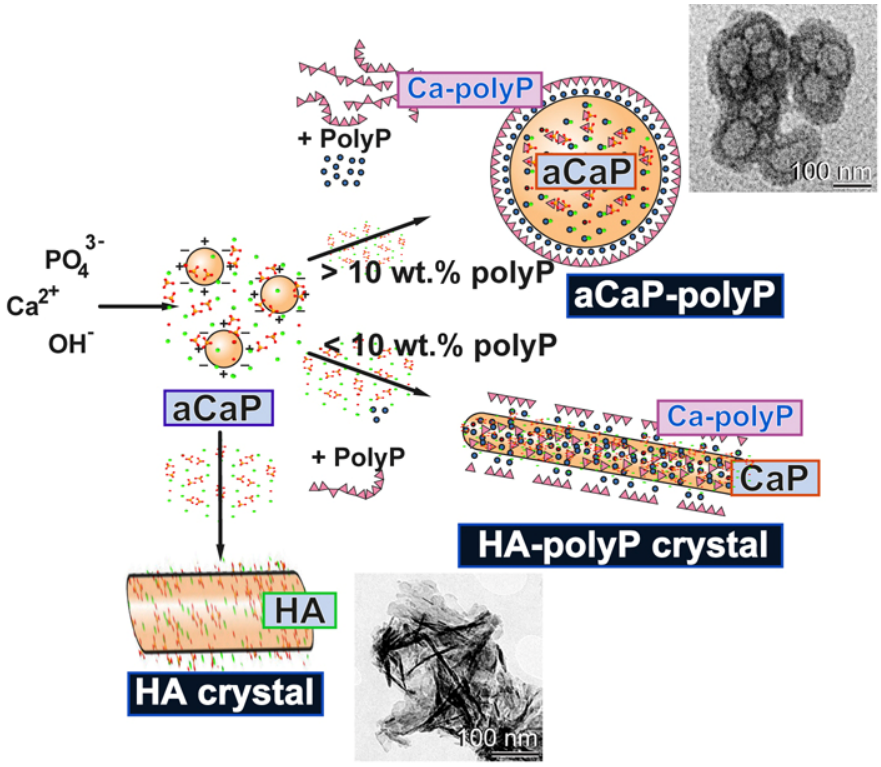

Figure 3.7.

Schematic outlines of the formation of amorphous CaP (aCaP) from the precursors Ca^{2+}, PO_4^{3-} and OH^-.The aCaP undergoes maturation to crystalline HA, or in the presence of <10 wt.% polyP likewise to crystalline CaP (see insert at bottom, showing CaP crystals; SEM image). If the content of polyP increases to P10 wt.% polyP in the CaP precipitates spheroidal amorphous aCaP–polyP is formed (see insert at top; SEM image).

3.6 References

1. E. Bonucci, Calcification in Biological Systems, CRC Press, Boca Raton, 1992.

2. M.J. Olszta, X. Cheng, S.S. Jee, R. Kumar, Y.Y. Kim, M.J. Kaufman, E.P. Douglas, L.B. Gower, Bone structure and formation: a new perspective, Mater. Sci. Eng. R. 58 (2007) 77–116.

3. N. Shepard, Role of proteoglycans in calcification, in: E. Bonucci (Ed.), Calcification in Biological Systems, CRC Press, Boca Raton, 1992, pp. 41–58.

4. G.J. Tortora, Chapter 5: histology of bone tissue, in: Principles of Human Anatomy, Harper Collines College Publishers, NY, 1995, pp. 796–834.

5. N. Reznikov, R. Shahar, S. Weiner, Three-dimensional structure of human lamellar bone: the presence of two different materials and new insights into the hierarchical organization, Bone 59 (2014) 93–104.

6. S. Boonrungsiman, E. Gentleman, R. Carzaniga, N.D. Evans, D.W. McComb, A.E. Porter, M.M. Stevens, The role of intracellular calcium phosphate in osteoblast mediated bone apatite formation, Proc. Nat. Acad. Sci. U.S.A. 109 (2012) 14170–14175.

7. M.J. Glimcher, Recent studies of the mineral phase in bone and its possible linkage to the organic matrix by protein-bound phosphate bonds, Philos. Trans. R. Soc. London B Biol. Sci. 304 (1984) 479–508.

8. H.C. Anderson, Molecular biology of matrix vesicles, Clin. Orthop. Relat. Res. 314 (1995) 266–280.

9. J. Mahamid, A. Sharir, L. Addadi, S. Weiner, Amorphous calcium phosphate is a major component of the forming fin bones of zebrafish: indications for an amorphous precursor phase, Proc. Nat. Acad. Sci. U.S.A. 105 (2008) 12748–12753.

10. J. Mahamid, A. Sharir, D. Gur, E. Zelzer, L. Addadi, S. Weiner, Bone mineralization proceeds through intracellular calcium phosphate loaded vesicles: a cryo-electron microscopy study, J. Struct. Biol. 174 (2011) 527–535.

11. W.E.G. Müller, H.C. Schröder, U. Schlossmacher, V.A. Grebenjuk, H. Ushijima, X. H. Wang, Induction of carbonic anhydrase in SaOS-2 cells, exposed to bicarbonate and consequences for calcium phosphate crystal formation, Biomaterials 34 (2013) 8671–8680.

12. W.E.G. Müller, H.C. Schröder, E. Tolba, M. Neufurth, B. Diehl-Seifert, X.H. Wang, Mineralization of bone-related SaOS-2 cells under physiological hypoxic conditions, FEBS J. (2015), http://dx.doi.org/10.1111/febs.13552.

13. H.S. Lee, T.H. Ha, K. Kim, Fabrication of unusually stable amorphous calcium carbonate in an ethanol medium, Mater. Chem. Phys. 93 (2005) 376–382.

14. X.H. Wang, H.C. Schröder, W.E.G. Müller, Enzyme-based biosilica and biocalcite: biomaterials for the future in regenerative medicine, Trends Biotechnol. 32 (2014) 441–447.

15. W.E.G. Müller, M. Neufurth, J. Huang, K. Wang, Q. Feng, H.C. Schröder, B. Diehl-Seifert, R. Muñoz-Espí, X.H. Wang, Non-enzymatic transformation of amorphous CaCO3 into calcium phosphate mineral after exposure to sodium phosphate in-vitro : implications for in vivo hydroxyapatite bone formation, ChemBioChem 16 (2015) 1323–1332.

16. W.E.G. Müller, M. Wiens, T. Adell, V. Gamulin, H.C. Schröder, I.M. Müller, Bauplan of Urmetazoa: basis for genetic complexity of Metazoa, Int. Rev. Cytol. 235 (2004) 53–92.

17. E.D. Pellegrino, R.M. Biltz, Calcium carbonate in medullary bone, Calcif Tissue Res. 6 (1970) 168–171.

18. S. Mann, S.B. Parker, M.D. Ross, A.J. Skarnulis, R.J. Williams, The ultrastructure of the calcium carbonate balance organs of the inner ear: an ultra-high resolution electron microscopy study, Proc. R. Soc. London B Biol. Sci. 218 (1983) 415–424.

19. F. Nudelman, K. Pieterse, A. George, P.H. Bomans, H. Friedrich, L.J. Brylka, P.A. Hilbers, G. de With, N.A. Sommerdijk, The role of collagen in bone apatite formation in the presence of hydroxyapatite nucleation inhibitors, Nat. Mater. 9 (2010) 1004–1009.

20. E. Beniash, R.A. Metzler, R.S. Lam, P.U. Gilbert, Transient amorphous calcium phosphate in forming enamel, J. Struct. Biol. 166 (2009) 133–143.

21. J. Mahamid, B. Aichmayer, E. Shimoni, R. Ziblat, C. Li, S. Siegel, O. Paris, P. Fratzl, S. Weiner, L. Addadi, Mapping amorphous calcium phosphate transformation into crystalline mineral from the cell to the bone in zebrafish fin rays, Proc. Nat. Acad. Sci. U.S.A. 107 (2010) 6316–6321.

22. D. Gebauer, A. Völkel, H. Cölfen, Stable prenucleation calcium carbonate clusters, Science 322 (2008) 1819–1822.

23. E.M. Pouget, P.H. Bomans, J.A. Goos, P.M. Frederik, G. de With, N.A. Sommerdijk, The initial stages of template-controlled CaCO3 formation revealed by cryo-TEM, Science 323 (2009) 1455–1458.

24. A.R. Ten Cate, Oral Histology: DEVELOPMENT, Structure, and Function, fourth ed., Mosby, Toronto, 1994.

25. A.S. Deshpande, E. Beniash, Bioinspired synthesis of mineralized collagen fibrils, Cryst. Growth Des. 8 (2008) 3084–3090.

26. P.A. Price, D. Toroian, J.E. Lim, Mineralization by inhibitor exclusion: the calcification of collagen with fetuin, J. Biol. Chem. 284 (2009) 17092–17101.

27. M. Hallman, A. Cederlund, S. Lindskog, S. Lundgren, L. Sennerby, A clinical histologic study of bovine hydroxyapatite in combination with autogenous bone and fibrin glue for maxillary sinus floor augmentation, Clin. Oral Implants Res. 12 (2001) 135–143.

28. D.W. Hutmacher, J.T. Schantz, C.X. Lam, K.C. Tan, T.C. Lim, State of the art and future directions of scaffold-based bone engineering from a biomaterials perspective, J. Tissue Eng. Regener. Med. 1 (2007) 245–260.

29. R.Z. LeGeros, Calcium phosphate-based osteoinductive materials, Chem. Rev. 108 (2008) 4742–4753.

30. J.H. Shepherd, S.M. Best, Calcium phosphate scaffolds for bone repair, JOM 63 (2011) 83–92.

31. M. Vallet-Regí, Ceramics for medical applications, J. Chem. Soc., Dalton Trans. (2001) 97–108.

32. K. Lin, C. Wu, J. Chang, Advances in synthesis of calcium phosphate crystals with controlled size and shape, Acta Biomater. 10 (2014) 4071–4102.

33. K. Kobayashi, T. Anada, T. Handa, N. Kanda, M. Yoshinari, T. Takahashi, O. Suzuki, Osteoconductive property of a mechanical mixture of octacalcium phosphate and amorphous calcium phosphate, ACS Appl. Mater. Interfaces 6 (2014) 22602–22611.

34. A.K. Nayak, Hydroxyapatite synthesis methodologies: an overview, Int. J. Chem. Tech. Res. 2 (2010) 903–907.

35. J. Fogh, J.M. Fogh, T. Orfeo, One hundred and twenty-seven cultured human tumor cell lines producing tumors in nude mice, J. Nat. Cancer Inst. 59 (1977) 221–226.

36. X.H. Wang, H.C. Schröder, W.E.G. Müller, Enzymatically synthesized inorganic polymers as morphogenetically active bone scaffolds: application in regenerative medicine, Int. Rev. Cell Mol. Biol. 313 (2014) 27–77.

37. W.E.G. Müller, E. Tolba, H.C. Schröder, B. Diehl-Seifert, X.H. Wang, Retinol encapsulated into amorphous Ca2+ polyphosphate nanospheres acts synergistically in MC3T3-E1 cells, Eur. J. Pharm. Biopharm. 93 (2015) 214–223.

38. W.E.G. Müller, E. Tolba, H.C. Schröder, S. Wang, G. Glaßer, R. Muñoz-Espí, T. Link, X.H. Wang, A new polyphosphate calcium material with morphogenetic activity, Mater. Lett. 148 (2015) 163–166.

39. S. Raynaud, E. Champion, D. Bernache-Assollant, P. Thomas, Calcium phosphate apatites with variable Ca/P atomic ratio I. Synthesis, characterisation and thermal stability of powders, Biomaterials 23 (2002) 1065–1072.

40. D.S.H. Lee, Y. Pai, S. Chang, Effect of thermal treatment of the hydroxyapatite powders on the micropore and microstructure of porous biphasic calcium phosphate composite granules, J. Biomat. Nanobiotechnol. 4 (2013) 114–118.

41. U. Schloßmacher, H.C. Schröder, X.H. Wang, Q. Feng, B. Diehl-Seifert, S. Neumann, A. Trautwein, W.E.G. Müller, Alginate/silica composite hydrogel as a potential morphogenetically active scaffold for three-dimensional tissue engineering, RSC Adv. 3 (2013) 11185–11194.

42. M. Wiens, X.H. Wang, H.C. Schröder, U. Kolb, U. Schlossmacher, H. Ushijima, W. E.G. Müller, The role of biosilica in the osteoprotegerin/RANKL ratio in human osteoblast-like cells, Biomaterials 31 (2010) 7716–7725.

43. M. Wiens, X.H. Wang, U. Schlossmacher, I. Lieberwirth, G. Glasser, H. Ushijima, H.C. Schröder, W.E.G. Müller, Osteogenic potential of biosilica on human osteoblast like (SaOS-2) cells, Calcif Tissue Int. 87 (2010) 513–524.

44. X.H. Wang, H.C. Schröder, V. Grebenjuk, B. Diehl-Seifert, V. Mailänder, R. Steffen, U. Schloßmacher, W.E.G. Müller, The marine sponge-derived inorganic polymers,

biosilica and polyphosphate, as morphogenetically active matrices/ scaffolds for differentiation of human multipotent stromal cells: potential application in 3D printing and distraction osteogenesis, Mar. Drugs 12 (2014) 1131–1147.

45. X.H. Wang, H.C. Schröder, U. Schlossmacher, M. Neufurth, Q. Feng, B. Diehl-Seifert, W.E.G. Müller, Modulation of the initial mineralization process of SaOS-2 cells by carbonic anhydrase activators and polyphosphate, Calcif Tissue Int. 94 (2014) 495 509.

46. H.C. Schröder, X.H. Wang, M. Wiens, B. Diehl-Seifert, K. Kropf, U. Schloßmacher, W.E.G. Müller, Silicate modulates the cross-talk between osteoblasts (SaOS-2) and osteoclasts (RAW 264.7 cells): inhibition of osteoclast growth and differentiation, J. Cell. Biochem. 113 (2012) 3197–3206.

47. L. Sachs, Angewandte Statistik, Springer, Berlin, 1984. p. 242.

48. M.C. Chang, C.C. Ko, W.H. Douglas, Preparation of hydroxyapatite-gelatin nanocomposite, Biomaterials 24 (2003) 2853–2862.

49. P.S. Prevéy, X-Ray diffraction characterization of crystallinity and phase composition in plasma-sprayed hydroxyapatite coatings, J. Therm. Spray Technol. 9 (2000) 369–376.

50. S. Mann, Molecular recognition in biomineralization, Nature 332 (1988) 119– 124.

51. K. Simkiss, K.M. Wilbur, Biomineralization – Cell Biology and Mineral Deposition, Academic Press, San Diego, CA, 1989. pp. 284–293.

52. T. Kokubo, Formation of biologically active bone-like apatite on metals, polymers by a biomimetic process, Thermochim. Acta 280–281 (1996) 479– 490.

53. P. Calvert, S. Mann, The negative side of crystal growth, Nature 386 (1997) 127–128.

54. S. Hayakawa, K. Tsuru, C. Ohtsuki, A. Osaka, Mechanism of apatite formation on a sodium silicate glass in a simulated body fluid, J. Am. Ceram. Soc. 82 (1999) 2155–2160.

55. G.K. Hunter, H.A. Goldberg, Modulation of crystal formation by bone phosphoproteins: role of glutamic acid-rich sequences in the nucleation of hydroxyapatite by bone sialoprotein, Biochem. J. 302 (1994)175–179.

56. N. Ito, M. Kamitakahara, K. Ioku, Observation of transformation behavior of octacalcium phosphate to hydroxyapatite, Key Eng. Mater. 529–530 (2013) 11–14.

57. S. Jiang, H. Pan, Y. Chen, X. Xu, R. Tang, Amorphous calcium phosphate phasemediated crystal nucleation kinetics and pathway, Faraday Discuss. 179 (2015) 451–461.

58. A.J. Nathanael, S.S. Han, T.H. Oh, Polymer-assisted hydrothermal synthesis of hierarchically arranged hydroxyapatite nanoceramic, J. Nanomater. (2013). doi.org/10.1155/2013/962026.

59. S.H. Jeon, P. Xu, B. Zhang, N.H. Mack, H. Tsai, L.Y. Chiang, H.L. Wang, Polymerassisted preparation of metal nanoparticles with controlled size and morphology, J. Mater. Chem. 21 (2011) 2550–2554.

60. H.C. Schröder, W.E.G. Müller (Eds.), Inorganic Polyphosphates; Biochemistry, Biology, Biotechnology, Progress in Molecular and Subcellular Biology, vol. 23, Springer Verlag, Berlin, 1999.

61. X.H. Wang, H.C. Schröder, W.E.G. Müller, Polyphosphate as a metabolic fuel in Metazoa: A foundational breakthrough invention for biomedical applications, Biotechnology J (2015), in press.

62. W.E.G. Müller, E. Tolba, H.C. Schröder, X.H. Wang, Polyphosphate: a morphogenetically active implant material serving as metabolic fuel for bone regeneration, Macromol. Biosci. (2015), http://dx.doi.org/10.1002/mabi.201500100.

63. D. Skrtic, J.M. Antonucci, E.D. Eanes, R.T. Brunworth, Silica- and zirconiahybridized amorphous calcium phosphate: effect on transformation to hydroxyapatite, J. Biomed. Mater. Res. 59 (2002) 597–604.

64. W.E.G. Müller, E. Tolba, Q. Feng, H.C. Schröder, J.S. Markl, M. Kokkinopoulou, X. H. Wang, Amorphous Ca2+ polyphosphate nanoparticles regulate the ATP level in bone-like SaOS-2 cells, J. Cell. Sci. (2015), http://dx.doi.org/10.1242/ jcs.170605.

65. M.C. Wang, H.T. Chena, W.J. Shih, H.F. Chang, M.H. Hon, I.M. Hung, Crystalline size, microstructure and biocompatibility of hydroxyapatite nanopowders by hydrolysis of calcium hydrogen phosphate de hydrate (DCPD), Ceram. Int. 41 (2015) 2999–3008.

66. S. Yokota, N. Nishiwaki, K. Ueda, T. Narushima, H. Kawamura, T. Takahashi, Evaluation of thin amorphous calcium phosphate coatings on titanium dental implants deposited using magnetron sputtering, Implant Dent. 23 (2014) 343–350.

67. P. Garnero, The role of collagen organization on the properties of bone, Calcif. Tissue Int. 97 (2015) 229–240.

68. E.E. Golub, K. Boesze-Battaglia, The role of alkaline phosphatase in mineralization, Curr. Opin. Orthop. 18 (2007) 444–448.

69. H.J. Prins, A.K. Braat, D. Gawlitta, W.J. Dhert, D.A. Egan, E. Tijssen-Slump, H. Yuan, P.J. Coffer, H. Rozemuller, A.C. Martens, In-vitro induction of alkaline phosphatase levels predicts in vivo bone forming capacity of human bone marrow stromal cells, Stem Cell Res. 12 (2014) 428–440.

70. K. Na, S.W. Kim, B.K. Sun, D.G. Woo, H.N. Yang, H.M. Chung, K.H. Park, Osteogenic differentiation of rabbit mesenchymal stem cells in thermoreversible hydrogel constructs containing hydroxyapatite and bone morphogenic protein-2 (BMP-2), Biomaterials 28 (2007) 2631–2637.

71. I. Cacciotti, A. Bianco, M. Lombardi, L. Montanaro, Mg-substituted hydroxyapatite nanopowders: Synthesis, thermal stability and sintering behavior, J. Eur. Ceram. Soc. 29 (2009) 2969–2978.

72. A. Zanotto, M.L. Saladino, D.C. Martino, E. Caponetti, Influence of temperature on calcium hydroxyapatite nanopowders, Adv. Nanoparticles 1 (2012) 21–28.

73. M. Sadat-Shojai, M.T. Khorasani, E. Dinpanah-Khoshdargi, A. Jamshidi, Synthesis methods for nanosized hydroxyapatite with diverse structures, Acta Biomater. 9 (2013) 7591–7621.

74. I.S. Harding, N. Rashid, K.A. Hing, Surface charge and the effect of excess calcium ions on the hydroxyapatite surface, Biomaterials 26 (2005) 6818–6826.

75. M. Rivas, J. Casanova, L.J. del Valle, O. Bertran, G. Revilla-López, P. Turon, J. Puiggalí, C. Alemán, An experimental-computer modeling study of inorganic phosphates surface adsorption on hydroxyapatite particles, Dalton Trans. 44 (2015) 9980–9991.

76. A.L. Boskey, A.S. Posner, Conversion of amorphous calcium phosphate to microcrystalline hydroxyapatite: a pH-dependent solution-mediated, solid-solid conversion, J. Phys. Chem. 77 (1973) 2313–2317.

Chapter 4:

High biocompatibility and improved osteogenic potential of amorphous calcium carbonate/vaterite

4.1 Introduction

Calcium carbonate ($CaCO_3$), the world largest geochemical reservoir for carbon (1) exists in three major crystalline polymorphs, as calcite, aragonite, and vaterite (reviewed in: ref.2). The amorphous calcium carbonate (ACC) is the least stable polymorph of $CaCO_3$ and vaterite the thermodynamically least stable form of crystalline $CaCO_3$. While calcite and aragonite are common in biological and geological samples, vaterite is metastable and rare in nature (reviewed in: ref.3). Vaterite is occasionally found in biological materials, *e.g.* as skeletal element in the mussel *Hyriopsis cumingii* and in otoliths (reviewed in: refs.4,5). It is remarkable that in fish two of the three pairs of otoliths, the sagittae and the lapilli are composed of aragonite, while the asteriscus are made of vaterite(6). Biochemical/chemical studies revealed that the mature crystals of otoliths are metabolically inert crystalline skeletal structures which run in parallel with organic matrices that vary. This observation suggested that those organics might act as templates as well as structure-guiding molecules during the deposition of the mineral phase from the amorphous to the distinct mineral phase (3) The importance of the organic components as structure and function orientating guide within the skeletal inorganic deposits has been postulated and finally proven in several biological systems, e.g. in shell layers of some mollusks (7) or in calcareous spicules from sponges (8). The crucial role of acidic matrix macromolecules, intimately involved in growth of biological crystals, has been highlighted already in 1985 (9) and later corroborated multifold, e.g. in the hic31 framework-matrix protein within the prismatic-layer of *H. Cumingii* (10).

The basic building blocks of bone comprise, besides of water and collagen, dahllite a form of carbonated apatite [$Ca_5(PO_4,CO_3)_3(OH)$] (reviewed in: refs.11,12). This crystalline

mineral is likely to be formed from amorphous calcium phosphate (ACP) (13). Very recently biochemical and dispersive spectroscopic evidence suggested that it is ACC that acts as bioseed for the formation of carbonated apatite (14), a process that is accelerated by carbonic anhydrase(s) (CA), very likely by the soluble CA-II isoform (14) and/or the cell-membrane-associated CA-IX (15-17). Based on these evidences the following three mechanically distinct phases resulting in bone hydroxyapatite (HA) formation can be distinguished (18); first, enzymatic formation of ACC bioseeds *via* CAes, second, non-enzymatic exchange of carbonate ions by phosphate (19) under formation of ACP and third, transition of ACP to the crystalline phase carbonated apatite/HA. It should be mentioned that polyphosphate (polyP), which is present in considerable amounts in the blood and in larger extent in blood platelets, has been implicated as a phosphate source for the formation of the bone calcium phosphate deposits (reviewed in:ref.18*).* From this polymer ortho-phosphate is enzymatically removed *via* the alkaline phosphatase (*ALP*) (20) which might serve as donor for bone mineralization. In addition, octacalcium phosphate and osteopontin, phosphorylated bone matrix glycoproteins, have been discussed as precursors of biological apatite crystal formation (21).

In the recent years, bioinspired as well as biomimetic approaches have been undertaken to develop functional materials capable of promoting bone tissue regeneration. Since collagen and HA are dominant in bone, biomaterials containing chemical-inducers of any of these materials or both have been extensively explored in bone tissue engineering with the hope to accelerate bone regeneration (reviewed in: ref.22). Calcium phosphate salts in general and HA in particular have been found to be superior as regenerative materials than their non-mineralized counterparts (reviewed in: ref.23). The application of ACC as a potential regeneration-inducing/supporting material has been hampered by the fact that ACC, as such, is not stable. Stabilization of ACC *in vivo* is regulated by specialized proteins, often in combination with Mg^{2+}, while under in-vitro conditions non-biogenic additives, like soluble polycarboxylates, again Mg^{2+}, triphosphate, or polyphosphonate species freeze ACC to a relative stable phase (see: refs.24,25); also freeze-drying has been determined to stabilize ACC (26). In contrast, vaterite is stable

enough to allow dissociation and in turn might act as a potential ion buffering system for bone regeneration and by that could modify transformation processes from $CaCO_3$ to HA (27).

In the present study we describe that polyP can stabilize the ACC phase. Previously it has been reported that soluble Na-polyP, spiked with defined molar ratios of Ca^{2+}, can be processed to solid nanoscaled nano-/microparticles that remain amorphous(28,29). In contrast, other polyP based ceramics have been prepared as crystalline materials at high temperature (30, 31) or as phosphate glass of variable chemical and physical structures as well as particle morphologies in the microsize range (32). In our procedure, at a level of 5% [w/w], polyP considerably suppresses the transformation of ACC to crystalline $CaCO_3$ and at a percentage of 10% [w/w] the polymer almost completely blocks this process. This finding might have important implications since polyP is a natural polymer which is abundantly present in the circulated blood and also in blood platelets (33, 34). Added to $CaCO_3$, polyP binds Ca^{2+} to the carbonate group and, by that, interferes with the transformation process to the crystalline forms of $CaCO_3$. Previously, polyP has been found to act as a morphogenetically active inorganic molecule on bone cells and induces their mineralization potency. The present study shows that $CaCO_3$, containing 5 or 10% [w/w] of polyP, comprises osteogenic potential in SaOS-2 cells as well as in human mesenchymal stem cells (MSC) by inducing *ALP* gene expression. In addition, it is shown that this calcium carbonate/calcium phosphate hybrid material is biocompatible and supports regeneration *in vivo*.

4.2 Material and Methods

4.2.1 Materials

Na-polyphosphate (Na-polyP) with an average chain length of ≈40 phosphate units was obtained from Chemische Fabrik Budenheim (Budenheim, Germany). Poly(D,L-lactide-*co*-glycolide) (PLGA; lactide:glycolide [75:25]; mol.wt. 66,000–107,000; P1941) was obtained from Sigma (Taufkirchen, Germany).

4.2.2 Preparation of Calcium carbonate microparticles

Ca-carbonate ($CaCO_3$) was prepared by direct precipitation in aqueous solutions (at room temperature), using $CaCl_2 \bullet 2H_2O$ solution (#223506; Sigma-Aldrich, Taufkirchen, Germany) and Na_2CO_3 solution (#85195; Fluka-Sigma) at equimolar concentration ratio between Ca^{2+} and CO_3^{2-} through rapid mixing. In brief, 20 ml of 0.1 M NaOH was added to 1.05 g Na_2CO_3 and then diluted with 30 mL of deionized water. This solution was combined with 50 mL of water containing 1.47 g $CaCl_2 \bullet 2H_2O$ and then rapidly stirred, immediately followed by filtration. The $CaCO_3$ precipitate (termed "CC") was rinsed with acetone to dry the solid material; scheme in **Fig. 4.1.**

To study the effect of polyP on precipitated $CaCO_3$ the solution of 20 ml of 0.1 M NaOH was supplemented with 0.05 g or 0.1 g of Na-polyP *to which* 1.05 g of Na_2CO_3 was added; subsequently this solution was diluted with 30 mL of deionized water. Then 50 mL water, containing 1.47 g $CaCl_2 \bullet 2H_2O$, was added. By this, 5% [w/w] (addition of 0.05 g Na-polyP) and 10% [w/w] (0.1 g Na-polyP) of polyP, respectively, was added to the $CaCO_3$precipitation assay. The suspensions obtained were filtrated, washed with acetone and dried at room temperature. The samples were termed "CCP5" (0.05 g Na-polyP per $CaCO_3$ precipitation assay) or "CCP10" (0.1 g).

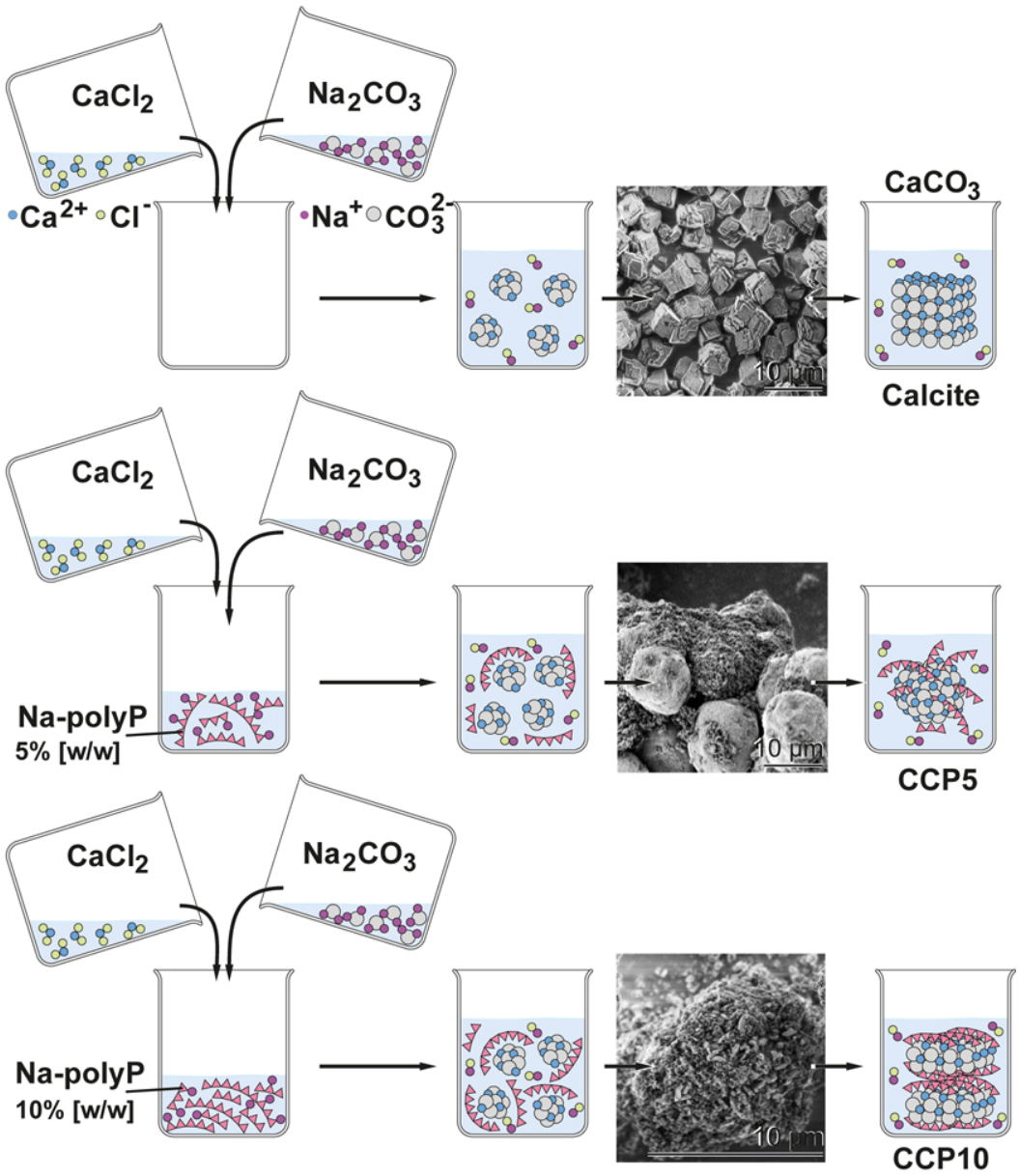

Figure 4.1.

Preparation of calcite and $CaCO_3$ supplemented with polyP (scheme). The inserts show the SEM images of the respective product.

4.3 Materials characterization

4.3.1 X-ray diffraction analyses

X-ray diffraction (XRD) experiments were performed as described previously (35). The patterns of dried powders were registered on a Philips PW 1820 diffractometer with $Cu_{K\alpha}$ radiation (λ = 1.5418 Å, 40 kV, 30 mA) in the range 2ϑ = 5–65° ($\Delta 2\vartheta$ = 0.02, Δt = 5 s). The calcite and vaterite phases were identified as described (36, 37).

4.3.2 Fourier transformed infrared spectroscopy

Fourier transformed infrared spectroscopic (FTIR) analyses were performed with micro-milled (agate mortar and pestle) mineral powder in an ATR (attenuated total reflectance)-FTIR spectroscope/Varian 660-IR spectrometer (Agilent, Santa Clara, CA), fitted with a Golden Gate ATR unit (Specac, Orpington, UK) (19). The spectra given represent the average of 100 scans with a spectral resolution of 4 cm^{-1} (typically 550-4000 cm^{-1}). The baseline correction, smoothing, and analysis of the spectra were achieved with the Varian 660-IR software package 5.2.0 (Agilent). Graphical display and annotation of the spectra were performed with Origin Pro (version 8.5.1; OriginLab, Northampton, MA).

4.3.3 Scanning electron microscopic studies

Scanning electron microscopic (SEM) analyses were performed with an SU 8000 instrument (Hitachi High-Technologies Europe, Krefeld, Germany), at low voltage (1 kV) as described (38). The particle size was determined with a particle size analyzer (ImageJ); 25-50 crystals were evaluated.

4.3.4 Release of Ca^{2+} from the $CaCO_3$ particles

In separate assays 100 µg/ml of either calcite or “CCP10” were added into an Eppendorf tube containing 1 mL of 1 M Tris-HCl (pH 7.4). After incubating at room temperature for 2 h, 2 d, 3 d and 8 d samples of 100 µl were taken, centrifuged and the supernatant analyzed for Ca^{2+} concentration. The determination was performed with the photometric test kit (Millipore/Merck Chemicals, Darmstadt, Germany; article no.

100858 “Calcium Cell Test”) as described in the Instructions of the Manufacturer. The blank values were subtracted from the test assays.

4.3.5 Cultivation of SaOS-2 cells

The human osteogenic sarcoma cells SaOS-2 were cultured in McCoy’s medium (Biochrom-Seromed, Berlin, Germany), supplemented with 2 mM L-glutamine and enriched with 15% heat-inactivated fetal calf serum (FCS) (39) Antibiotics, 100 units/mL penicillin and 100 µg/mL streptomycin, were likewise added. The cells were incubated in 25-cm^2 flasks or in 6-well plates (growth area 9.5 cm^2; Corning Costar cell culture plates; #CLS3516 Sigma) at 37°C. The cultures were inoculated with 1×10^4 cells/well in a total volume of 3 mL. Where indicated, the cultures were first incubated for a period of 3 d in the absence the mineralization-activating cocktail (MAC). Then the cultures were continued to be incubated for additional 7 d in the absence or presence of the MAC, comprising 5 mM β-glycerophosphate, 50 mM ascorbic acid and 10 nM dexamethasone to induce biomineralization (40) The $CaCO_3$ samples (“CC”, “CCP5” or “CCP10”) were added to each well at the beginning of the experiments. Every third day the culture medium was replaced by fresh medium/serum and, where indicated, also with MAC. The cells were subsequently used for the quantification of the *ALP* gene expression.

4.3.6 Cell viability assay

SaOS-2 cells were seeded into the 6-well plates and cultured for 3 d in McCoy’s medium/15% FCS. Where indicated, the cultures were supplemented with 30 µg (in 3 mL) of the respective $CaCO_3$ preparation. Then, after a 2 or 3 d incubation period, the cells were incubated with fresh medium containing 200 µL of 3-[4,5-dimethyl thiazole-2-yl]-2,5-diphenyl tetrazolium (MTT; #M2128, Sigma) for 4 h in the dark. Subsequently the remaining MTT dye was aspirated and 200 µL of DMSO were added to solubilize the formazan crystals. Finally, the optical densities (OD) were determined at 560 nm (14). Ten parallel experiments each were performed.

4.3.7 Human mesenchymal stem cells

The expression of *ALP* was determined, in parallel in SaOS-2 cells, and also in human mesenchymal stem cells (MSC). The cells were isolated using previously described methods; the experiments had been approved from the ethics committee (41, 42). The deep-frozen, preserved MSCs were thawed, and suspended in 75-cm^2 flasks. They were cultivated in α-MEM (Cat. no. F0915; Biochrom, Berlin, Germany), supplemented with 20% FCS supplemented with 0.5 mg/mL of gentamycin, 100 units penicillin, 100 µg/mL of streptomycin and 1 mM pyruvate (#P2256 Sigma-Aldrich). The incubation was performed in a humidified incubator at 37°C. After the pre-incubation period of 3 d the non-adherent cells were discarded, and the adherent cells were continued to be incubated with α-MEM/FCS.

4.3.8 Quantitative real-time polymerase chain reaction: *ALP* expression

The SaOS-2 or MSCs cells were pre-cultivated for 3 d in medium/serum. Then the cultures were split and incubated either in the absence of any $CaCO_3$ (control) or with 50 µg/mL of "CCP5", *"CCP10"* or calcite and the cultivation was continued for an additional 7 d in the absence or presence of MAC. Subsequently, the cells were harvested, RNA extracted and subjected for quantitative real-time RT [reverse transcription]-polymerase chain reaction (qRT-PCR) as described (43). The following primer pairs were used: *ALP* [alkaline phosphatase; NM_000478.4] Fwd: 5'-TGCAGTACGAGCTGAACAGGAACA-3' [nt_{1141} to nt_{1164}] and Rev: 5'-TCCACCAAATGTGAAGACGTGGGA-3' [nt_{1418} to nt_{1395}; product size of 278 bp] and as reference GAPDH [glyceraldehyde 3-phosphate dehydrogenase; NM_002046.3] Fwd: 5'-CCGTCTAGAAAAACCTGCC-3' [nt_{929} to nt_{947}] and Rev: 5'-GCCAAATTCGTTGTCATACC-3' [nt_{1145} to nt_{1126}; 199 bp]. The qRT-PCR determinations were performed in an iCycler (Bio-Rad, Hercules, CA, USA), and the mean C_t values and efficiencies were calculated by iCycler software (Bio-Rad); the estimated PCR efficiencies were in the range of 93%-103% (39).

4.3.9 Preparation of PLGA-based implant microspheres

The microspheres, used for the animal experiments were produced as described in details (44). The implant microspheres lacking $CaCO_3$/polyP were fabricated with 4 ml of a PLGA/dichloromethane solution (volume ratio 1:5); they are termed "cont-mic". For the fabrication of the implant spheres containing $CaCO_3$/polyP, "CCP10" was added to the PLGA/dichloromethane mixture at a concentration of 20%. The viscous reaction mixture was pressed through a syringe with an aperture of 0.8 mm. By this approach, implant microspheres, termed "polyP-mic", with an average diameter of ≈ 830 were obtained (see under "Results"). The content of polyP in the microspheres was determined after treatment of the samples with 1 M sulfuric acid to hydrolyze polyP; the resulting orthophosphate was determined with ammonium molybdate (#277908; Sigma-Aldrich) as described (45).

4.3.10 Determination of the mechanical properties

The mechanical properties of the microspheres were determined with a nanoindenter, equipped with a cantilever that has been fused to the top of a ferruled optical fiber (44, 46). Using this technique the reduced Young's modulus (RedYM) was determined.

4.3.11 Compatibility studies *in vivo*

Wistar rats of male gender, weighting between 240 g and 290 g (age: two months), were included in this study; 3 animals from each group were used. Diet and water were provided *ad libitum* during the total experimental period. Prior to surgery the animals were treated with Ciprofloxacins (Bayer, Leverkusen, Germany) 10 mL/kg of body weight for antibiotic prophylaxis. Then the animals were narcotized with chlorpromazine (Smith, Kline, French & Philadelphia, PA)/ Ketamin (Ketanest; Pfizer, Groton, CT) *via* intramuscular injection. Following routine disinfection, incisions of ≈1 cm were made in the right and left half, perpendicularly to the vertebral axis at the upper limbs level. Following skin incision, the muscle was incised and dissected to accommodate the microspheres. The implant microspheres (≈20 mg in a volume of 100 µL) were introduced into the muscle and stabilized there in the deeper layer (44, 47, 48).

After a period of 2, 4, or 8 weeks the animals were sacrificed and the specimens with the surrounding tissue were dissected and sliced. The samples were inspected macroscopically for inflammation, infection and discoloration. The samples were fixed in formalin, sliced, stained with Mayer's hematoxylin (#MHS1; Sigma) and then analyzed by optical microscopy (with an Olympus AHBT3 microscope) (49).

4.3.12 Statistical analysis

After finding that the values follow a standard normal Gaussian distribution, the results were statistically evaluated using paired Student's *t*-test (50).

4.4 Results

4.4.1 Effect of polyP on calcite formation: FTIR and XRD spectra

For all $CaCO_3$solids the following FTIR signals were recorded: v_1 (symmetric stretching) at ≈1080 cm^{-1}; v_2 (out of-plane bending) at ≈870 cm^{-1}; v_3 (doubly degenerate planar asymmetric stretching) at ≈1400 cm^{-1} and v_4 (doubly degenerate planar bending) at 700 cm^{-1}. The published IR data (36), which were obtained with FTIR/KBr pellets, include peaks located at around 1400 cm^{-1} (v3), 876 cm^{-1} (v_2), and 714 cm^{-1} (v_4) for calcite and 1090 cm^{-1} (v_1), 870 cm^{-1} (v_2), and 745 cm^{-1} (v_4) for vaterite (**Fig. 4.2**). Our samples prepared in the absence of polyP are characterized as follows. For calcite the typical vibration bands 1391, 872 and 712 cm^{-1} were recorded, while the samples prepared in presence of polyP showed the adsorption peaks at 1398, 869 and 742 cm^{-1} for "CCP5" polyP as well as the bands at 1398, 869 and 741cm^{-1} for "CCP10" proving the formation of vaterite. It is apparent that the strength of the signal for vaterite around 741 cm^{-1} decreases at higher content of polyP in the fabricated $CaCO_3$ solids, "CCP10" *versus* "CCP5". This is indicative for the formation of ACC. Beside of the CO_3^{2-} absorption peaks, the peaks from 1200 cm^{-1} to 950 cm^{-1} correspond to the absorption peaks of phosphate in polyP.

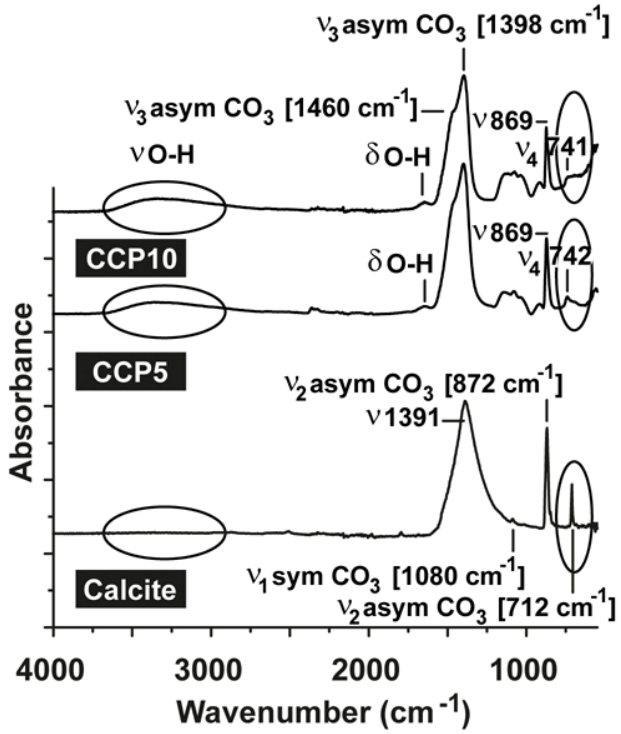

Figure 4.2.

FTIR spectra of calcite as well as "CCP5" (0.05 g of Na-polyP/assay) and "CCP10" (0.1 g of Na-polyP). The major distinguishing vibration regions/signals for calcite versus ACC, the vibration range for O-H (around 3250 cm^{-1}) and the asymmetric ν_2 line for CO_3 at 725/712 $cm^{-1}$are circled.

The above result, vaterite to be formed in small portions in ACC solids, was confirmed with XRD in which the diffraction peaks of the sample prepared in absence of polyP, at approximately 23°, 30°, 36° and 40°, is given; those signals correspond to calcite. In contrast, the samples prepared in the presence of polyP ("CCP5") showed peaks at approximately 24°, 27°, 32° and 44°, which also reflect the existence of vaterite. Furthermore, these data prove that the $CaCO_3$ solids, prepared in the absence of polyP were pure calcite (**Fig. 4.3A**). In contrast, the "CCP5" samples were composed of vaterite in association with ACC, as can be deduced from the low intensities of the signals and also the broadening of the diffraction peaks for sample "CCP5" (**Fig. 4.3B**). In consequence, the increase of polyP amount, as in "CCP10", causes a decrease transformation rate of ACC to vaterite. This is evident from the XRD pattern of "CCP10"

sample which exhibits the amorphous nature of the sample, but also containing small amounts of vaterite.

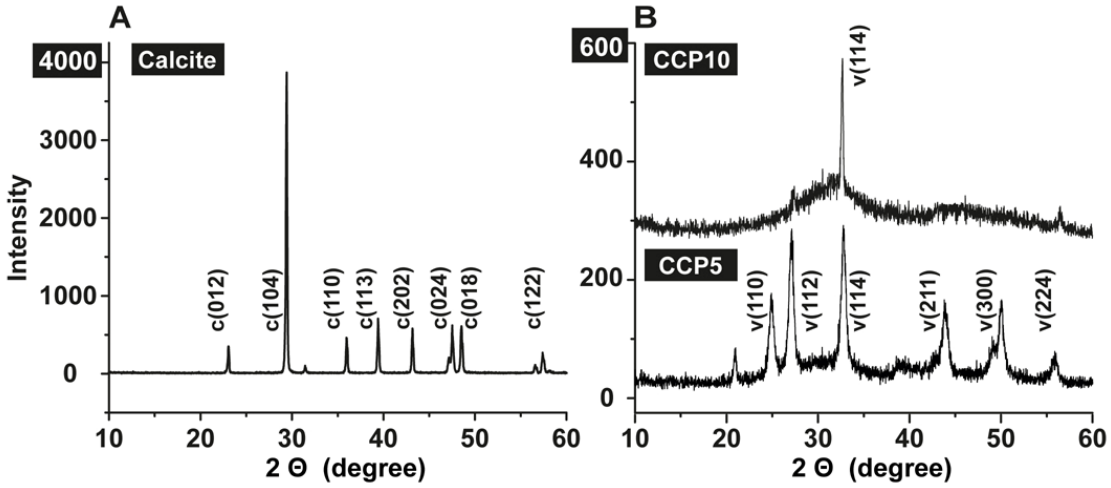

Figure 4.3

XRD pattern obtained from (**A**) calcite and (**B**) the two $CaCO_3$ preparations, containing two different concentrations of polyP, "CCP5" or "CCP10".The characteristic signals are highlighted and marked with the respective Miller indices, given in parentheses(36). Please note the different scale of the ordinate captions between (**A**) and (**B**).

4.4.2 Morphology of the solids formed

The solids formed by precipitation from $CaCl_2 \bullet 2H_2O$ and Na_2CO_3 were studied by SEM. The photomicrographs of the particles, formed in the absence of polyP, show the typical crystalline calcite, the rhombohedral crystals surrounded by {104} faces; (51) **Fig. 4.3A, B**. The size of the particles varies between 5.3 to 8.9±2.4 µm. In contrast, those solids formed from $CaCl_2 \bullet 2H_2O$ and Na_2CO_3 in the presence of polyP show a different morphology. At the lower polyP concentration, the "CCP5" particles show a spherical appearance with an average size of the spherical crystals of 9.4±3.7 µm (**Fig. 4.4C, D**); we attribute these particles to vaterite. They are surrounded by very abundantly accumulating small nanoparticles with a size range of 100 to 200 nm, which we assigned as ACC. Increasing the polyP, as in "CCP10", the globular particles disappear and are replaced by penta/hexagonal flake shaped vaterite (**Fig. 4.4E, F**). High-magnification of the samples by SEM revealed that those individual large flakes, vaterite crystals, are formed by numerous globular to platelets-like, mostly ACC, each about 500 nm. The

latter two morphologies, the globular particles and the flake like particles match described crystalline vaterite grains (37).In turn, the data (XRD, FTIR and SEM) indicate that the "CCP5" and "CCP10" particles consist, to a different proportion, of ACC together with vaterite.

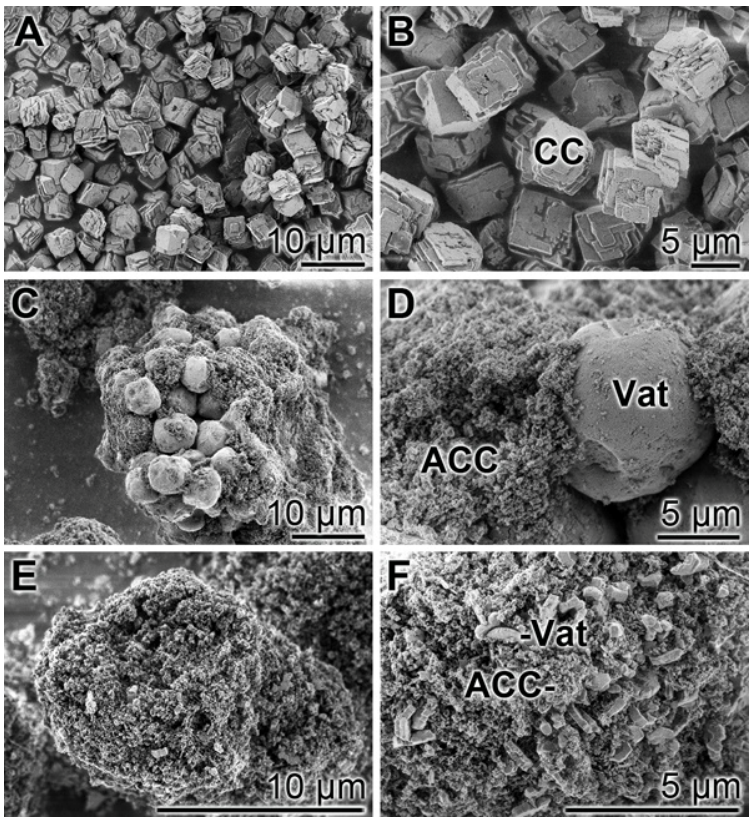

Figure 4.4.

Morphology of the solids formed from $CaCl_2 \bullet 2H_2O$ and Na_2CO_3; SEM analysis. (**A** and **B**) in the absence of polyP calcite crystals are formed. This morphology is changed after addition of polyP during the precipitation process. (**C** and **D**) In the presence of 5% polyP, the "CCP5" particles show a spherical appearance. (**E** and **F**) at 10% polyP, "CCP10", thesolids show a platelet-like shape, corresponding to vaterite crystals (Vat).

4.4.3 Effect of $CaCO_3$ samples on cell growth/viability

The cell growth/viability of SaOS-2 cells after exposure to the $CaCO_3$ preparations was determined by applying the MTT assay. The $CaCO_3$ samples were added at a concentration of 50 µg/ mL. In parallel a control series of experiments lacking any $CaCO_3$ solids was performed (**Fig. 4.5**). The results revealed that the increase in cell growth/viability from 0.70±0.11 at time 0 to approximately 1.1 absorbance units after 2

d and 2.35 units after 3 days changes only non-significantly among the control assays and the three $CaCO_3$ series ("CCP5", "CCP10" or calcite).

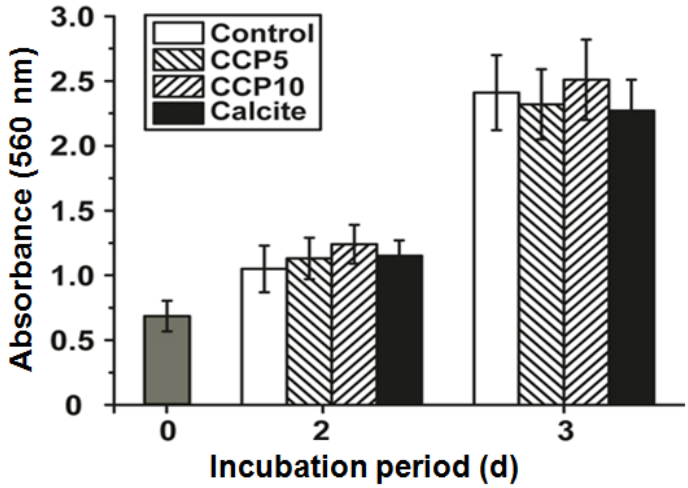

Figure 4.5.
Cell viability/growth of SaOS-2 cells after cultivation for 2 d and 3 d, respectively, in the absence of any $CaCO_3$ solids (control; open bars) or after exposure to 50 µg/mL of "CCP5" (left hatched bars), "CCP10" (right hatched bars) or calcite (filled bars). After terminating the cultivation, the assays were subjected to the MTT assay and the absorbance at 560 nm was determined. The absorbance value at time zero is likewise given (grey bars). Data represent means ± SD of ten independent experiments.

4.4.4 Stability of the $CaCO_3$ solids in the culture medium

SaOS-2 cells grow in an adherent manner (52).If the cultures are exposed to either calcite or "CCP5" solids the growth behavior onto the surfaces of the culture dishes is similar in assays containing either "CCP10" (**Fig. 4.6A, B**) or calcite (**Fig. 4.6C**, **D**). After 3 d the cells grow almost to confluency. However, it is remarkable that the number of mineral particles, floating in the culture medium, after this period of time, is strongly reduced in the assays containing "CCP10" (**Fig. 4.6A**, **B**), compared to those seen in calcite assays (**Fig. 4.6C, D**). This observation can be taken as an indication that the "CCP10" particles undergo dissolution during the 5 d incubation period. This finding is supported by the determination revealing that after 3 d incubation period in simulated body fluids(53) the amount of calcite particles decreases only by 5-10%, while only 35%

of the "CCP10" particles can be recovered, as measured on the basis of sedimentable carbonate (data not shown).

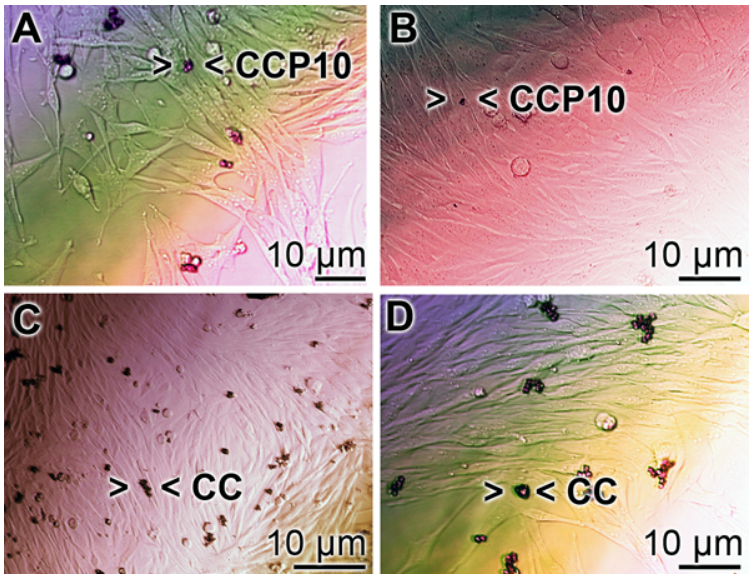

Figure 4.6.
Growth pattern of SaOS-2 cells in the presence of 50 µg/mL of "CCP10" (**A** and **B**) or calcite (**C** and **D**) after a 3 d incubation period**.** The cells were identified by phase contrast/Nomarski optics. The $CaCO_3$ particles in the assays became visible in the phase contrast images and are marked (><).

4.4.5 Release of Ca^{2+} from the $CaCO_3$ particles

In separate assays either calcite or "CCP10" was added into a 1 mL assay, buffered with 1 M Tris-HCl (pH 7.4). While almost no Ca^{2+} is released from the calcite sample, already 6.8±1.1 µg/ml (68% of the total Ca^{2+} in the reaction mixture) was released from the "CCP10" after a period of 48 hr; this extent increases further during the total 192 hr of incubation (**Fig. 4.7**).

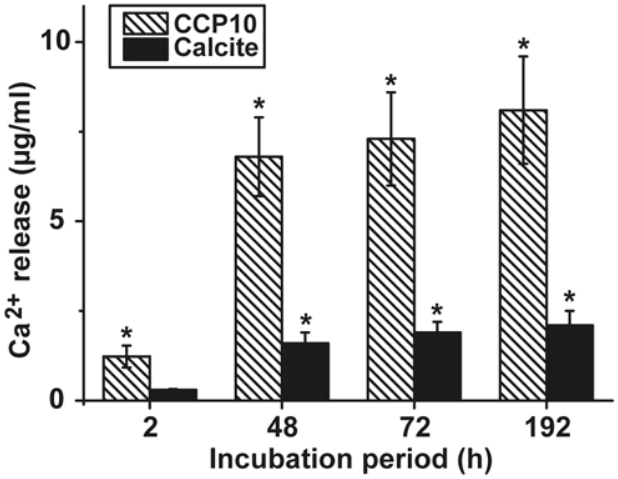

Figure 4.7.
Release of Ca^{2+} from the $CaCO_3$ particles."CCP10" or calcite was incubated in Tris-HCl buffer (pH 7.4) for various time periods and the supernatant was analyzed for Ca^{2+} concentration. The results are means from 6 parallel experiments; * *P*< 0.01.

4.4.6 Expression of the *ALP* in SaOS-2 cells as well as in MSCs

The morphogenetic activity of the $CaCO_3$ samples towards SaOS-2 cells as well as the MSCs was determined in the absence and presence of MAC. Using SaOS-2 cells it was determined that in the absence of MAC the expression ratio between the *ALP* and the reference gene expression (GAPDH) significantly increases from 0.31±0.9 arbitrary units to ≈0.6. Within the sets of experiments without the MAC no significant differences are measured, irrespectively of the absence (control) or presence of the $CaCO_3$ samples in the assays (**Fig. 4.8A**). However, if the expression ratio (*ALP*:GAPDH) is determined in MAC activated cells then a significant increase of the ratio to 0.87±0.12 (in the control), to 1.74±0.23 ("CCP5") or to 1.86±0.29 (*"*CCP10*"*)is measured. In contrast, no response of the cells in assays with calcite is determined (0.14±0.05).

A similar expression pattern of the *ALP*, if correlated to the reference *GAPDH* gene expression, is found if MSCs are used for the experiments. Again, in the presence of the MAC a significant increase of the expression ratio is seen assays in the absence of any $CaCO_3$ solid, as well as in the presence of both "CCP5" and *"*CCP10*"*. No inducing effect is determined in cells exposed to calcite (**Fig. 4.8B**).

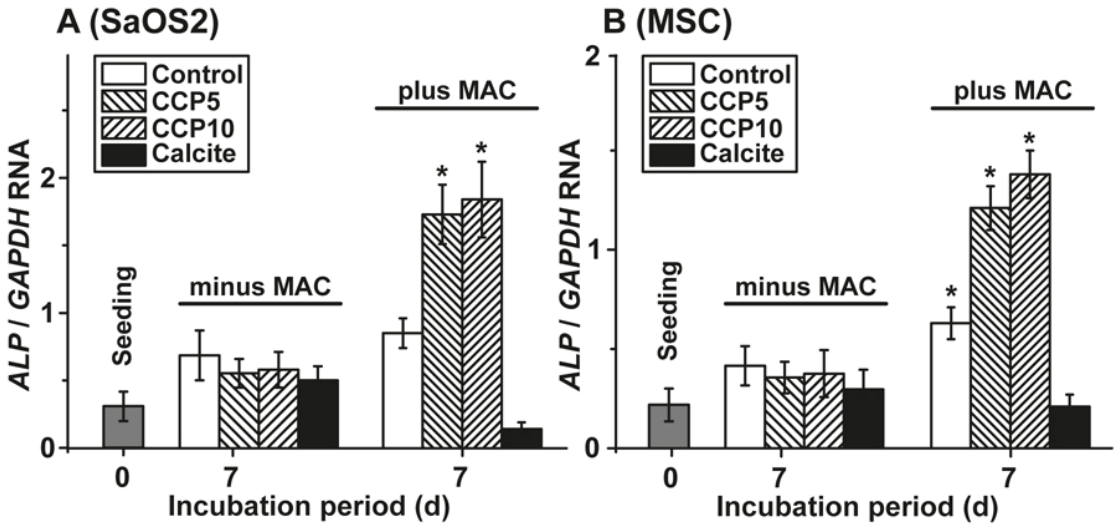

Figure 4.8.

Steady-state expression levels of the *ALP*gene both in (A) SaOS-2 cells and in (B) MSCs. The cells remained without any $CaCO_3$ solids (control), or were exposed to 50 µg/mL of "CCP5" (left hatched bars), "CCP10" (right hatched bars), or calcite (filled bars). After the 3 d pre-incubation period in the absence of MAC the cells were continued to be incubated in the absence of MAC (minus MAC) or were exposed to MAC (plus MAC). After the 7 d incubation the cells were harvested, their RNA extracted and subjected to qRT-PCR analyses. The expression values are given as ratios to the reference gene GAPDH; the ratios at time zero are in grey. The results are means from 5 parallel experiments; * $P< 0.01$; the values are computed against the expression measured in cells during seeding.

4.4.7 Implant microspheres, used for the animal studies

The control spheres, the "cont-mic" had a size of (≈845 µm [820±60 µm]; n=50), while those containing polyP were insignificantly slightly smaller (≈838 µm [816 ± 65 µm]); **Fig. 4.9A, B.** The texture of the microspheres surfaces was porous and had pores of 25-30 nm (not shown here). The content of polyP in the "polyP-mic" was 7.26±0.92%. The hardness of the particles (RedYM) was determined with a nanoindenter and found to be for the "cont-mic" 26.99±6.22 MPa and the "polyP-mic" 23.96±5.49 MPa.

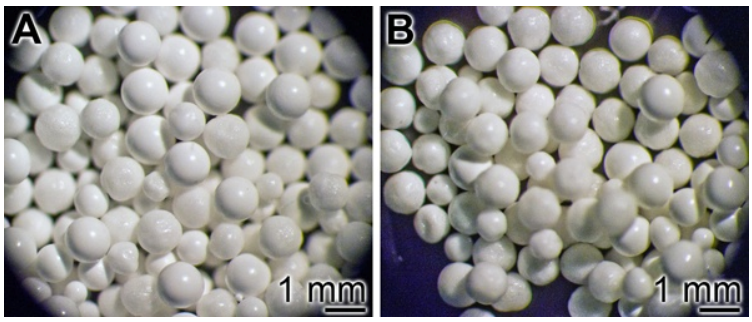

Figure 4.9.
Morphology of the microspheres; (**A**) control spheres "cont-mic" and (**B**) polyP loaded spheres, "polyP-mic".

4.4.8 Compatibility studies in rats

The implant microsphere samples (20 mg), both "cont-mic" and "polyP-mic" were inserted in the muscles of the back of rats, as described under "Materials and Methods" (**Fig. 4.10A, B**). After 2, 4, or 8 weeks tissue samples with the microspheres were removed, sliced and stained with hematoxylin solution. In none of the excised specimens any sign for a histopathological alteration could be seen in all of the three sacrificed laboratory animals per group both for the "cont-mic" (**Fig. 4.10C, E, G**) and the "polyP-mic" series (**Fig. 4.10D, F, H**). Typical images for the sample sections, stained with hematoxylin are shown. It is evident that after 2 weeks the regions, where the implant microspheres had been placed into the muscle, harbor a few cells which are scattered within the implanted microsphere areas (**Fig. 4.10C, D**). However, after a 4 (**Fig. 4.10E**) and 8 weeks (**Fig. 4.10G**) stay of the "cont-mic" microspheres in the muscle area the implant spheres appear to be empty or close to be cell-free. In contrast, within the "polyP-mic" microspheres already after 4 weeks (**Fig. 4.10F**) an accumulation of the cells within the spheres are evident. Even more, after 8 weeks the spheres are almost filled with infiltrating cells (**Fig. 4.10H**).

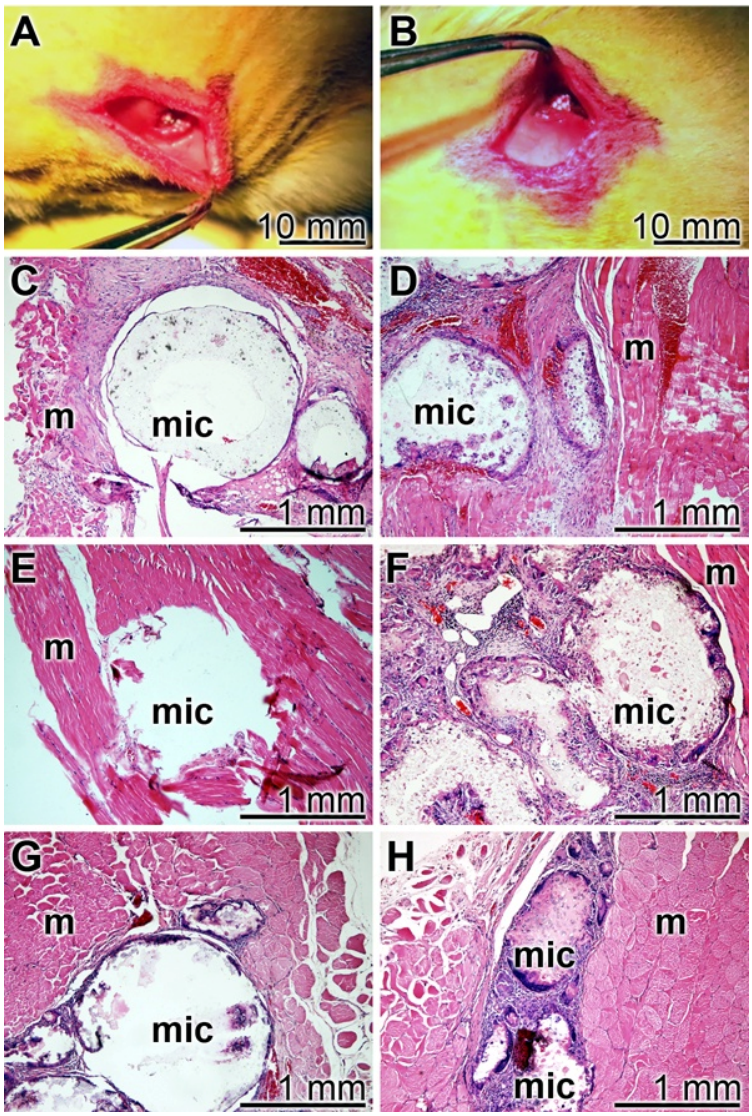

Figure 4.10.

Implantation of the implant microspheres (A and B) into muscle of the back of a test animal. (**C** to **H**) Cytochemical analysis of the regions around the microspheres after a period of 2 weeks (**C**, **D**), 4 weeks (**E**, **F**) and 8 weeks (**G**, **H**) of transplantation. The animals received either "cont-mic" implant microspheres (**C**, **E**, **G**) or implant microspheres ("polyP-mic"), filled with "CCP10"; staining of the slices was performed with hematoxylin. Microspheres (mic) and muscle areas are marked (**m**).

4.5 Discussion

As any organ in the human body, the skeletal elements are dynamic systems, prone to anabolic and catabolic processes. In contrast e.g. to the liver, the inorganic components and especially the crystalline HA part of the bones show a comparably slow metabolic turnover with the relatively low rate of 2 to 3%/y (45). Basically it can be taken as a rule that crystalline minerals in an organism are biologically inert; typical examples are bladder stones that are formed from crystalline creatinine, oxalate, citrate, uric acid, sulfate, chloride and/or ammonium under supersaturated and acidic conditions (55). In turn, bone implant materials that should elicit regenerative activity might preferentially be formed of amorphous material, like e.g. bioactive glass (56). Amorphous precursors from HA, e.g. ACC or ACP, (57) are metastable phases which give rise to the mature carbonated and subsequently crystalline HA apatite (reviewed in: ref.12). At physiological conditions, the turnover of HA is, if at all, very low, while the transition from ACC to calcium phosphate runs readily and is only dependent on the substrate/product concentrations (19). In any event, concentration-dependent reactions in the body are driven enzymatically, since both the process of oversaturation, a result of active metabolic pumping, and the through put *via* the flow equilibrium are energetically coupled to exergonic reactions that are enzyme-dependent.

Recently, distinct evidence accumulated that ACC, as the (presumed) bioseed for bone mineral formation, is formed enzymatically *via* CA-II or CAI-IX (17, 19). The metastable ACC, readily formed at slightly alkaline conditions, undergoes rapid transformation to vaterite, and/or aragonite and calcite, unless this reactions chain is not blocked by inorganic or organic molecules (19). In turn, in the present study we fabricated $CaCO_3$ solids, an ACC polymorph that contains a small amount of vaterite, and assessed their potential to act as (potential) bone implant material. These $CaCO_3$/polyP deposits retain the potency to undergo transformation to the stable aragonite and calcite, and additionally, after exchange of carbonate by phosphate, have the ability to form ACP and perhaps finally also HA (to be studied). Such an implant material would be superior

to a biologically inert HA implant scaffold that merely functions as a mechanical place holder and platform for cells to adhere and to proliferate but not as an osteogenic material (58).

It is established that parallel with the enthalpy increment, crystallization of ACC to the other polymorphs (vaterite [≈-15 kJ mol^{-1} relative to ACC], aragonite [≈-19 kJ mol^{-1}], or to calcite [≈-19 kJ mol^{-1}]) (59), the solubility of ACC to vaterite, aragonite and finally calcite drops considerably between ACC and vaterite. In the present study the Na^+ salt of the anionic polymer polyP was added to the precursors of $CaCO_3$ ($CaCl_2$ and Na_2CO_3) during the synthesis of ACC. This polymer prevented, at a final concentration of 10%, the transformation process of ACC to its crystalline polymorphs vaterite, aragonite and calcite almost totally. It has been shown that the $CaCO_3$ polymorph transformation kinetics, following the Ostwald step rule, from ACC *via* the first nucleation step, the metastable spherical vaterite polymorph, then to aragonite and finally to the stable rhombohedral calcite polymorph, decreases to the same extent as the "impurities" in the assay increases(60). Such an "impurity" is the morphogenetically active polyP that prevents the transformation from ACC to the crystalline polymorphs; only small fractions of vaterite within the ACC solid are formed.

Both the $CaCO_3$solids (61, 62) and the polyP physiological metabolite (18, 62, 63), tested separately, have osteogenic potential and could serve as constituents of bioactive bone grafts. In turn, the scaffold developed in the present study exploits not only the morphogenetic potential of polyP but also utilizes the property of this polymer to freeze the $CaCO_3$ solids at the ACC stage. This material is superior to calcite with respect to the osteogenic activity; both "CCP5" and "CCP10" are determined to be significant inducers of the gene *ALP*, a known marker for bone formation *via* stimulation of osteoblasts. This result has been obtained from studies with bone-like SaOS-2 cells and also with MSC. Using a $CaCO_3$ formulation with 10% [w/w] polyP, "CCP10", the release of Ca^{2+}, and simultaneously of CO_3^{2-}, is fast during the first 48 h of incubation, allowing the release of the biologically active anions CO_3^{2-} and PO_4^{3-} from the scaffold; the ortho-phosphate

will be enzymatically and exohydrolytically liberated from polyP (64). In turn, the CO_3^{2-} as well as the HCO_3^- anions induce the mineralization process onto bone-forming cells,[14] very likely *via* modulating the efficiency of the HCO_3^-/Cl^- anion exchanger, inserted into the plasma membrane not only of osteoclasts but also of osteoblasts (65). Very recently, this view has been corroborated by the finding that the baso-lateral anion exchanger Ae2a,b in differentiating ameloblasts secretes bicarbonates into the extracellular space under simultaneous deposition of HA/enamel (66).

To assess the biocompatibility of the $CaCO_3$/polyP material *in vivo*, "CCP10" was encapsulated into PLGA ("polyP-mic") microspheres. In parallel, the control implant spheres remained without $CaCO_3$/polyP ("cont-mic"). Those pearls were inserted in the muscles of the back of rats. After an observation period of 2, 4, and 8 weeks tissue samples were taken from the rats and inspected microscopically after slicing and staining with Mayer's hematoxylin. The inspections show that in the "polyP-mic" series an advanced repopulation of the implant region with cells became evident after 4 weeks and 8 weeks, resp. In contrast, the microspheres lacking $CaCO_3$/polyP were devoid of any cells. From these experiments we conclude that the "CCP10" biomaterial is not only biocompatible but also supports the cellular regeneration potency of the impaired implant region.

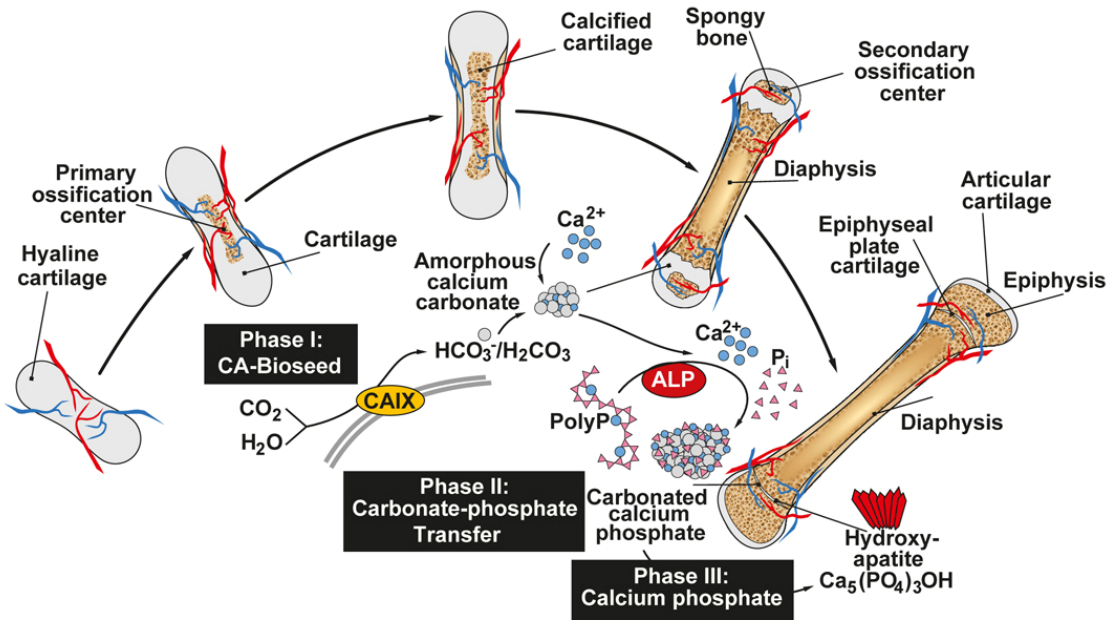

Figure 4.11.

Schematic presentation of the process of endochondral ossification and the proposed phases of bone mineral deposition. After penetration of blood vessels the hyaline cartilage at the primary ossification centers in the diaphysis starts to calcify ($CaCO_3$ deposits). The formation of spongy bone at the secondary ossification centers in the epiphyses starts later. Two regions of hyaline cartilage remain the articular cartilage at the surface of the epiphysis and the epiphyseal plate (growth region) between the epiphysis and diaphysis. The mineral deposition in the growth region is subdivided into the following three steps. Phase I: amorphous calcium carbonate (ACC) bioseeds are formed, a process with might be mediated by the membrane-associated CA-IX. Phase II: polyP released from platelets undergoes *ALP*-mediated hydrolysis under formation of ortho-phosphate that act as phosphate donor for the carbonate-phosphate transfer reaction. Finally phase III: the phosphate units are used for the (carbonated) calcium phosphate formation.

4.6 Conclusion

The recently gathered findings on the $CaCO_3$ nature of the bioseeds, the anion exchange of CO_3^{2-} by PO_4^{3-} and the supply of ortho-phosphate from polyP, the following series of mechanistically distinct processes, describing bone formation, can be sketched. In the *first phase* during bone mineral deposition, like in the endochondral ossification, the cartilage in the metaphysis comprising the growth center between the epiphysis and the diaphysis of the long bone, calcifies. It is likely that this process of calcification is enzymatically driven by CA-II and/or CA-IX. *Secondly*, platelets which accumulate with

the osteoblasts both in regions of bone formation and also at bone fracture sites release polyP into the extracellular space where the polymer undergoes *ALP*-mediated exohydrolysis under the release of ortho-phosphate. *Thirdly*, the available phosphate units, formed in a spatial vicinity to the bioseed synthesis, serve as the source for the formation of ACP and ultimately to carbonated HA, **Fig. 4.11.** Considering this background, the $CaCO_3$/polyP material fabricated in this paper appears to be a promising biocompatible and osteogenic scaffold that provides both the substrate for the bioseed development ($CaCO_3$ [CO_3^{2-}]) and for the subsequent transformation to the calcium phosphate (polyP [PO_4^{3-}]).

4.7 Notes and references

1. O. Braissant, G. Cailleau, C. Dupraz and E. P. Verrecchia, Bacterially induced mineralization of calcium carbonate in terrestrial environments: the role of exopolysaccharides and amino acids. J. Sed. Res., 2003, 73, 485–490.

2. F. C. Meldrum and H. Cölfen, Controlling mineral morphologies and structures in biological and synthetic systems. Chem. Rev., 2008, 108, 4332-4432.

3. F. C. Meldrum, Calcium carbonate in biomineralisation and biomimetic chemistry. Intern. Mater. Rev., 2003, 48, 187-224.

4. D. Ren, Q. Feng and X. Bourrat, Effects of additives and templates on calcium carbonate mineralization in-vitro . Micron, 2011, 42, 228-245.

5. J. Tomás, A. J. Geffen, I. S. Allen and J. Berges, Analysis of the soluble matrix of vaterite otoliths of juvenile herring (Clupea harengus): do crystalline otoliths have less protein? Comp. Biochem. Physiol. A Mol. Integr. Physiol., 2004, 139, 301-308.

6. A. M. Oliveira, M. Farina, I. P. Ludka and B. Kachar, Vaterite, calcite, and aragonite in the otoliths of three species of Piranha. Naturwiss., 1996, 83, 133-135.

7. G. Falini, S. Albeck, S. Weiner and L. Addadi, Control of aragonite or calcite polymorphism by mollusk shell macromolecules. Science, 1996, 271, 67– 69.

8. W. E. G. Müller, M. Neufurth, U. Schlossmacher, H. C. Schröder, D. Pisignano and X. H. Wang, The sponge silicatein-interacting protein silintaphin-2 blocks calcite formation of calcareous sponge spicules at the vaterite stage. RSC Advances, 2014, 4, 2577–2585.

9. L. Addadi and S. Weiner, Interactions between acidic proteins and crystals: stereochemical requirements in biomineralization. Proc. Natl. Acad. Sci. U.S.A., 1985, 82, 4110-4114.

10. X. Liu, S. Zeng, S. Dong, C. Jin and J. Li, A novel matrix protein hic31 from the prismatic layer of Hyriopsis cumingii displays a collagen-like structure. PLoS One, 2015, 10(8), e0135123.

11. S. Weiner and H. D. Wagner, The material bone: structure–mechanical function relations. Ann. Rev. Mat. Sci., 1998, 28, 271–98.

12. N. Reznikov, R. Shahar and S. Weiner, Bone hierarchical structure in three dimensions. Acta Biomater., 2014, 10, 3815-3826.

13. Y. Wang, S. Von Euw, F. M. Fernandes, S. Cassaignon, M. Selmane, G. Laurent, G. Pehau-Arnaudet, C. Coelho, L. Bonhomme-Coury, M. M. Giraud-Guille, F. Babonneau, T. Azaïs and N. Nassif, Water-mediated structuring of bone apatite. Nat. Mater., 2013, 12, 1144-1153.

14. X. H. Wang, H. C. Schröder, U. Schlossmacher, M. Neufurth, Q. Feng, B. Diehl-Seifert and W. E. G. Müller, Modulation of the initial mineralization process of SaOS-2 cells by carbonic anhydrase activators and polyphosphate. Calcif. Tissue Int., 2014, 94, 495–509

15. S. Y. Liao, M. I. Lerman and E. J. Stanbridge, Expression of transmembrane carbonic anhydrases, CAIX and CAXII, in human development. BMC Dev. Biol., 2009, 9, 22; 10.1186/1471-213X-9-22.

16. X. Chang, Y. Zheng, Q. Yang, L. Wang, J. Pan, Y. Xia, X. Yan and J. Han, Carbonic anhydrase I (CA1) is involved in the process of bone formation and is susceptible to ankylosing spondylitis. Arthritis Res., 2012, 14, R176.

17. WEG Müller, HC Schröder, E Tolba, M Neufurth, B Diehl-Seifert, XH Wang (2015) Mineralization of bone-related SaOS-2 cells under physiological hypoxic conditions. FEBS J.; in press.

18. X. H. Wang, H. C. Schröder and W. E. G. Müller, Polyphosphate as a metabolic fuel in Metazoa: A foundational breakthrough invention for biomedical applications. Biotechnol J., 2015, doi: 10.1002/biot.201500168.

19. W. E. G. Müller, M. Neufurth, J. Huang, K. Wang, Q. Feng, H. C. Schröder, B. Diehl-Seifert, R. Muñoz-Espí and X. H. Wang, Non-enzymatic transformation of amorphous CaCO3 into calcium phosphate mineral after exposure to sodium phosphate in-vitro: Implications for in vivo hydroxyapatite bone formation. ChemBioChem, 2015, 16, 1323-1332.

20. S. Omelon, J. Georgiou, F. Variola and M. N. Dean, Colocation and role of polyphosphates and alkaline phosphatase in apatite biomineralization of elasmobranch tesserae. Acta Biomater., 2014, 10, 3899-3910.

21. W. E. Brown, J. P. Smith, J. R. Lehr and A. W. Frazier, Crystallographic and chemical relations between octacalcium phosphate and hydroxyapatite. Nature, 1962, 196, 1050-1055.

22. S. Bose, M. Roy and A. Bandyopadhyay, Recent advances in bone tissue engineering scaffolds. Trends Biotechnol., 2012, 30, 546–554.

23. R. Guzmán, S. Nardecchia, M. C. Gutiérrez, M. L. Ferrer, V. Ramos, F. del Monte, A. Abarrategi and J. L. López-Lacomba, Chitosan scaffolds containing calcium phosphate salts and rhBMP-2: in-vitro and in vivo testing for bone tissue regeneration. PLoS One, 2014, 9(2), e87149.

24. M. Kellermeier, E. Melero-García, F. Glaab, R. Klein, M. Drechsler, R. Rachel, J. M. García-Ruiz and W. Kunz, Stabilization of amorphous calcium carbonate in inorganic silica-rich environments. J. Am. Chem. Soc., 2010, 132, 17859-17866.

25. K. Sawada, The mechanisms of crystallization and transformation of calcium carbonates. Pure Appl. Chem., 1997, 69, 921-928.

26. J. Ihli, A. N. Kulak and F. C. Meldrum, Freeze-drying yields stable and pure amorphous calcium carbonate (ACC). Chem. Commun. (Camb.), 2013, 49, 3134-3136.

27. R. Schröder, H. Pohlit, T. Schüler, M. Panthöfer, R. E. Unger, H. Frey and W. Tremel, Transformation of vaterite nanoparticles to hydroxycarbonate apatite in a hydrogel scaffold: Relevance to bone formation. J. Mater. Chem. B, 2015, 3, 7079-7089.

28. W. E. G. Müller, E. Tolba, H. C. Schröder, S. Wang, G. Glaßer, R. Muñoz-Espí, T. Link and X. H. Wang, A new polyphosphate calcium material with morphogenetic activity. Materials Letters, 2015, 148, 163-166.

29. W. E. G. Müller, E. Tolba, H. C. Schröder, B. Diehl-Seifert and X. H. Wang, Retinol encapsulated into amorphous Ca2+ polyphosphate nanospheres acts synergistically in MC3T3-E1 cells. Eur. J. Pharm. Biopharm., 2015, 93, 214-223.

30. R. M. Pilliar, M. J. Filiaggi, J. D. Wells, M. D. Grynpas and R. A. Kandel, Porous calcium polyphosphate scaffolds for bone substitute applications – in-vitro characterization. Biomaterials, 2001, 22, 963–972.

31. Y. Shanjani, J. N. De Croos, R. M. Pilliar, R. A. Kandel and E. Toyserkani, Solid freeform fabrication and characterization of porous calcium polyphosphate structures for tissue engineering purposes, J. Biomed. Mater. Res. B Appl. Biomater., 2010, 93, 510–519.

32. B. Lee, M. Kim, S. Choi and Y. K. Lee, Amorphous calcium polyphosphate bone regenerative materials based on calcium phosphate glass, Key Eng. Mater., 2009, 396–398, 209-212.

33. J. H. Morrissey, S. H. Choi and S. A. Smith, Polyphosphate: an ancient molecule that links platelets, coagulation, and inflammation. Blood, 2012, 119, 5972-5979.

34. L. Faxälv, N. Boknäs, J. O. Ström, P. Tengvall, E. Theodorsson, S. Ramström and T. L. Lindahl, Putting polyphosphates to the test: evidence against platelet-induced activation of factor XII. Blood, 2013, 122, 3818-3824.

35. S. Raynaud, E. Champion, D. Bernache-Assollant and P. Thomas, Calcium phosphate apatites with variable Ca/P atomic ratio I. Synthesis, characterisation and thermal stability of powders. Biomaterials, 2002, 23, 1065-1072.

36. K. Saito, H. Omori, S. Kanno, Y. Hirata, T. Okada, S. Mori and K. Nakadate, Chemical and crystallographic studies on 33 cases of calcium carbonate gallstone (so-called limy bile). Gastroenterol. Jpn., 1986, 21, 162-166.

37. Q. Hu, J. Zhang, H. Teng and U. Becker, Growth process and crystallographic properties of ammonia-induced vaterite. Amer. Mineral, 2012, 97, 1437-1445.

38. U. Schloßmacher, H. C. Schröder, X. H. Wang, Q. Feng, B. Diehl-Seifert, S. Neumann, A. Trautwein and W. E. G. Müller, Alginate/silica composite hydrogel

as a potential morphogenetically active scaffold for three-dimensional tissue engineering. RSC Advances, 2013, 3, 11185-11194.

39. M. Wiens, X. Wang, H. C. Schröder, U. Kolb, U. Schlossmacher, H. Ushijima and W. E. G. Müller, The role of biosilica in the osteoprotegerin/RANKL ratio in human osteoblast-like cells. Biomaterials, 2010, 31, 7716-7725.

40. M. Wiens, X. Wang, U. Schlossmacher, I. Lieberwirth, G. Glasser, H. Ushijima, H. C. Schröder and W. E. G. Müller, Osteogenic potential of biosilica on human osteoblast-like (SaOS-2) cells. Calcif. Tissue Int., 2010, 87, 513-524.

41. M. R. Lorenz, V. Holzapfel, A. Musyanovych, K. Nothelfer, P. Walther, H. Frank, K. Landfester, H. Schrezenmeier and V. Mailänder, Uptake of functionalized, fluorescent-labeled polymeric particles in different cell lines and stem cells. Biomaterials, 2006, 27, 2820-2828.

42. X. H. Wang, H. C. Schröder, V. Grebenjuk, B. Diehl-Seifert, V. Mailänder, R. Steffen, U. Schloßmacher and W. E. G. Müller, The marine sponge-derived inorganic polymers, biosilica and polyphosphate, as morphogenetically active matrices/scaffolds for differentiation of human multipotent stromal cells: Potential application in 3D printing and distraction osteogenesis. Marine Drugs, 2014, 12, 1131-1147.

43. H. C. Schröder, X. H. Wang, M. Wiens, B. Diehl-Seifert, K. Kropf, U. Schloßmacher and W. E. G. Müller, Silicate modulates the cross-talk between osteoblasts (SaOS-2) and osteoclasts (RAW 264.7 cells): inhibition of osteoclast growth and differentiation. J. Cellular Biochem., 2012, 113, 3197-3206.

44. S. F. Wang, X. H. Wang, F. G. Draenert, O. Albert, H. C. Schröder, V. Mailänder, G. Mitov and W. E. G. Müller, Bioactive and biodegradable silica biomaterial for bone regeneration. Bone, 2014, 67, 292–304.

45. M. S. Mahadevaiah, Y. Kumar, M. S. Abdul-Galil, M. S. Suresha, M. A. Sathish and G. Nagendrappa, A simple spectrophotometric determination of phosphate in sugarcane juices, water and detergent samples. E-Journal of Chemistry, 2007, 4, 467-473.

46. D. Chavan, T. C. van de Watering, G. Gruca, J. H. Rector, K. Heeck, M. Slaman and D. Iannuzzi, Ferrule-top nanoindenter: an optomechanical fiber sensor for nanoindentation. Rev. Sci. Instrum., 2012, 83, 115110. doi: 10.1063/1.4766959.

47. S. Vidya, A. Parameswaran and V. G. Sugumaran, Comparative evaluation of tissue. Compatibility of three root canal. Sealants in Rattus norwegicus: A Histopathological study. Endodontology, 1994, 6, 7-17.

48. J. M. Anderson, Biological responses to materials. Annu. Rev. Mater. Res., 2001, 31, 81-110.

49. H. R. Lee, H. J. Kim, J. S. Ko, Y. S. Choi, M. W. Ahn, S. Kim, S. H. Do, Comparative characteristics of porous bioceramics for an osteogenic response in-vitro andin vivo. PLoS One, 2013, 8, e84272.

50. L. Sachs, Angewandte Statistik, Springer, Berlin, 1984, p. 242.

51. I. W. Kim, J. L. Giocondi, C. Orme, S. Collino and J. S. Evans, Morphological and kinetic transformation of calcite crystal growth by prismatic-associated asprich sequences. Cryst. Growth Des., 2008, 8, 1154-1160.

52. C. Pautke, M. Schieker, T. Tischer, A. Kolk, P. Neth, W. Mutschler and S. Milz, Characterization of osteosarcoma cell lines MG-63, SaOS-2 and U-2 OS in comparison to human osteoblasts. Anticancer Res., 2004, 24, 3743-3748.

53. A. Oyane, H. M. Kim, T. Furuya, T. Kokubo, T. Miyazaki and T. Nakamura, Preparation and assessment of revised simulated body fluids. J. Biomed. Mater. Res. A, 2003, 65, 188-195.

54. B. Clarke, Normal bone anatomy and physiology. Clin. J. Am. Soc. Nephrol., 2008, 3 (Suppl 3), S131–S139.

55. M. R. Wiederkehr and O. W. Moe, Uric acid nephrolithiasis: A systemic metabolic disorder. Clin. Rev. Bone Miner. Metab., 2011, 9, 207–217.

56. M. N. Rahaman, D. E. Day, B. S. Bal, Q. Fu, S. B. Jung, L. F. Bonewald and A. P. Tomsia, Bioactive glass in tissue engineering. Acta Biomater., 2011, 7, 2355-2373.

57. J. D. Termine and A. S. Posner, Amorphous/crystalline interrelationships in bone mineral. Calcif. Tissue Res., 1967, 1, 8-23.

58. H. Wang, Y. Li, Y. Zuo, J. Li, S. Ma and L. Cheng, Biocompatibility and osteogenesis of biomimetic nano-hydroxyapatite/polyamide composite scaffolds for bone tissue engineering. Biomaterials, 2007, 28, 3338-3348.

59. A. V. Radha, T. Z. Forbes, C. E. Killian, P. U. Gilbert and A. Navrotsky, Transformation and crystallization energetics of synthetic and biogenic amorphous calcium carbonate. Proc. Natl. Acad. Sci. U.S.A., 2010, 107, 16438-16443.

60. A. Richter, D. Petzold, H. Hofmann and B. Ullrich, Production, properties and application of calcium carbonate powders. 3. Investigations to the transition of vaterite and aragonite in aqueous systems. Chemische Technik, 1996, 48, 271-275,

61. K. Kuroda, M. Moriyama, R. Ichino, M. Okido and A. Seki, Formation and in vivo evaluation of carbonate apatite and carbonate apatite/CaCO3 composite films using the thermal substrate method in aqueous solution. Mat Transact, 2008, 49, 1434-1440.

62. X. H. Wang, H. C. Schröder and W. E. G. Müller, Enzyme-based biosilica and biocalcite: biomaterials for the future in regenerative medicine. Trends Biotechnol., 2014, 32, 441-447.

63. W. E. G. Müller, E. Tolba, H. C. Schröder, M. Neufurth, S. Wang, T. Link, B. Al-Nawas and X. H. Wang (2015k) A new printable and durable N,O-carboxymethyl chitosan-Ca2+-polyphosphate complex with morphogenetic activity. J. Mat. Chem. B, 3, 1722-1730.

64. W. E. G. Müller, X. H. Wang, B. Diehl-Seifert, K. Kropf, U. Schloßmacher, I. Lieberwirth, G. Glasser, M. Wiens and H. C. Schröder, Inorganic polymeric phosphate/polyphosphate as an inducer of alkaline phosphatase and a modulator of intracellular Ca2+ level in osteoblasts (SaOS-2 cells) in-vitro . Acta Biomaterialia, 2011, 7, 2661-2671.

65. J. Green, D. T. Yamaguchi, C. R. Kleeman and S. Muallem, Cytosolic pH regulation in osteoblasts. Regulation of anion exchange by intracellular pH and Ca2+ ions. J. Gen. Physiol., 1990, 95, 121-145.

66. R. Jalali, B. Zandieh-Doulabi, P. K. DenBesten, U. Seidler, B. Riederer, S. Wedenoja, D. Micha and A. L. Bronckers, Slc26a3/Dra and Slc26a6 in murine ameloblasts. J. Dent. Res., 2015, doi: 10.1177/0022034515606873.

Extended summary

This part provides a general discussion and conclusions of the overall work presented in this thesis. Significant contributions of the research are also briefly summarized. Finally, future directions are presented.

As mentioned before in **chapter 1**, bone tissue engineering has been emerged as a potential alternative to the conventional use of bone grafts, due to their limited supply and problem of infections and disease transmissions [1-3]. While this approach is based on a deep understanding of natural healing mechanisms of bone tissue, i.e. the principles of cellular, molecular developmental biology and morphogenesis, it is very much guided by the development of an artificial extracellular matrix known as a scaffold [3, 4]. This matrix plays an important role in manipulating and maintaining the functions of bone forming cells via providing the favorable environments for promoting cell proliferation and differentiation, and in targeting the cells to the site of the bone defect in order to initiate tissue regeneration [2, 5]. However, in spite of numerous previous studies, there is no final conclusive data on which type of materials is the best for bone tissue engineering scaffolds. Since this important field is still at the infant stage, it needs extensive work and more detailed analyses to optimize the processing and characterization methods and to assess the biological response based on *in vitro* and *in vivo* evaluation of the resultant materials. In this context, this thesis represents an approach to fabricate different biomaterials based on polyP as bioactive degradable matrices for bone tissue regeneration and to highlight their role in hard tissue mineralization and associated requirements for effective bone tissue engineering.

In an attempt to exploit the potential of polyP as an inducer for bone formation, a number of studies have previously shown that exogenously administered polyphosphate effect cell proliferation and reduce mineralization in a dose- dependent manner [6, 7]. While the molecular mechanism of action of polyP has not been fully understood, it has been demonstrated that polyP inhibits crystalline calcium hydroxyapatite nucleation and growth from solution as long as the polymer is not

hydrolyzed [8]. However, previous studies have shown that temperature, pH, and some enzymes enhanced their hydrolytic degradation, decreasing the polyP concentration and therefore reducing their inhibitory activity [9-12]. Thus, the major challenge concerning the successful use of polyP is their stability, their ability to be taken up efficiently into the cell in intact form and the appropriate concentration in the extracellular space [13-15].

The results in **chapter 2** implicate a more active role for Ca-polyP nanoparticles, in regulating osteogenic cell behavior and biomineralization than Na-polyP. However, the mechanism of the morphogenetic activity of Ca-polyP resulting in the promotion of bone mineralization needs further elucidation; most likely they involve multiple pathways:

- Regulation of the extracellular pools of calcium and phosphate ions, similar to the chemical composition of the natural bone mineral, in turn modulating osteogenic cell response.
- Induction of cell differentiation through higher steady-state-expression of the *ALP* gene, which is a marker and essential for the mineralization process.
- Activation of osteoblast-like a SaOS-2 cell that is reflected by an accumulation of mitochondria and the translocation of the polyP-degrading enzyme ALP to the cell surface.

In conclusion, our results demonstrate that Ca-polyP nanoparticles can be used as a smart bioavailable reserve for calcium and phosphate ions and a morphogenetically active substrate for bone-forming cells during bone formation.

Mineralization of hard tissues, essential for its mechanical properties, involves a well orchestrated process in which inorganic mineral HA crystals are produced by bone-forming cells and deposited in precise amounts and arrangement within the bone's organic fibrous extracellular matrix [16-19]. By studying the molecular components involved in this process, scientists gain a more insight into the principles of bone

formation and its disturbances under abnormal conditions. These research efforts will change and help us to find out new therapeutic targets for treatment of bone diseases and complete healing bone defects. Although, the composition of bone as nature biocomposite material has been known for a long time [18, 20], there is still much doubt about the chemical and physical identity of building units of the bone matrix. Thus, finding out the composition and phase transformations of initial products obtained during calcification, i.e. the entity of the bone mineral immediately after deposition, will considerably help to understand the basic mechanism of calcification.

Recently, amorphous calcium phosphate (ACP) has been found in human bone matrix. It is well known that ACP formed as an intermediate phase during the formation of hydroxyapatite (HA) as well as other types of calcium phosphates [21, 22]. ACP could be consider as a bone mineral precursor in which it is spontaneously transformed into the most thermodynamically stable under physiological environment calcium phosphate phase HA. It is well known that the presence of magnesium, fluoride, carbonate, pyrophosphate, diphosphonates or nucleotides, at definite amounts, will delay and inhibit the fast transformation of ACP into hydroxyapatite [23, 24]. Therefore, mimicking natural mineralization in the laboratory in order to fabricate and develop new types of calcium phosphate based biomaterials which are thought to be intermediate phases during crystalline hydroxyapatite deposition, is an attractive target for bone tissue regenerative therapy.

It has been, **in chapter 3**, proposed an approach to optimize and modulate nucleation and growth hydroxyapatite crystal via an in-situ precipitation method in the presence of polyP. It was found that addition of low concentrations of polyP (<10 wt.%) results in spindle-like hydroxyapatite crystallites. While at higher polyP concentrations (>10 wt.%) the formation of crystalline HA was inhibited and amorphous calcium phosphate-polyP nanoparticles were formed. Further studies revealed that the polyP–CaP particles cause a strong upregulation of the expression of the genes encoding for two marker proteins of bone formation, collagen type I and alkaline phosphatase (ALP). Based on their

morphogenetic activity the amorphous polyP–CaP particles offer a promising material for the development of bone implants, formed from physiological inorganic precursors/polymers.

In the same context, one of the challenges in elucidating biomineralization processes is the ability to identify mineral compositions at the nanometer scale, during tissue formation and disease [16, 25]. *In vitro* studies have suggested that carbonated mineral might be a precursor for deposition of bone apatite [26, 27].Recently biochemical and dispersive spectroscopic evidence suggest that amorphous calcium carbonate could also act as a bioseed for the formation of carbonated apatite [28-30]. In this context, **chapter 4** describes that polyP can stabilize the amorphous calcium carbonate phase. Furthermore, the $CaCO_3$/polyP material appears to be a promising biocompatible and osteogenic scaffolding material that acts as nucleating centers for mineralization deposition.

Taken together, the thesis highlights the novel function of polyP in mineralization and paramount importance not only for fundamental biomineralization research, but also for the design and development of new biomaterials for hard tissue repair and regeneration applications. Thus, we are optimistic that the incorporation of polyP with common types of calcium phosphate or carbonates will find many applications ranging from bone implants to drug carriers which were specially designed to find out the right surrounding microenvironment for bone regeneration. Finally, with all these materials at hand further experiments will be performed to determine material degradation mechanism, cellular uptake as well as *in vivo* evaluations are required to assess the potential for clinical application.

References

1. Amini A. R., Laurencin C. T., & Nukavarapu S. P. (2012). Crit Rev Biomed Eng. 40: 363-408.

2. Dimitriou R., Jones E., McGonagle D. & Giannoudis P. V. (2011). BMC Med. 9: 66.

3. Putnam A. J. & Mooney D. J. (1996). Nat Med. 2: 824-826.

4. Place E. S, Evans N. D & Stevens M. M. (2009). Nat Mater. 8: 457-470.

5. Kanczler J. M. & Oreffo R. O. (2008). Eur Cell Mater. 2: 100-14.

6. Hoac B., Kiffer-Moreira T., Millán J. L. & McKee M. D. (2013). Bone 53: 478-486.

7. Francis M. D. (1969). Calcif Tissue Res. 3: 151-62.

8. Fleisch H., Russell R. G. & Straumann F. (1966). Nat. 212: 901-3.

9. Omelon S., Georgiou J., Henneman Z. J., Wise L. M., Sukhu B., Hunt T., Wynnyckyj C., Holmyard D., Bielecki R. & Grynpas M. D. (2009). PLoS One. 4: e5634.

10. Kawazoe Y., Shiba T., Nakamura R., Mizuno A., Tsutsumi K., Uematsu T., Yamaoka M., Shindoh M. & Kohgo T.(2004). J Dent Res. 83:613-618.

11. Ariganello M. B., Omelon S., Variola F., Wazen R. M., Moffatt P. & Nanci A. (2014). J Cell Biochem. 115: 2089-2102.

12. Wang X.H., Schröder H.C., Schlossmacher U., Neufurth M., Feng Q., Diehl-Seifert B. & Müller W.E.G. (2014). Calcif Tissue Int. 94: 495-509.

13. Müller W. E. G., Wang X. H., Diehl-Seifert B., Kropf K., Schloßmacher U., Lieberwirth I., Glasser G., Wiens M. & Schröder, H. C. (2011). Acta Biomater. 7: 2661-2671.

14. Schröder H. C., Kurz L., Müller W. E. G. & Lorenz B. (2000). Biochem (Moscow). 65: 296-303.

15. Tsutsumi K., Saito N., Kawazoe Y., Ooi, H. K. & Shiba T. (2014). PLoS One. 9: e86834.

16. Sommerdijk N. A. J. M. & Cölfen H. (2011). MRS Bulletin. 35: 116–121.

17. Fernandez-yague M. A., Akogwu S., Mcnamara L., Zeugolis D. I., Pandit A., & Biggs M. J. (2015). Adv Drug Deliv Rev. 84: 1–29.

18. Rey C., Combes C., Drouet C. & Glimcher M. J. (2009). Osteoporosis Int. 20: 1013-1021.

19. Glimcher M. J. (1987). Instr Course Lect. 36: 49–69.

20. Meyers M. A., Chen P. Y., Lin A. Y. M. & Seki Y. (2008). Prog Mater Sci. 53: 1–206.

21. Habraken W., Habibovic P., Epple M. & Bohner M. (2016). Mater Today. 19 69-87

22. Combes C. & Rey C. (2010). Acta Biomater. 6: 3362–78.

23. Olszta M. J., Odom D. J., Douglas E. P. & L.B. Gower. (2003). Connect Tissue Res. 44: 326-334.

24. Andersen A. (1989). J Cryst Growth. 94: 767-777.

25. Pellegrino E. D., Biltz R. M., & Rogers P. J. (1965). Trans Am Clin Climatol Assoc. 76: 181-191.

26. Klosowski M. M., Friederichs R. J., Nichol R., Antolin N., Carzaniga R., Windl W., Best S. M., Shefelbine S. J., McComb D. W. &Porter A. E. (2015). Acta Biomater. 20: 129-139.

27. Borowitzka M. A. (1989). Chemical and Biochemical Perspectives. Ed. Mann S., Webb J. & Williams R. J. P., VCH, Weinheim, Germany. 63-94.

28. Wang X. H., Schröder H. C., Schlossmacher U., Neufurth M., Feng Q., Diehl-Seifert B. & Müller W. E. G. (2014). Calcif Tissue Int. 94: 495-509.

29. Liao S. Y., Lerman M. I. & Stanbridge E. J. (2009). BMC Dev Biol. 9: 22.

30. Chang X., Zheng Y., Yang Q., Wang L., Pan J., Xia Y., Yan X. & Han J. (2012). Arthritis Res Ther. 14: R176.

List of Figures

Curriculum Vitae

Name	: Emad Tolba Adnan Tolba Eldeyaste
Nationality	: Egyptian
Date of birth	: 4th July 1983
Current position	: Researcher Assistant
Tel. No.	: +4915213459856
E-Mail	: Emad_nrc@yahoo.com (or) Etolbaad@uni-mainz.de.

Education

Apr. 2014	: PhD Candidate, University Medical Center of the Johannes Gutenberg University Mainz, Germany.
Jul. 2010	: M.Sc. in Biophysics, Faculty of Science, Mansoura University, Egypt. *Thesis entitled*: Design, synthesis and characterization of apatite based nanocomposites with tailored biomedical specifications.
May 2005	: B.Sc. in Biophysics (GPA: Very good), Faculty of Science, Mansoura University, Egypt.

Career

Since 2014	: Researcher Assistant, Institute for Physiological Chemistry, University Medical Center of the Johannes Gutenberg University Mainz.
Aug.2011: Dec.2013	: Researcher Assistant, Biomaterials Department, National Research Centre, Egypt. *Research topic*: Fabrication and characterization of biomaterials for biomedical application.
Jan.2011: Apr.2011	: A Junior Scientist, Fraunhofer Institute for Mechanics of Materials IWM, Freiburg, Germany. *Research topic*: "Electrospun non-woven for engineering artificial blood vessels"
Jun.2006: Nov.2010	: Assistant Researcher, Biomaterials Department, National Research Center, Egypt.

Research Interests

Biomaterials field is an interdisciplinary area and typically involves in the development of biological substitutes to restore, maintain, improve or regenerate damaged tissue structure and function. Specific research areas within this field:

- Fabrication and characterization of biomaterials for medical and biotechnological applications, i.e. bioceramics, biopolymers and their composites.
- Processing technologies for soft and hard tissue engineering scaffolds and matrices.
- Material/cell interaction mechanisms to direct stem cell fate for tissue engineering and regenerative medicine purposes, including cellular attachment, proliferation and differentiation as well as nanoparticles cellular uptake, cytotoxicity and intracellular targeting.

Workshops & Conferences

12th: 13thJul.2007	: The 2nd International Conference on Inorganic Chemical Industries& Mineral Resources (Future Aspects). National Research Center, Egypt.
29thJan.: 4thFeb.2006	: The US-Egypt workshop "Tissue Engineering" (Research Applications and Technology Development). National Research Center, Egypt.
1st: 2ndMar.2015	: The International conference of the Egyptian Society for Science and Technology of Biomaterials (ESSTB). Transfer of Biomaterials into Technology. National Research Center, Egypt.
2nd: 4thSept.2015	: Creating life in 3D"Frontiers in Material and Life Sciences". Brno, Czech Republic.
15th: 16thApr.2016	: The 1st International Conference on"3D Printing in Medicine". Mainz, Germany.

Publications

2016

- Wang XH, Ackermann M, Wang S, **Tolba E**, Neufurth M, Feng Q, Schröder HC & Müller WEG. (2016). Amorphous polyphosphate/amorphous calcium carbonate implant material with enhanced bone healing efficacy in a critical-size defect in rats. Biomed Mater. 11: 035005.
- Müller WEG, Neufurth M, Wang S, **Tolba E**, Schröder HC & Wang XH. (2016). Morphogenetically active scaffold for osteochondral repair (Polyphosphate /alginate/ N, O-carboxymethyl chitosan). Eur Cell Mater. 31: 174-190.
- Müller WEG, Neufurth M, **Tolba E**, Wang S, Geurtsen W, Feng Q, Schröder HC & Wang XH. (2016). A biomimetic approach to ameliorate dental hypersensitivity by amorphous polyphosphate microparticles. Dent Mater. 32: 775-785.
- Müller WEG, Schröder HC, **Tolba E**, Neufurth M, Diehl-Seifert B & Wang XH. (2016). Mineralization of bone related SaOS-2 cells under physiological hypoxic conditions. FEBS J. 283: 74–87.
- Müller WEG, **Tolba E**, Schröder HC, Muñoz-Espí R, Diehl-Seifert B &Wang XH. (2016). Amorphous polyphosphate-hydroxyapatite: A morphogenetically active substrate for bone-related SaOS-2 cells in-vitro. Acta Biomat. 31: 358- 367.
- **Tolba E**, Müller WEG, Abd El-HadyB M, Neufurth M, WurmFR, Wang S, Schröder HC &Wang XH. (2016). High biocompatibility and improved osteogenic potential of amorphous calcium carbonate/vaterite. J Mater Chem B. 4: 376-386.

2015

- Müller WEG, **Tolba E**, Schröder HC, Neufurth M, Wang S, Link T, Al-Nawas B & Wang XH. (2015). A new printable and durable N,O-carboxymethyl chitosan-Ca^{2+}-polyphosphate complex with morphogenetic activity. J Mat Chem B. 3: 1722-1730.
- Müller WEG, **Tolba E**, Schröder HC, Diehl-Seifert B & Wang XH. (2015). Retinol encapsulated into amorphous Ca^{2+} polyphosphate nanospheres acts synergistically in MC3T3-E1 cells. Eur J Pharm Biopharm. 93: 214-223.
- Müller WEG, **Tolba E**, Schröder HC, Wang S, Glasser G, Diehl-Seifert B & Wang XH. (2015). Biologizing titanium alloy implant material with morphogenetically active polyphosphate. RSC Advances. 5: 75465-75473.
- Neufurth M, Wang XH, **Tolba E**, Dorweiler B, Schröder HC, Link T, Diehl-Seifert B & Müller WEG. (2015). Modular small diameter vascular grafts with bioactive functionalities. PLoS ONE. 10: e0133632.

- Müller WEG, **Tolba E**, Dorweiler B, Schröder HC, Diehl-Seifert B & Wang XH. (2015). Electrospun bioactive mats enriched with Ca-polyphosphate/retinol nanospheres as potential wound dressing. Biochem Biophys Rep. 3: 150-160.
- Müller WEG, **Tolba E**, Schröder HC & Wang XH. (2015). Polyphosphate: a morphogenetically active implant material serving as metabolic fuel for bone regeneration. Macromol. Biosci. 15: 1182- 1197.
- Müller WEG, **Tolba E**, Schröder HC, Wang S, Glaßer G, Muñoz-Espí R, Link T & Wang XH. (2015). A new polyphosphate calcium material with morphogenetic activity. Mater Lett. 148: 163-166.
- Müller WEG, **Tolba E**, Feng Q, Schröder HC, Markl JS, Kokkinopoulou M & Wang XH. (2015). Amorphous Ca2+polyphosphate nanoparticles regulate ATP level in bone-like SaOS-2 cells. J Cell Sci. 128: 2202- 2207.

2014

- Wang XH, **Tolba E**, Schröder HC, Neufurth M, Feng Q, Diehl-Seifert B & Müller WEG. (2014). Effect of Bioglass on Growth and Biomineralization of SaOS-2 Cells in Hydrogel after 3D Cell Bioprinting. PLoS ONE. 9: e112497.
- Müller WEG, **Tolba E**, Schröder HC, Diehl-Seifert B, Link T & Wang XH. (2014). Biosilica-loaded poly (Ɛ-caprolactone) nanofibers mats provide a morphogenetically active surface scaffold for the growth and mineralization of the osteoclast-related SaOS-2 cells. Biotechnology J. 9: 1312-1321.

2012

- El-Gohary MI, El-Dyn SM, Abd El-moniem BM, Al-Ashkar E, Saleh S, **Tolba E**& Soliman I. (2012). Synthesis and microstructure characterization of novel Sr-HA prepared by co-precipitation with enhanced bioactivity. Egypt J Biophys Biomed Engng. 13: 73- 85.

2010

- **Tolba E**, Abd-Elhady BM., Elkholy B, Elkady H & Eltonsy M. (2010). Biomimetic synthesis of guided-tissue regeneration hydroxyapatite / polyvinyl alcohol nanocomposite scaffolds: influence of alginate addition on mechanical and biological properties. J Am Sci. 6: 239-249.

2009

- **Tolba E**, Abd-Elhady BM, Elkholy B & Eltonsy M. (2009). Biomimetic synthesis of guided-tissue regeneration hydroxyapatite / polyvinyl alcohol nanocomposite scaffolds: influence of processing parameters on construct microstructure. Egyptain Journal of Applied Science. 24(12B) .3.

ERKLÄRUNG

Hiermit erkläre ich, die vorliegende Arbeit selbständig und nur mit Hilfe der angegebenen Personen und Mittel (Literatur, Apparaturen, Material) angefertigt zu haben. Bei den von mir durchgeführten Untersuchungen habe ich die Grundsätze guter wissenschaftlicher Praxis, wie sie in der Satzung der Johannes Gutenberg-Universität Mainz niedergelegt sind, eingehalten.

_____ _____

Ort, Datum **Emad Tolba**